AFRL-VA-WP-TR-2007-3086

AIR VEHICLE TECHNOLOGY INTEGRATION PROGRAM (AVTIP)

Delivery Order 0020: Prediction of Manufacturing Tolerances for Laminar Flow, Task 6

Anne M. Bender
Aaron Drake

Northrop Grumman Corporation
Air Combat Systems
1 Hornet Way
El Segundo, CA 90245

SEPTEMBER 2006

Final Report for 01 March 2006 – 30 September 2006

Approved for public release; distribution unlimited.

STINFO COPY

AIR VEHICLES DIRECTORATE
AIR FORCE MATERIEL COMMAND
AIR FORCE RESEARCH LABORATORY
WRIGHT-PATTERSON AIR FORCE BASE, OH 45433-7542

NOTICE AND SIGNATURE PAGE

AFRL-VA-WP-TR-2007-3086 HAS BEEN REVIEWED AND IS APPROVED FOR PUBLICATION IN ACCORDANCE WITH ASSIGNED DISTRIBUTION STATEMENT.

*//Signature//

Jeffrey R. Komives, 1st Lt, USAF
Aerospace Engineer
Aerospace Vehicle Integration and Demo Branch

//Signature//

Michael L. Zeigler
Chief
Aerospace Vehicle Integration and Demo Branch

//Signature//

Douglas C. Blake
Chief
Aeronautical Sciences Division

This report is published in the interest of scientific and technical information exchange, and its publication does not constitute the Government's approval or disapproval of its ideas or findings.

*Disseminated copies will show "//signature//" stamped or typed above the signature blocks.

REPORT DOCUMENTATION PAGE

Form Approved
OMB No. 0704-0188

1. REPORT DATE *(DD-MM-YY)*	2. REPORT TYPE	3. DATES COVERED *(From - To)*
September 2006	Final	01 March 2006 – 30 September 2006

4. TITLE AND SUBTITLE
AIR VEHICLE TECHNOLOGY INTEGRATION PROGRAM (AVTIP)
Delivery Order 0020: Prediction of Manufacturing Tolerances for Laminar Flow, Task 6

5a. CONTRACT NUMBER
F33615-00-D-3054-0020

5b. GRANT NUMBER

5c. PROGRAM ELEMENT NUMBER
0602201

6. AUTHOR(S)
Anne M. Bender
Aaron Drake

5d. PROJECT NUMBER
A071

5e. TASK NUMBER

5f. WORK UNIT NUMBER
0A

7. PERFORMING ORGANIZATION NAME(S) AND ADDRESS(ES)
Northrop Grumman Corporation
Air Combat Systems
1 Hornet Way
El Segundo, CA 90245

8. PERFORMING ORGANIZATION REPORT NUMBER

9. SPONSORING/MONITORING AGENCY NAME(S) AND ADDRESS(ES)
Air Vehicles Directorate
Air Force Research Laboratory
Air Force Materiel Command
Wright-Patterson Air Force Base, OH 45433-7542

10. SPONSORING/MONITORING AGENCY ACRONYM(S)
AFRL/VAAI

11. SPONSORING/MONITORING AGENCY REPORT NUMBER(S)
AFRL-VA-WP-TR-2007-3086

12. DISTRIBUTION/AVAILABILITY STATEMENT
Approved for public release; distribution unlimited.

13. SUPPLEMENTARY NOTES
Report contains color. PAO Case Number: AFRL/WS 06-8776, 29 Nov 2006.

14. ABSTRACT

The ultimate goal of the MEATLOAF study is to develop generalized criteria for the allowable size of an excrescence on a laminar flow wing to prevent premature transition. A salient feature of the study is the nondimensionalization of the critical parameters such that the results are applicable to future work and not specific to a particular airframe. Task 1 provided a database of step effects at Reynolds numbers up to approximately 7.5x105. Task 6 is the first step towards extending the Reynolds numbers range to chord Reynolds numbers more applicable to aircraft such as Global Hawk for small pressure gradients. The feasibility of additional testing to include the full-range of pressure gradients at these higher Reynolds numbers was assessed. Figures 1-3 show the approximate range of chord Reynolds numbers for the initial testing of Task 6 in comparison to the completed Task 1 testing.

15. SUBJECT TERMS
laminar flow, laminar, manufacturing tolerances, excrescence, drag

16. SECURITY CLASSIFICATION OF:			17. LIMITATION OF ABSTRACT:	18. NUMBER OF PAGES	19a. NAME OF RESPONSIBLE PERSON (Monitor)
a. REPORT	b. ABSTRACT	c. THIS PAGE			1Lt Jeffrey Komives
Unclassified	Unclassified	Unclassified	SAR	56	19b. TELEPHONE NUMBER *(Include Area Code)* N/A

Standard Form 298 (Rev. 8-98)
Prescribed by ANSI Std. Z39-18

Table of Contents

1.0 Introduction

The original Prediction of Manufacturing Tolerances for Laminar Flow (MEATLOAF) study was successfully completed in June 2005. The study focused on developing generalized criteria for manufacturing tolerances to prevent premature transition on laminar flow wings. The study consisted primarily of an experimentally-based low-speed unswept parametric investigation. It was concluded that accounting for pressure gradient effects had the potential to significantly loosen manufacturing tolerance requirements for laminar flow aircraft. However, the study needed to be expanded to higher Reynolds numbers before results could be incorporated into manufacturing tolerance requirements with an acceptable risk level.

Task 6 was a low-speed unswept investigation conducted at the Towing Wind Tunnel facility in Hyuga, Japan. The goal of the investigation was to assess the suitability of the Towing Wind Tunnel for extensive laminar flow testing and to extend the database of step effects developed in Task 1 to higher chord Reynolds numbers than was previously possible. The maximum chord Reynolds number with the existing MEATLOAF model is approximately 5 times greater than was possible in Task 1. If a new model were built, the maximum chord Reynolds number could be approximately 10 times greater than was possible in Task 1. The Towing Wind Tunnel is a unique facility, which was identified as a potential test site for additional MEATLOAF testing in August 2005.

The report serves as an addendum to the original MEATLOAF report, AFRL-VA-WP-TR-2005-3060 20050826. The original report should be referenced for background information and results from the original study.

1.1 Project Overview

The ultimate goal of the MEATLOAF study is to develop generalized criteria for the allowable size of an excrescence on a laminar flow wing to prevent premature transition. A salient feature of the study is the nondimensionalization of the critical parameters such that the results are applicable to future work and not specific to a particular airframe. Task 1 provided a database of step effects at Reynolds numbers up to approximately 7.5×10^5. Task 6 is the first step towards extending the Reynolds numbers range to chord Reynolds numbers more applicable to aircraft such as Global Hawk for small pressure gradients. The feasibility of additional testing to include the full-range of pressure gradients at these higher Reynolds numbers was assessed. Figures 1-3 show the approximate range of chord Reynolds numbers for the initial testing of Task 6 in comparison to the completed Task 1 testing.

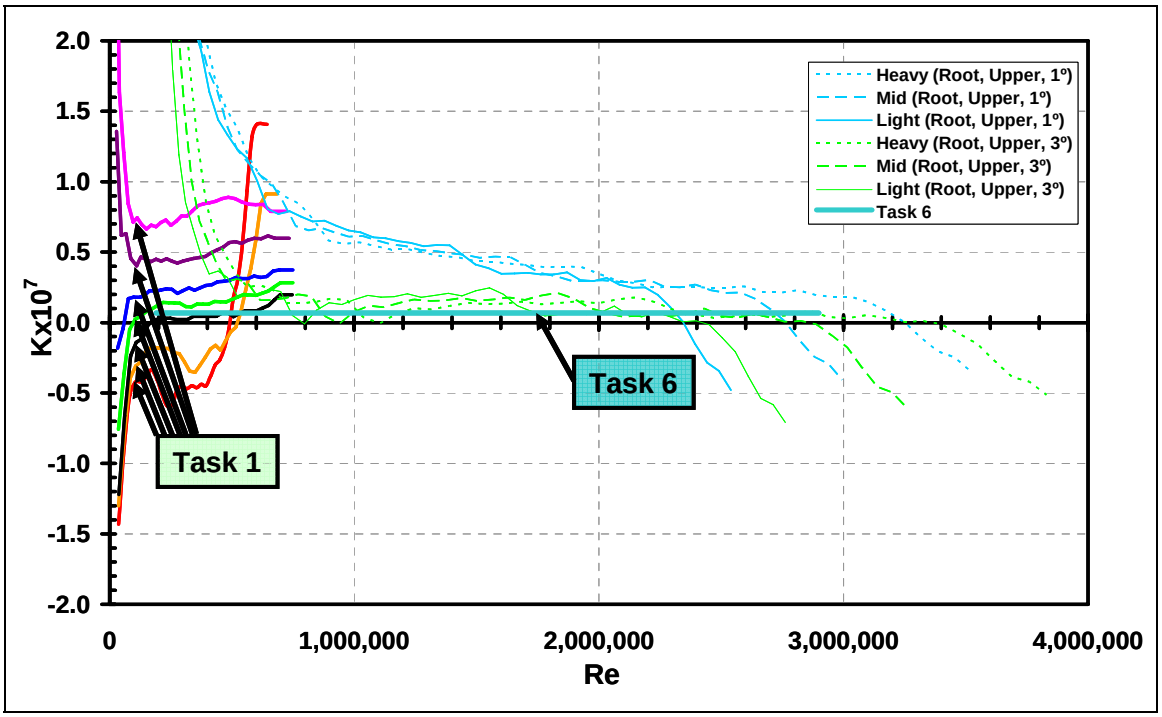

Figure 1. Global Hawk-type wing root upper surface pressure distribution (root)

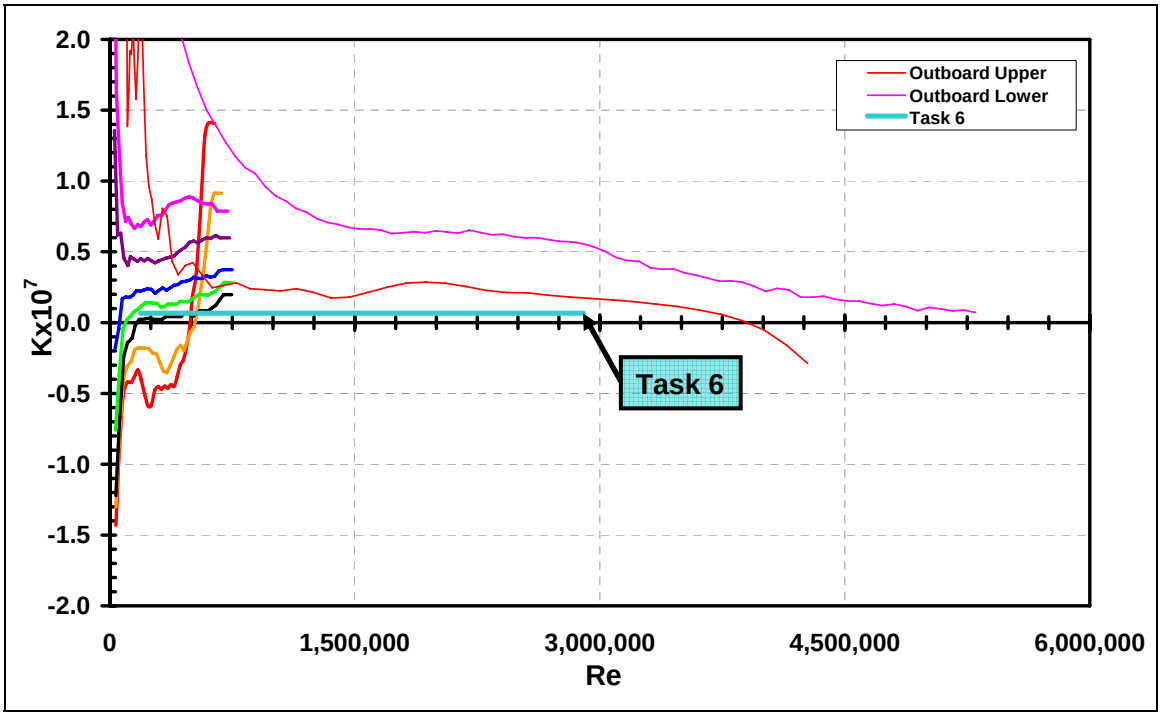

Figure 2. SensorCraft-type surface pressure distribution (outboard)

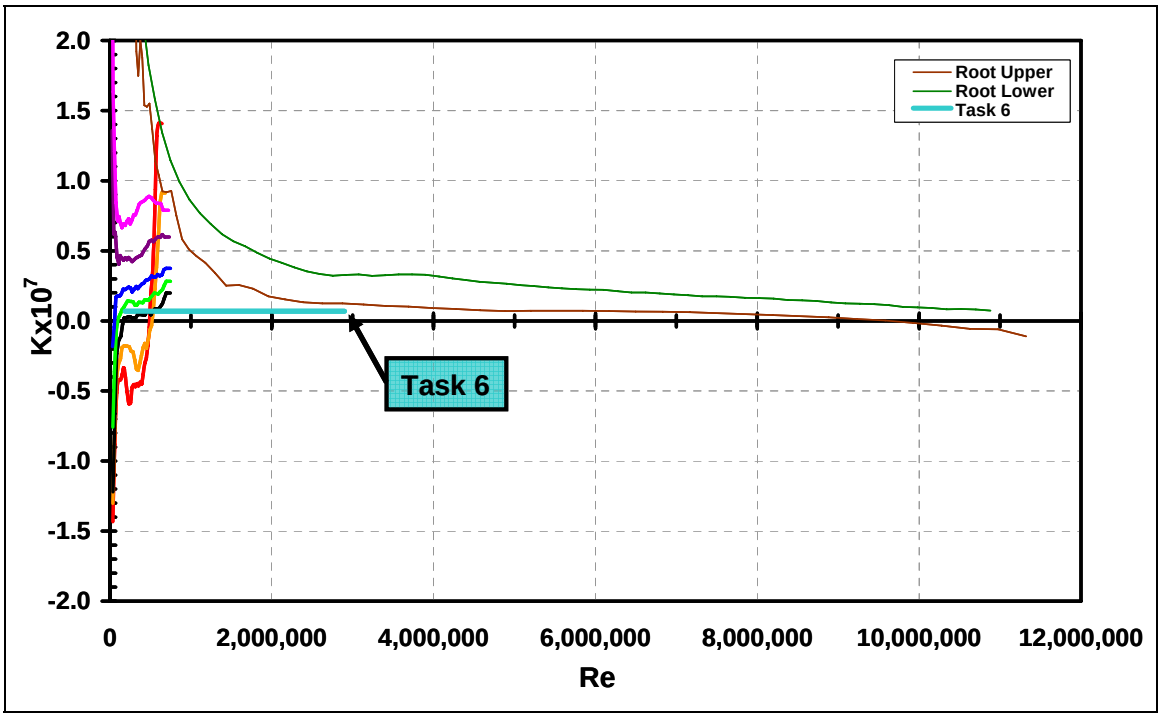

Figure 3. SensorCraft-type surface pressure distribution (root)

2.0 Experimental Expansion of Step Effects Database in Reynolds Number

Task 6 of the Prediction of Manufacturing Tolerances for Laminar Flow contract was an experimental expansion of step effects database in Reynolds number. The objectives were twofold: to assess the feasibility of more extensive laminar flow testing at the Towing Wind Tunnel facility and to take the first step towards extending the existing step effect database from Task 1 in Reynolds number.

2.1 Test Facility

The Towing Wind Tunnel is jointly owned by Tohoku and Miyazaki Universities. The Towing Wind Tunnel is a 2 km long track on which an electrically driven vehicle runs. The vehicle is called the Hyuga Aerodynamic Research by Towing (HART) vehicle. The model is placed on the HART vehicle, and is supported by a hydraulically actuated support arm to minimize vibrations. The first 910 m of the track is the acceleration region, the next 515 m is the measurement region, and the last 475 m is the deceleration region. The measurement region is covered by a hood, which shields the car from external noise and winds. The surface of the test track is paved asphalt. A diagram of the Towing Wind Tunnel is shown in Figure 4.

The HART vehicle is approximately 8.5 m long, by 3.4 m wide by 0.7 m tall and weighs approximately 2.7 t. The vehicle has 8 tires underneath its body, 4 of which are electrically driven. 4 tires on the side of the vehicle brace against vertical guide walls that run alongside the track. The maximum speed of the HART vehicle on the track is 50 m/s. The HART vehicle is shown in Figures 5-6.

Initial Internal Research and Development (IRAD) testing by Northrop Grumman Corporation (NGC) in December 2005 at the facility indicated that it was suitable for laminar flow testing.

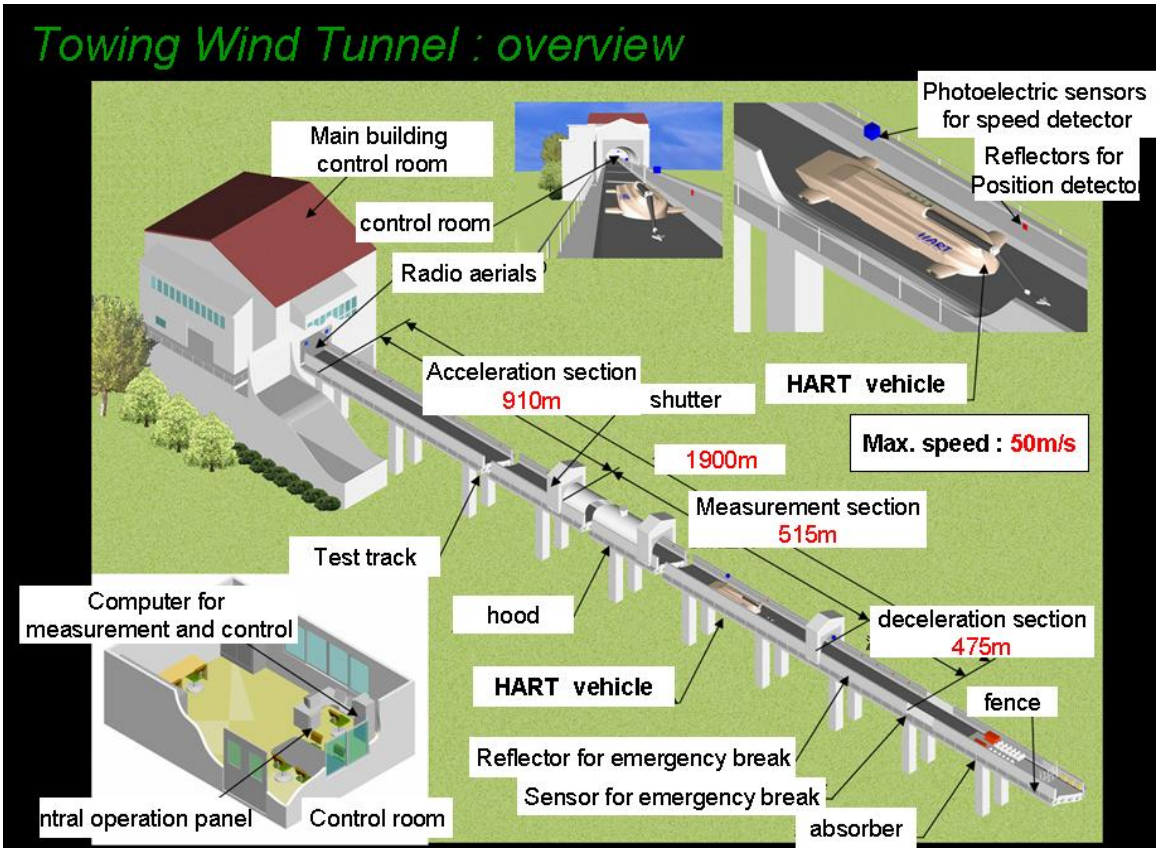

Figure 4. Towing Wind Tunnel diagram

Figure 5. HART vehicle moving to beginning of test track with facility's flat plate model

Figure 6. HART vehicle at beginning of test track during NGC IRAD testing

2.2 Model

The approach was to utilize an existing test article for this investigation. This existing model is called the Task 0 model and was used extensively in NGC IRAD testing. Like the Task 1 model, the Task 0 model is a flat plate model with a super-ellipse leading edge. The derivative of the surface contour of a super-ellipse goes to zero at the minor axis such that there is no second-derivative discontinuity where the super-ellipse meets the flat plate. This is important because having noncontinuous second derivatives can cause separation and transition. The Task 0 plate has a continuously-adjustable step located 9 inches from the leading edge of the 48-inch long plate. Because of the construction of the plate, the steps created are pure two-dimensional steps, with no blendouts. The same model is used for every step case, enabling all test conditions to be changed without having to change physical parts or the actual test surface. The model is shown in Figures 7-10.

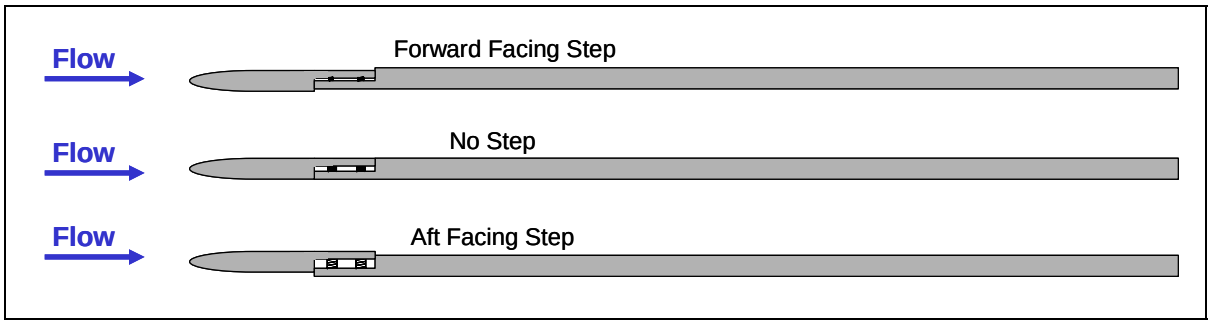

Figure 7. Task 0 (Task 6) model diagram, side view

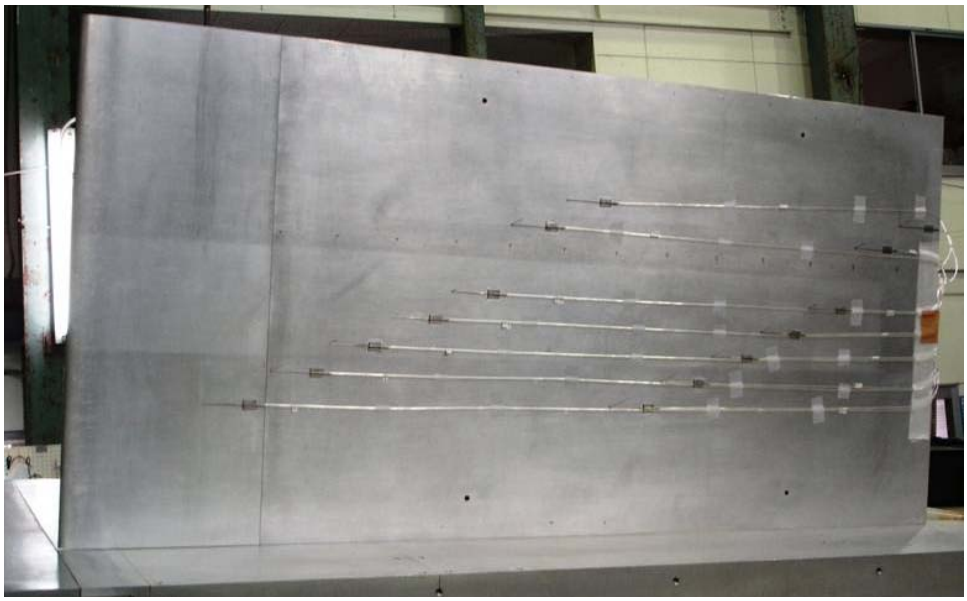

Figure 8. Upper surface of model instrumented with Preston tubes

Figure 9. Lower surface of model

Figure 10. Washer used to set incidence

The model was mounted vertically and held in place with braces. Washers were inserted between the braces and the plate in order to give the plate a slight nose down orientation, to ensure a mildly favorable pressure gradient and attached flow.

2.3 Instrumentation

A self-contained instrumentation package was developed for the Task 6 testing (Figures 11-12). The instrumentation package includes Preston tubes, static pressure taps, and a Pitot tube to measure skin friction, pressure gradient, and air speed. A row of pressure taps in the model allowed measurement of the static pressure distribution on the plate and a Preston tube array was used to measure the chordwise distribution of skin friction. From these skin friction distributions, the transition location was determined.

Locating transition via Preston tube skin friction measurements was a technique successfully employed during the Task 1 work. The nondimensionalization of critical parameters and the analysis methods that were developed in Task 1 was also used in the Task 6 work.

Figure 11. Instrumentation box and plate

Figure 12. Top view of instrumentation

The instrumentation package consists of two groups of pressure ports, each consisting of seven Preston tubes, seven surface static pressures, and a reference dynamic pressure. A data logger and lithium-polymer batteries make the instrumentation package a fully self-contained device for measuring and recording skin friction distributions on the plate. All the components of the instrumentation are commercially-available, off-the-shelf parts. The data logger is a DATAQ Instruments Inc., Model DI-710-UHS. The pressure sensors are Silicon Microstructures Inc., Model 5852-001-S-3-L and 5852-003-S-3-L (nine of each). The two batteries are lithium-polymer (3-cell, 11.1 V, approx. 1500 mAhr). The pressure sensors are on a fiberglass board with traces, and are hard soldered (not socketed) to the board for robustness.

2.4 Experimental Results

2.4.1 Pressure Gradients

The model is equipped with thirty static pressure taps, fourteen of which were instrumented for the Task 6 work. The chordwise locations of the instrumented pressure taps coincide with each of the chordwise locations of the Preston tubes for the skin friction measurements.

There are two sets of Preston tube locations, forward and aft, each having seven Preston tube/static tap pairs. Only one set of locations was tested at one time. The data logger recorded sixteen single-ended channels. Seven channels were for the static taps, seven channels were for the Preston tubes, and two channels were for the Pitot tube (static and total pressure). With a

model with a larger span and a data logger with more channels, more locations could be measured simultaneously. The sample rate for each channel was 5 samples per second.

Static pressure distribution measurements were made using the pressure sensors, model 5852-003-D-3L. The signal range is 0.5 – 4.5 volts and the sensors were designed for an operating pressure range from 0-0.15 psi. The differential sensors minimum and maximum are -0.3 psi and 0.3 psi.

The measured pressure distribution for each run was averaged and this average was converted into the dimensionless pressure gradient, K. A plot of dimensionless pressure gradient versus velocity is shown in Figure 13. The value of K varies a negligible amount with velocity, thus the same K is assigned for all runs tested. The value of K for the Task 6 testing is $K = 0.068 \times 10^{-7}$ as indicated by the dashed black line in the figure. This K value represents a very mild favorable pressure gradient.

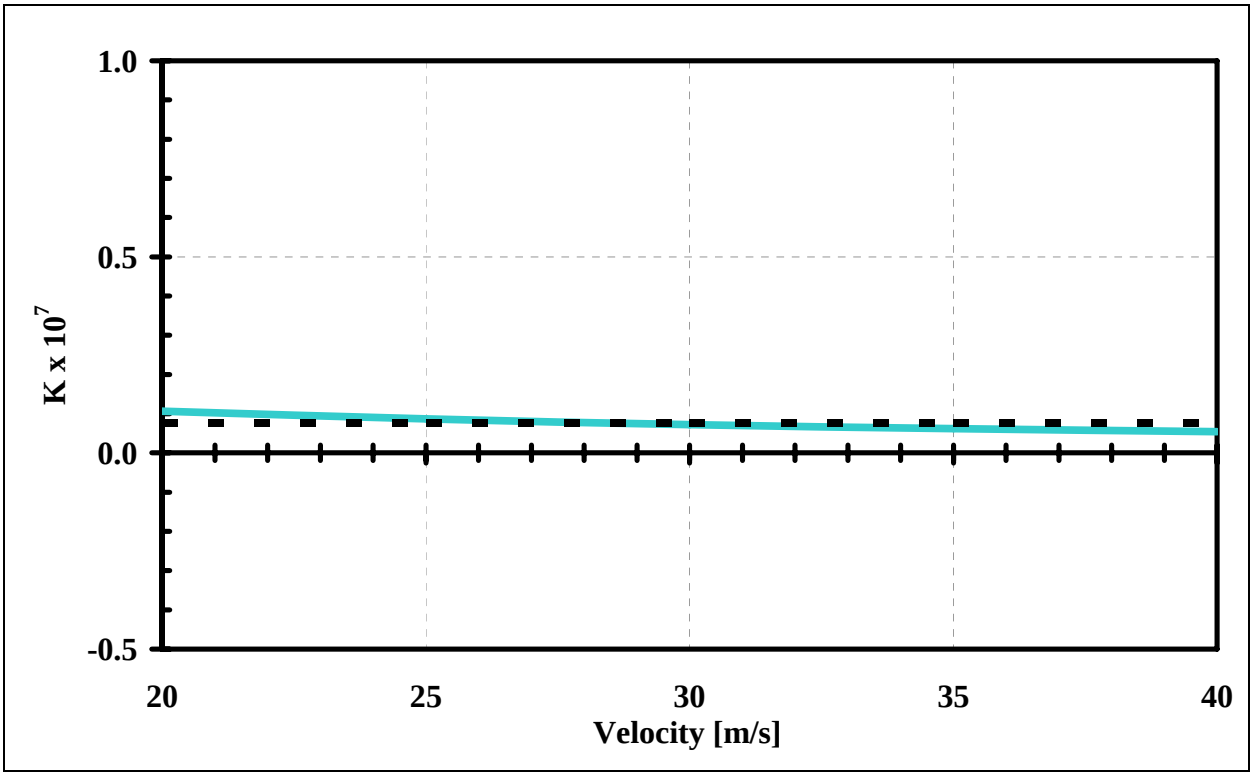

Figure 13. Dimensionless pressure gradient vs. velocity

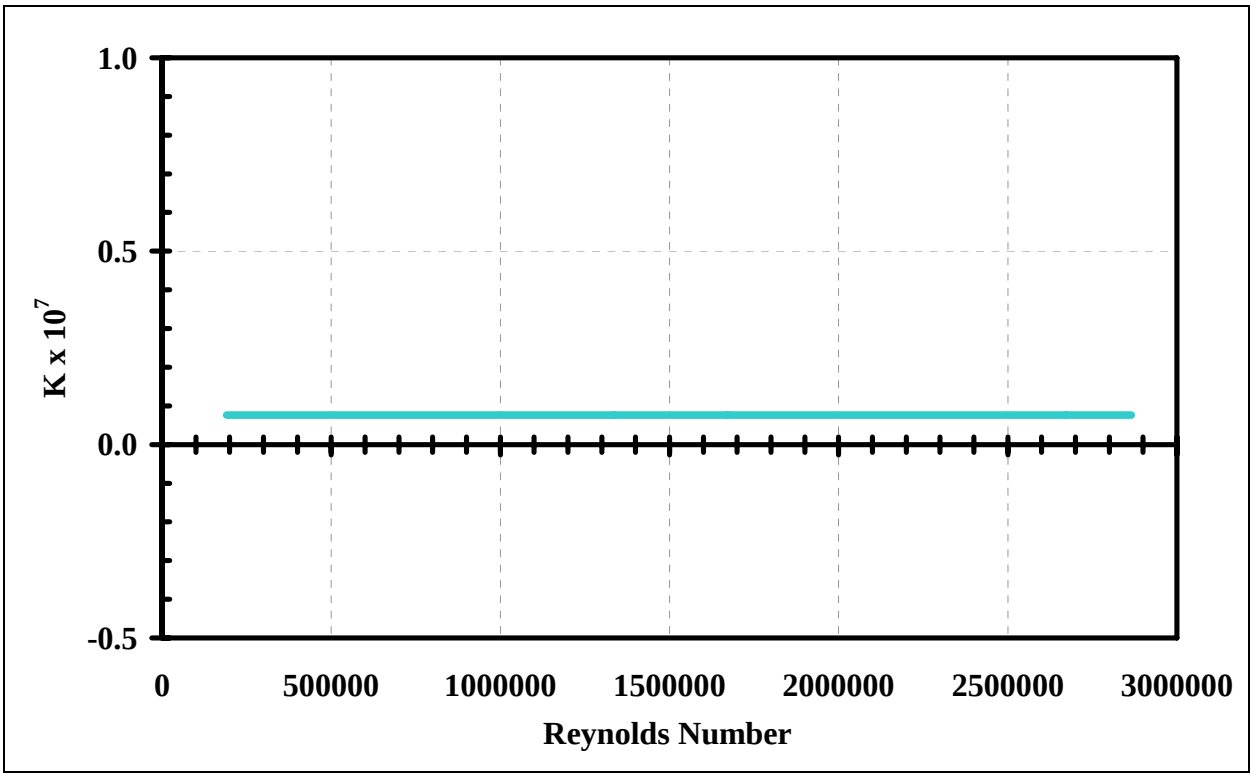

Figure 14. Dimensionless pressure gradient vs. Reynolds number

2.4.2 Boundary Layer Velocity Profiles

To determine the excrescence height Reynolds number (Re_k), it is necessary to have boundary layer velocity profiles at the excrescence location for each speed tested. The boundary layer velocity profiles were obtained computationally using a code called IBL. IBL computes 2-D laminar, transitional, or turbulent boundary layers with or without prescribed arbitrary distributions of surface pressure, heat transfer, and/or mass transfer. The input to IBL in this case was the measured pressure distribution for each speed tested. The velocity profiles obtained are shown in Figure 15. For cases where the measured speed fell between two velocities, the Re_k value was interpolated.

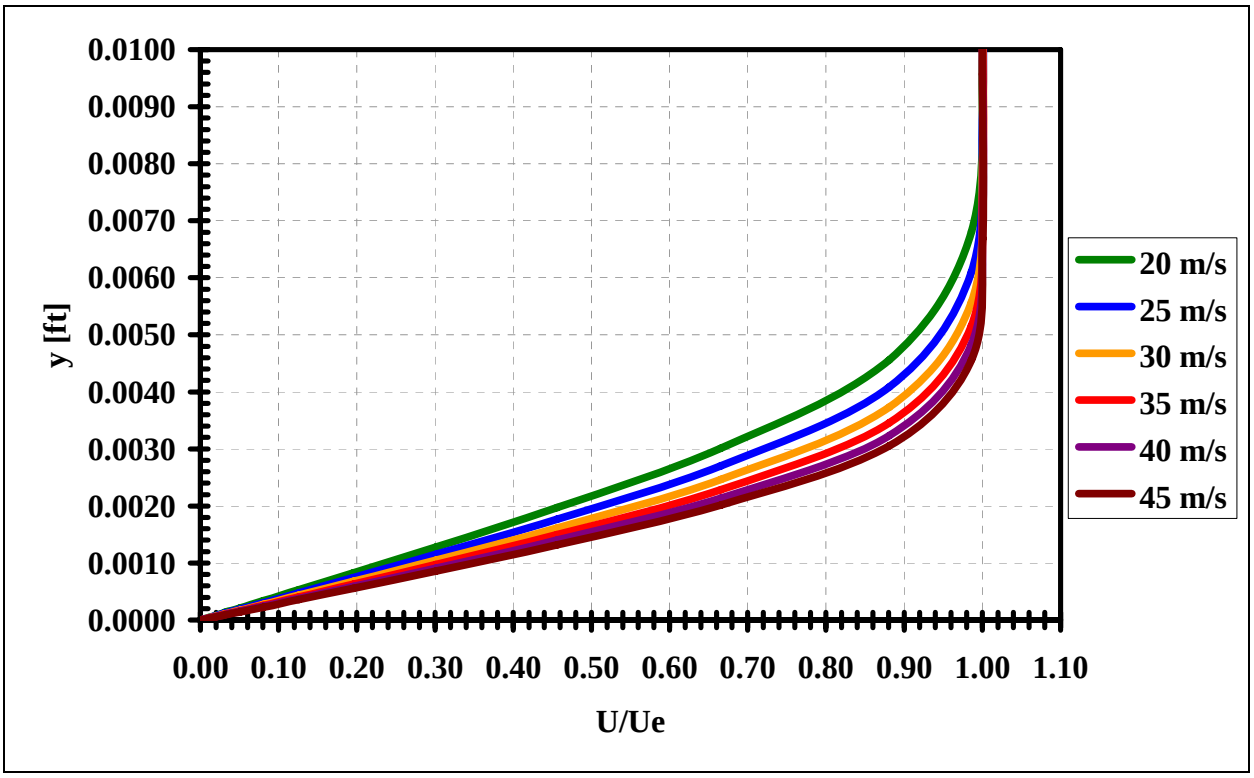

Figure 15. Boundary layer velocity profiles

2.4.3 Skin Friction Distributions

Skin friction distributions for each combination of excrescence geometry and speed were measured using Preston tubes. The outer diameter of the Preston tubes was 0.032 inches. The Preston tube measurements were made using the array of Preston tubes affixed to the model surface. The model was instrumented with fourteen Preston tubes in all; however the instrumentation was only capable of reading data from seven Preston tubes at a time. Therefore, cases are divided into those with the forward Preston tubes or the aft Preston tubes. Preston tube chordwise locations ranged from x = 6 inches to x = 45 inches, with a Preston tube every three inches (the Preston tube that would have been at x = 9 inches, the location of the step, was located at x = 9.25 inches). Each Preston tube had a corresponding static tap located at the same chordwise location. The resulting pressure differences were converted to skin friction coefficients using Patel's calibration for turbulent boundary layers and Poll's calibration for laminar boundary layers, as was done in the Task 1 testing.

The skin friction distribution results for each case tested in Task 6 are presented in Figures 16-79 and transition trends are presented in Figures 80-83. Though each set of Preston tubes had seven Preston/static pairs, in many of the plots, fewer than seven measurement locations are shown. The aft tap at x=45 inches was found to be too close to the edge to obtain reliable data so it is omitted from the plots. In other cases, Preston tubes were moved to ensure that the spanwise spacing was appropriate and some taps were omitted during this study.

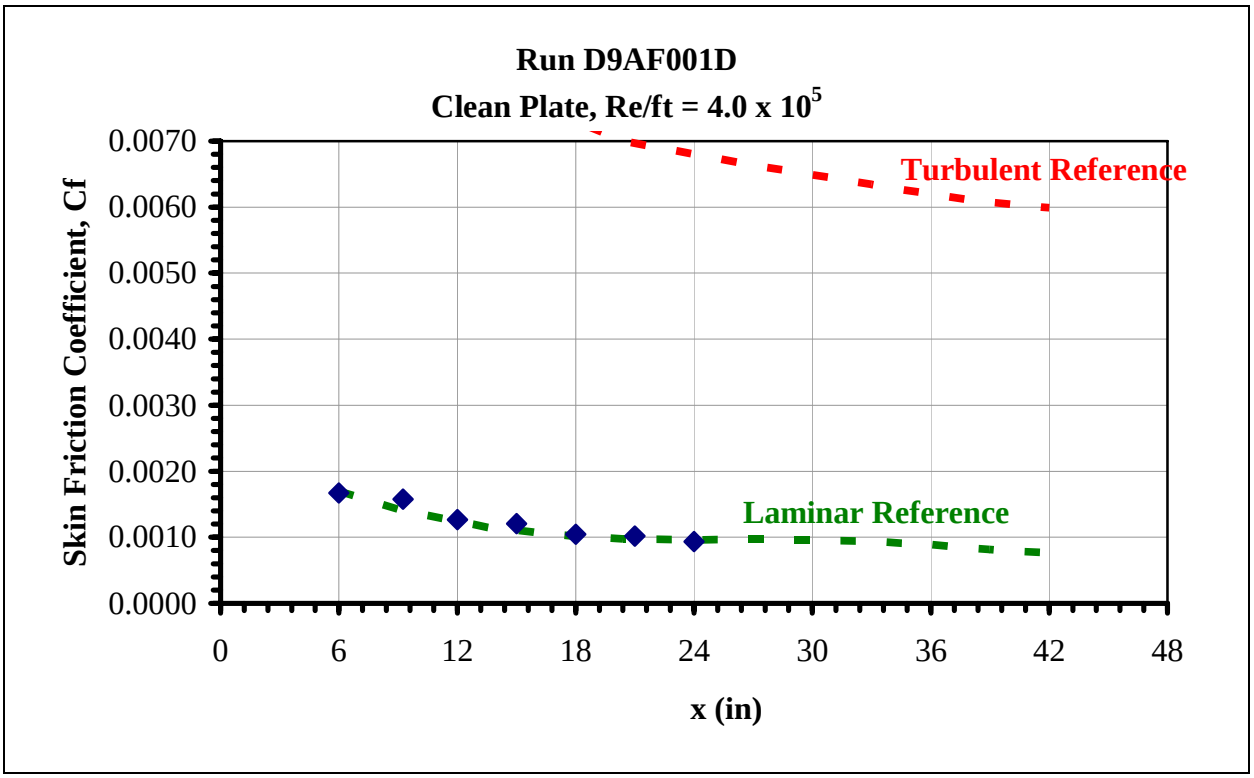

Figure 16. Clean plate skin friction distribution, run D9AF001D

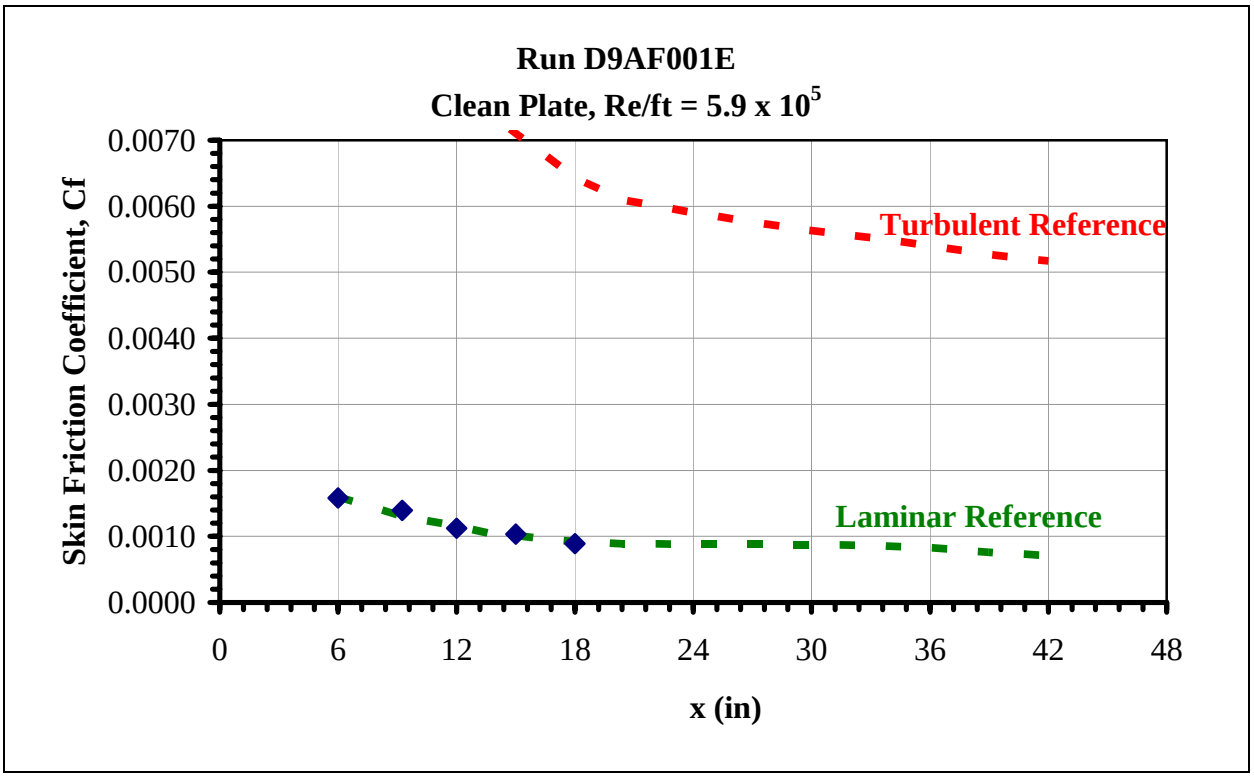

Figure 17. Clean plate skin friction distribution, run D9AF001E

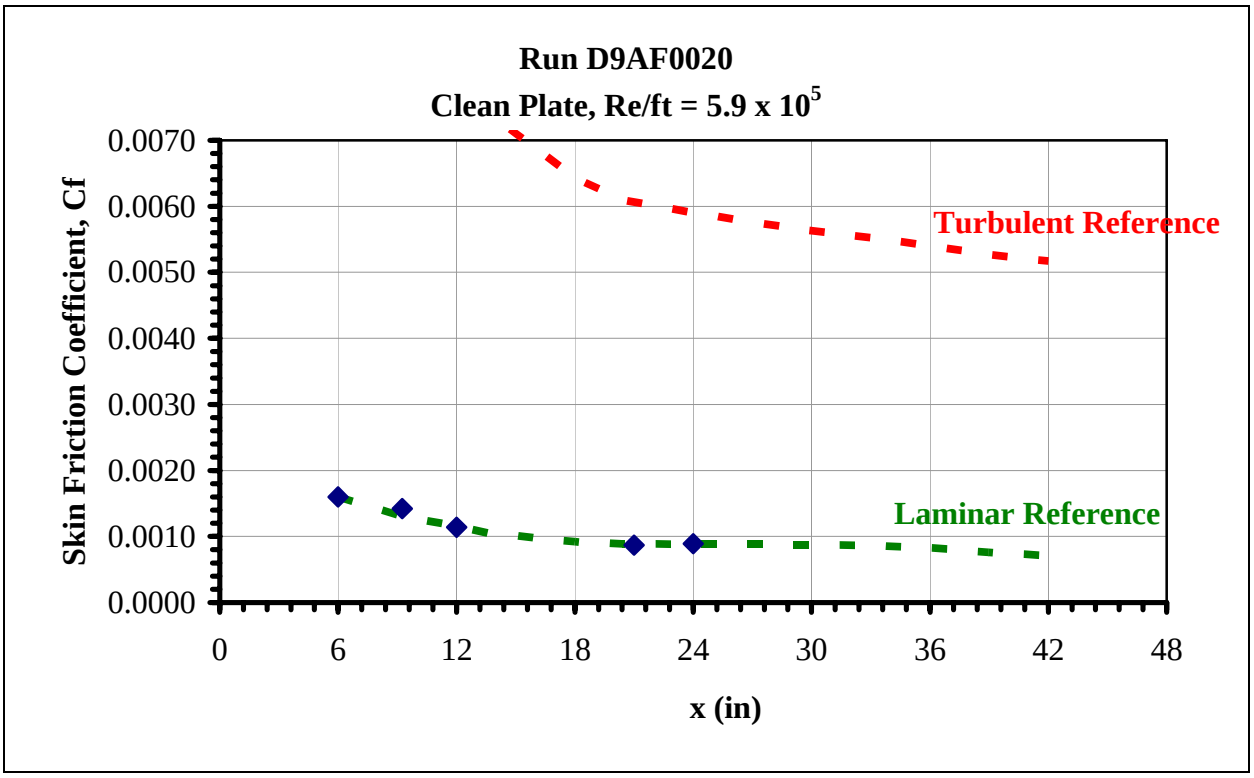

Figure 18. Clean plate skin friction distribution, run D9AF0020

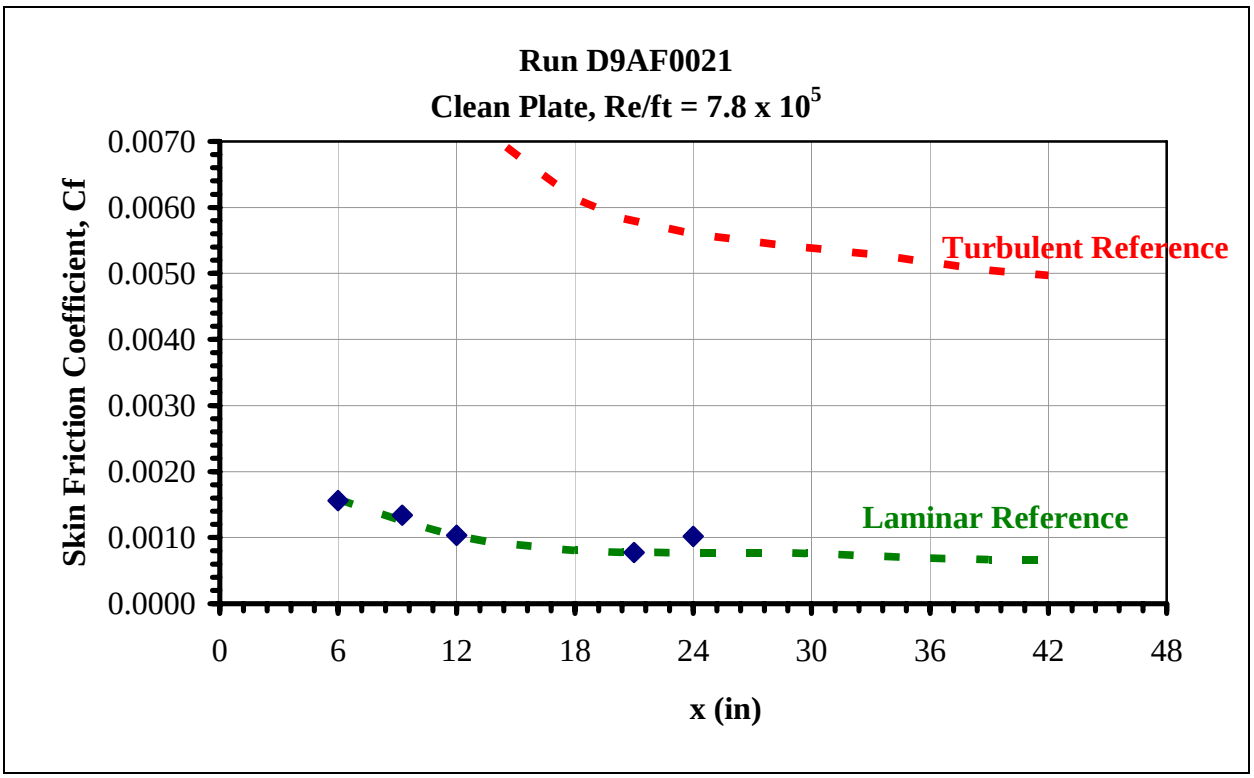

Figure 19. Clean plate skin friction distribution, run D9AF0021

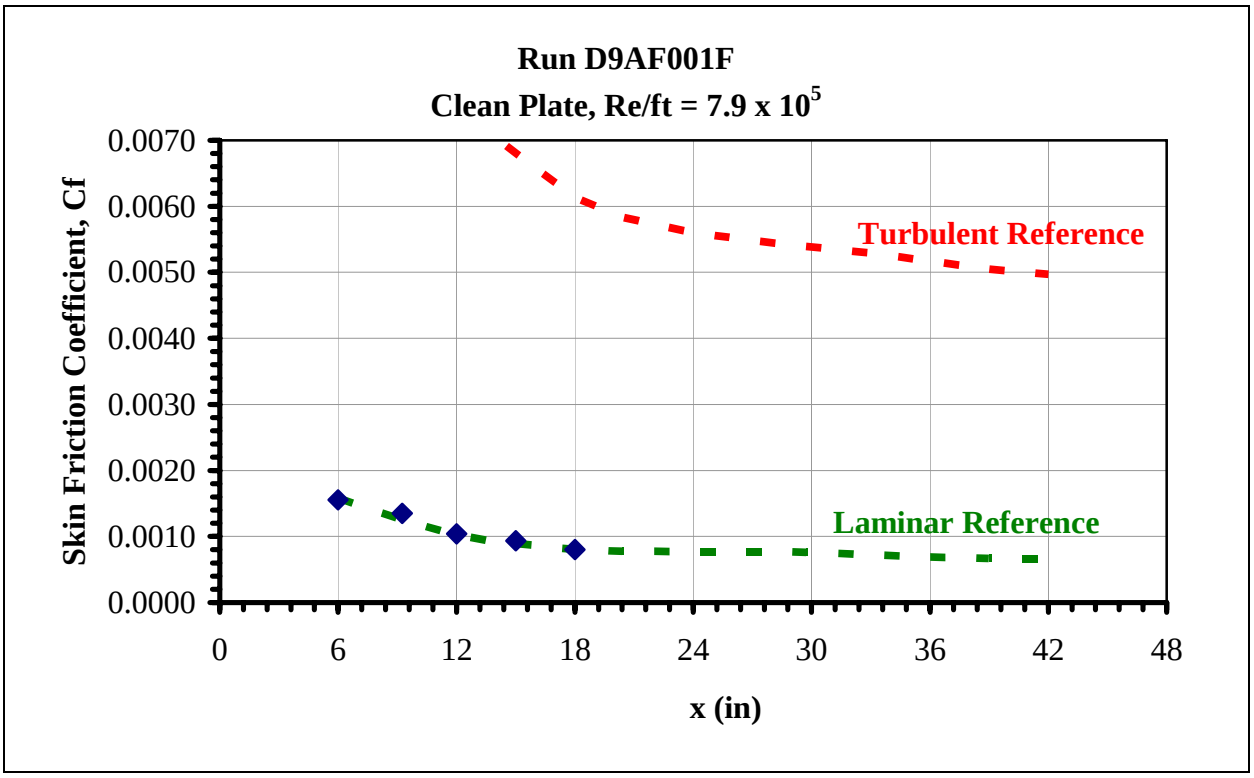

Figure 20. Clean plate skin friction distribution, run D9AF001F

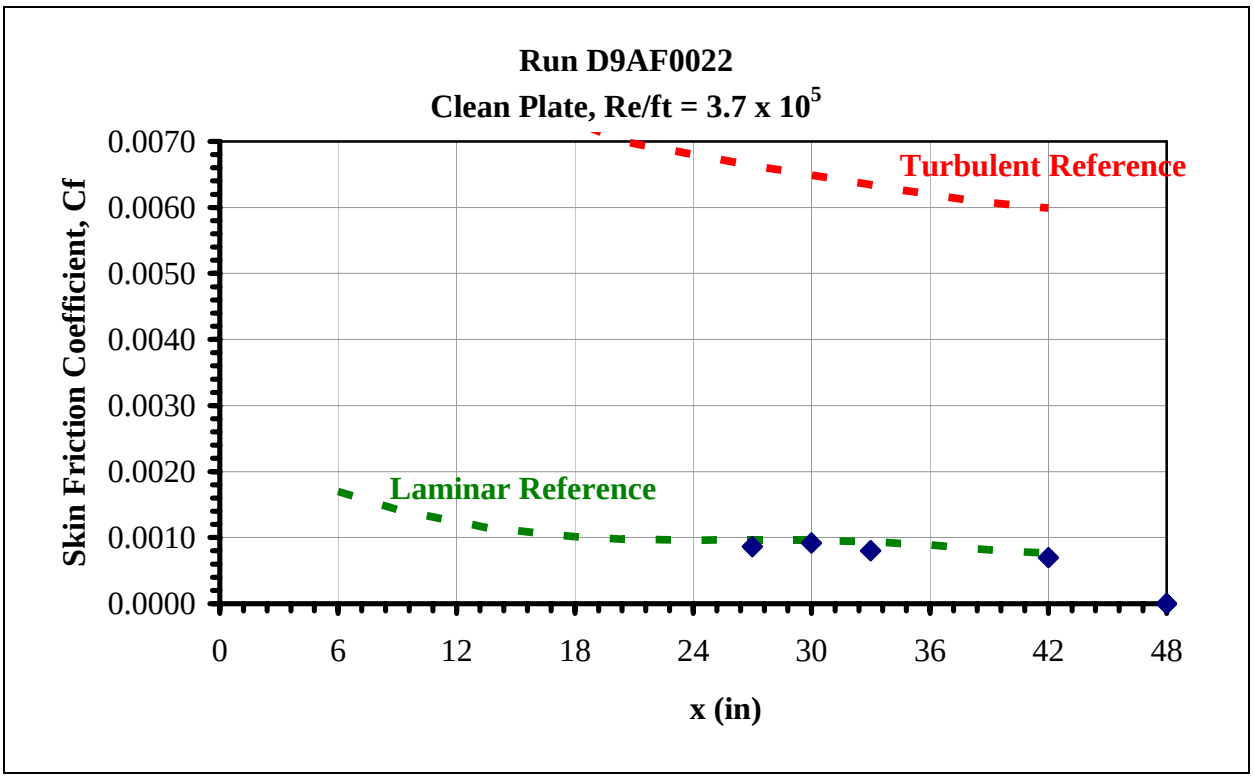

Figure 21. Clean plate skin friction distribution, run D9AF0022

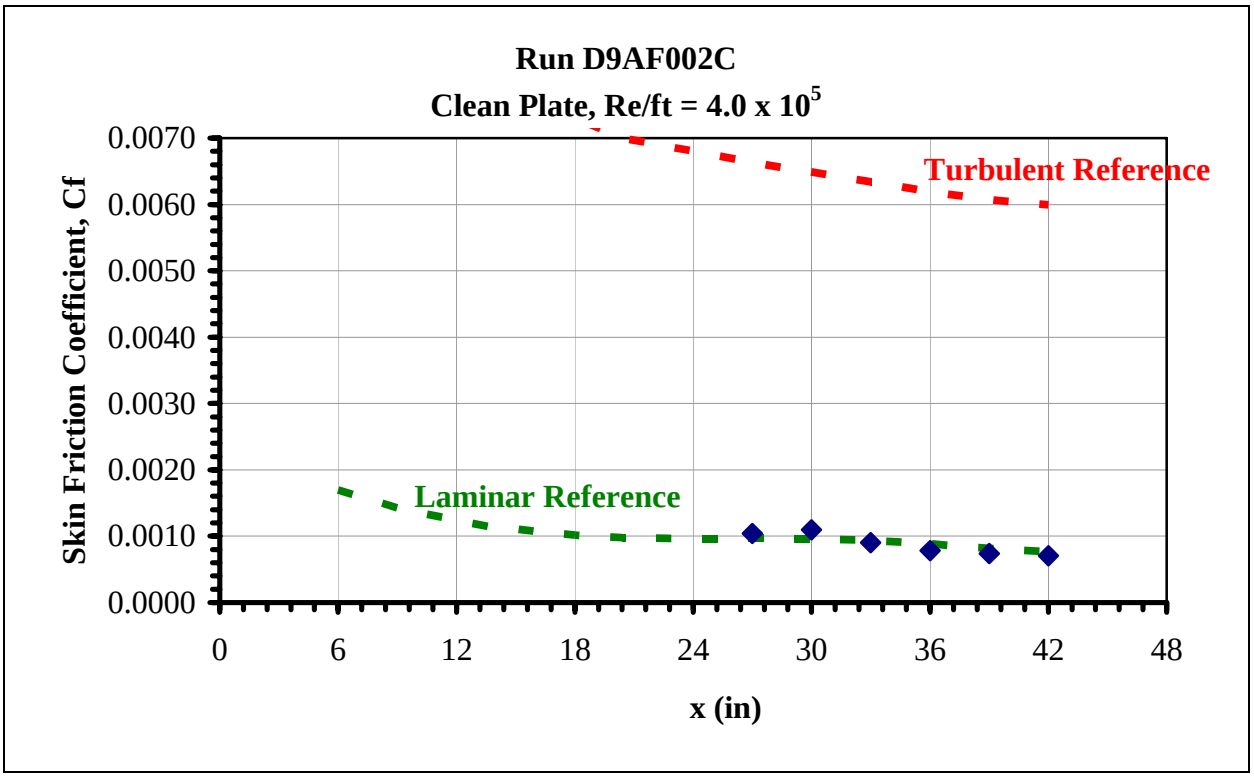

Figure 22. Clean plate skin friction distribution, run D9AF002C

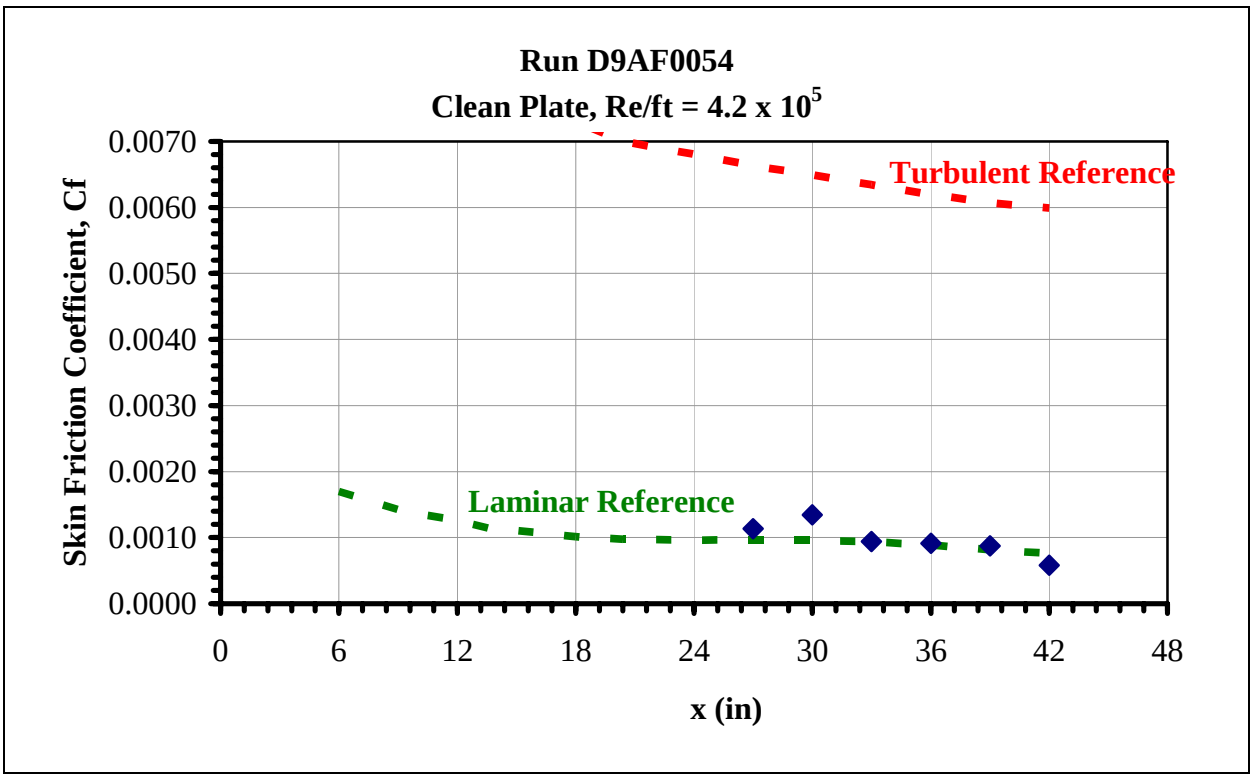

Figure 23. Clean plate skin friction distribution, run D9AF0054

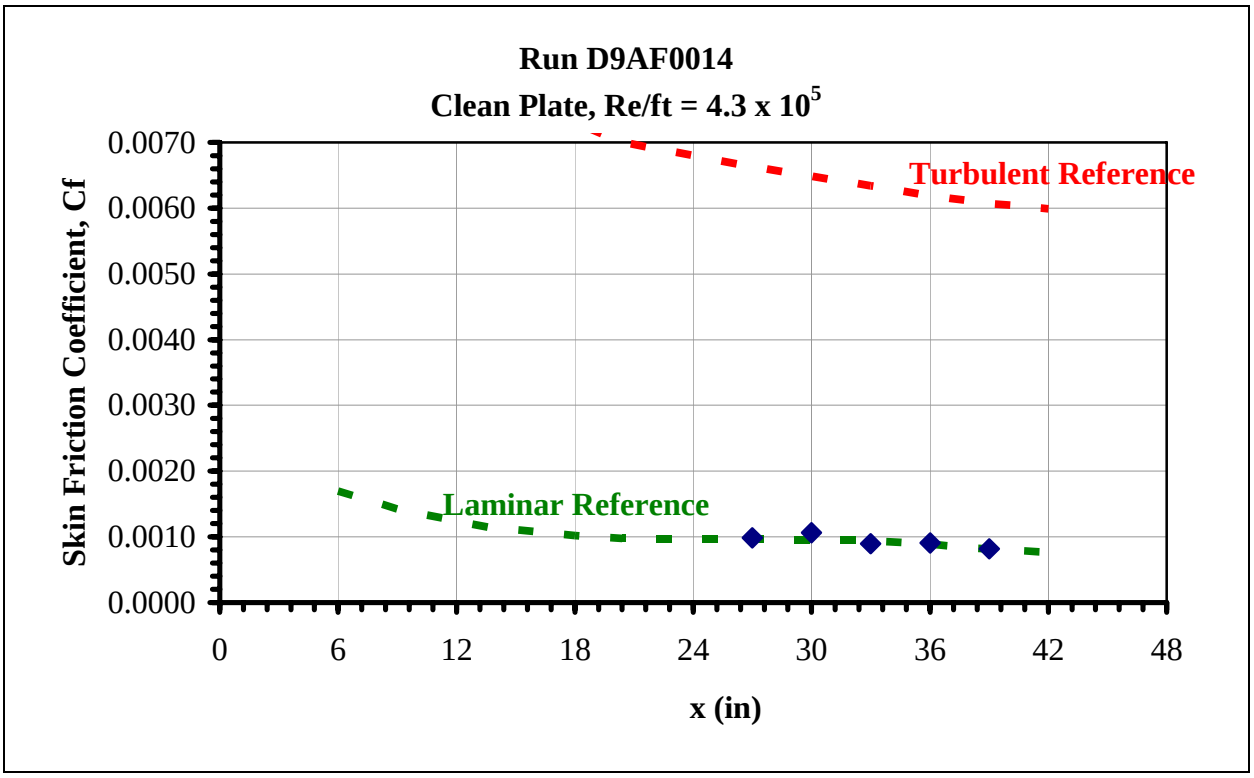

Figure 24. Clean plate skin friction distribution, run D9AF0014

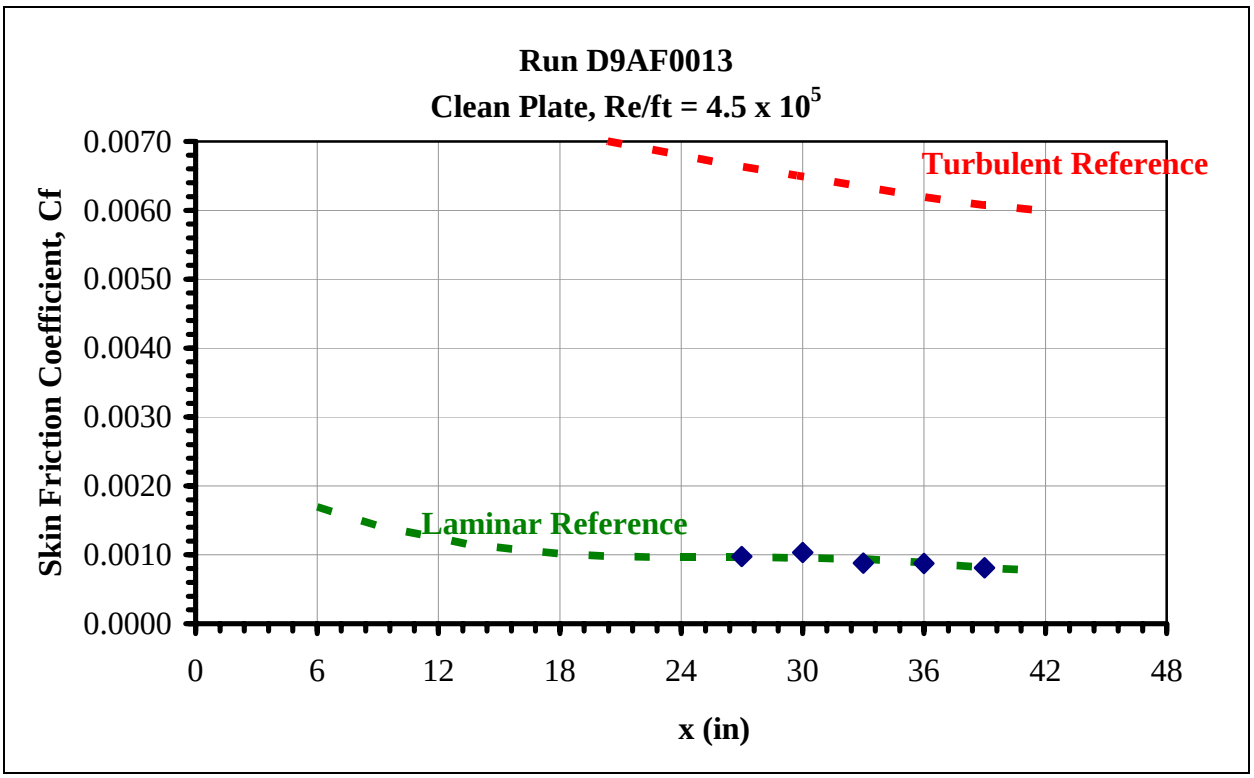

Figure 25. Clean plate skin friction distribution, run D9AF0013

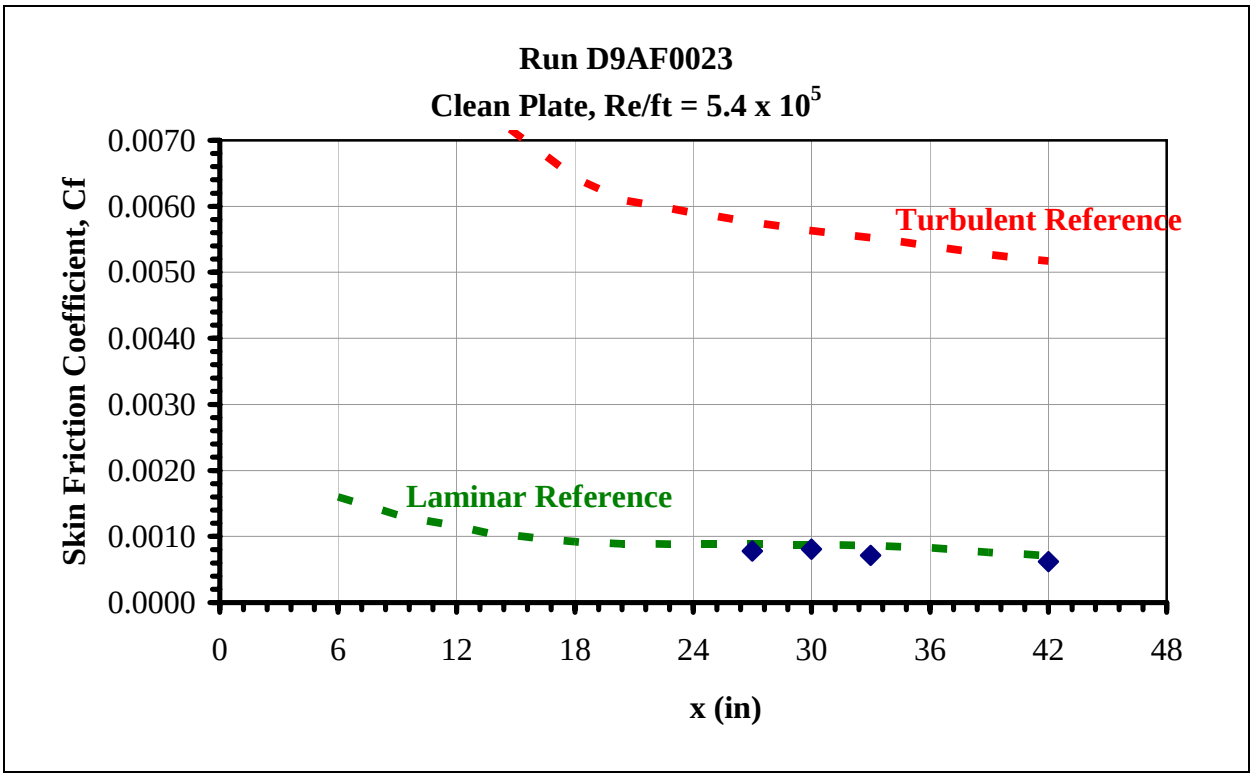

Figure 26. Clean plate skin friction distribution, run D9AF0023

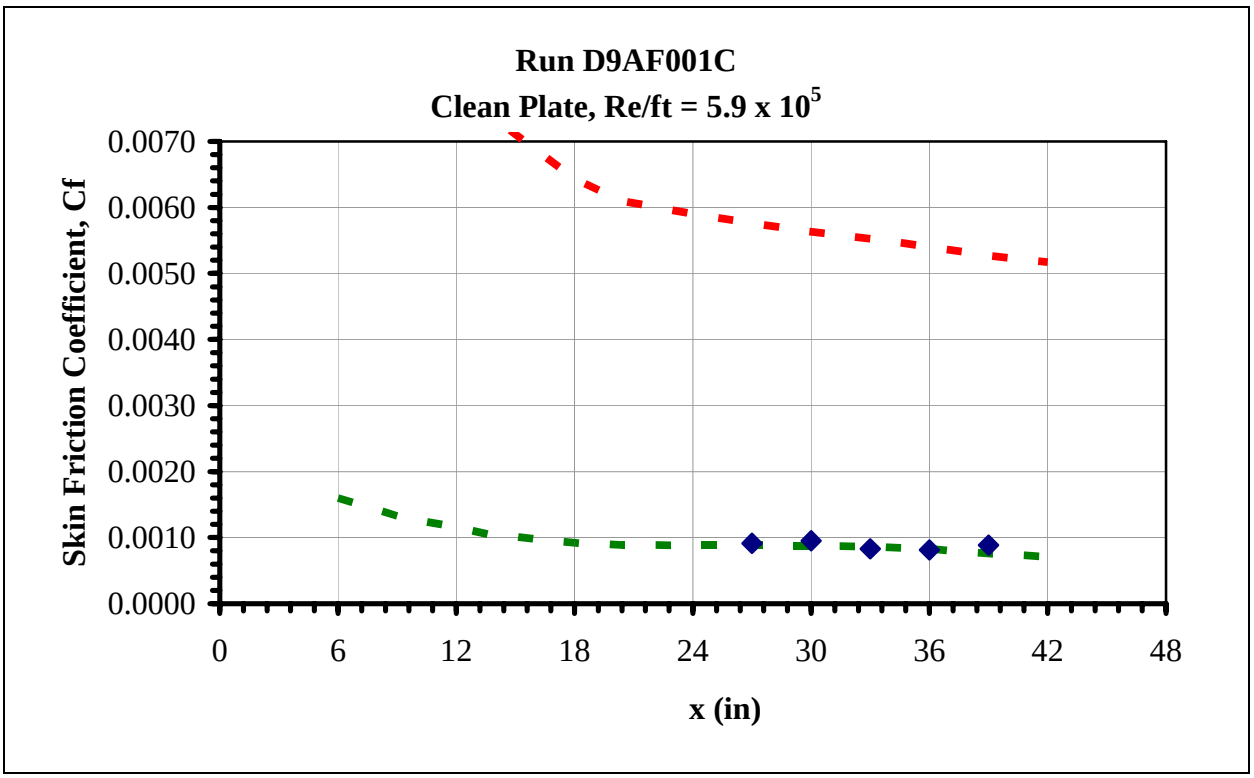

Figure 27. Clean plate skin friction distribution, run D9AF001C

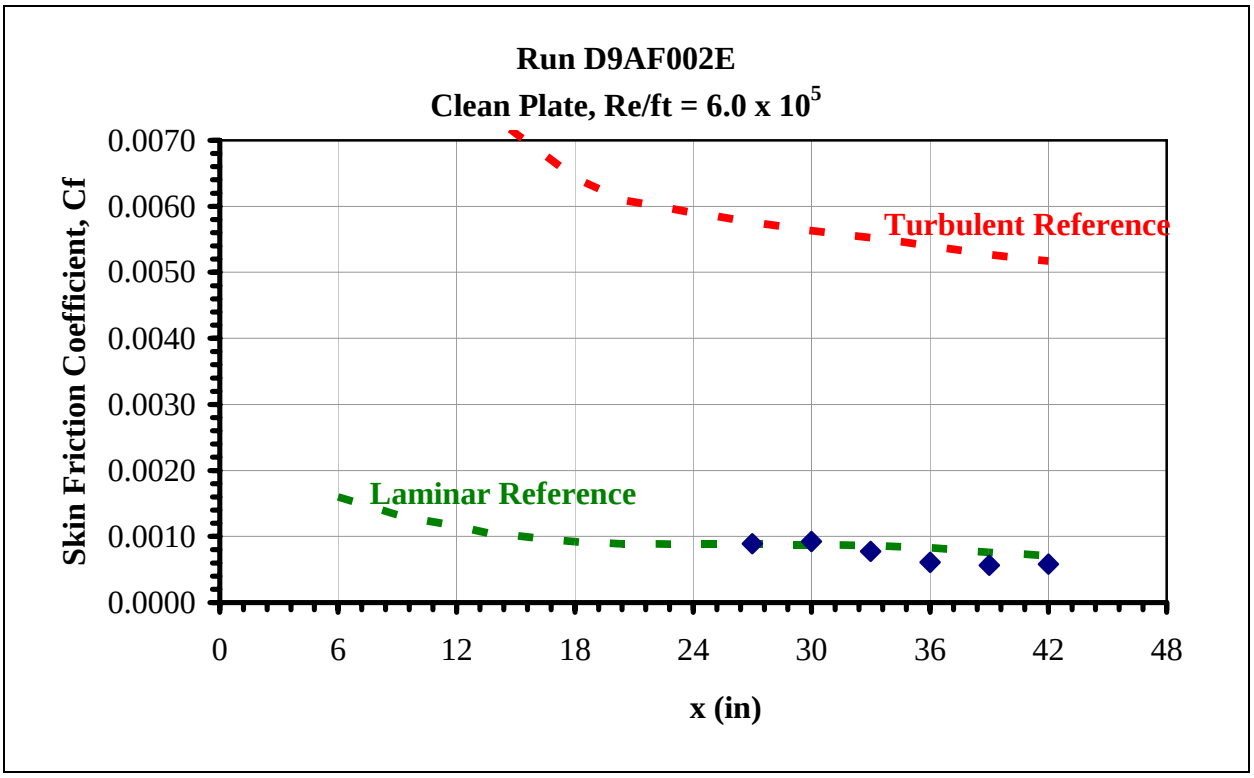

Figure 28. Clean plate skin friction distribution, run D9AF002E

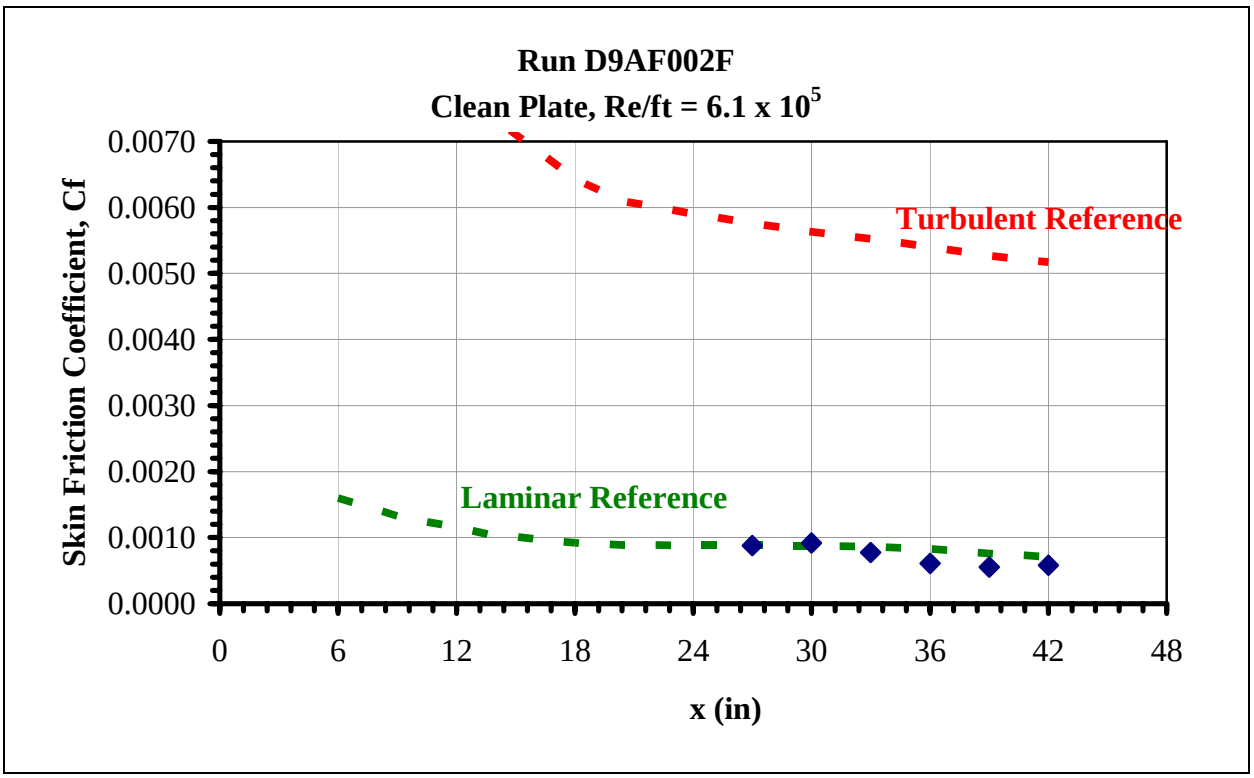

Figure 29. Clean plate skin friction distribution, run D9AF002F

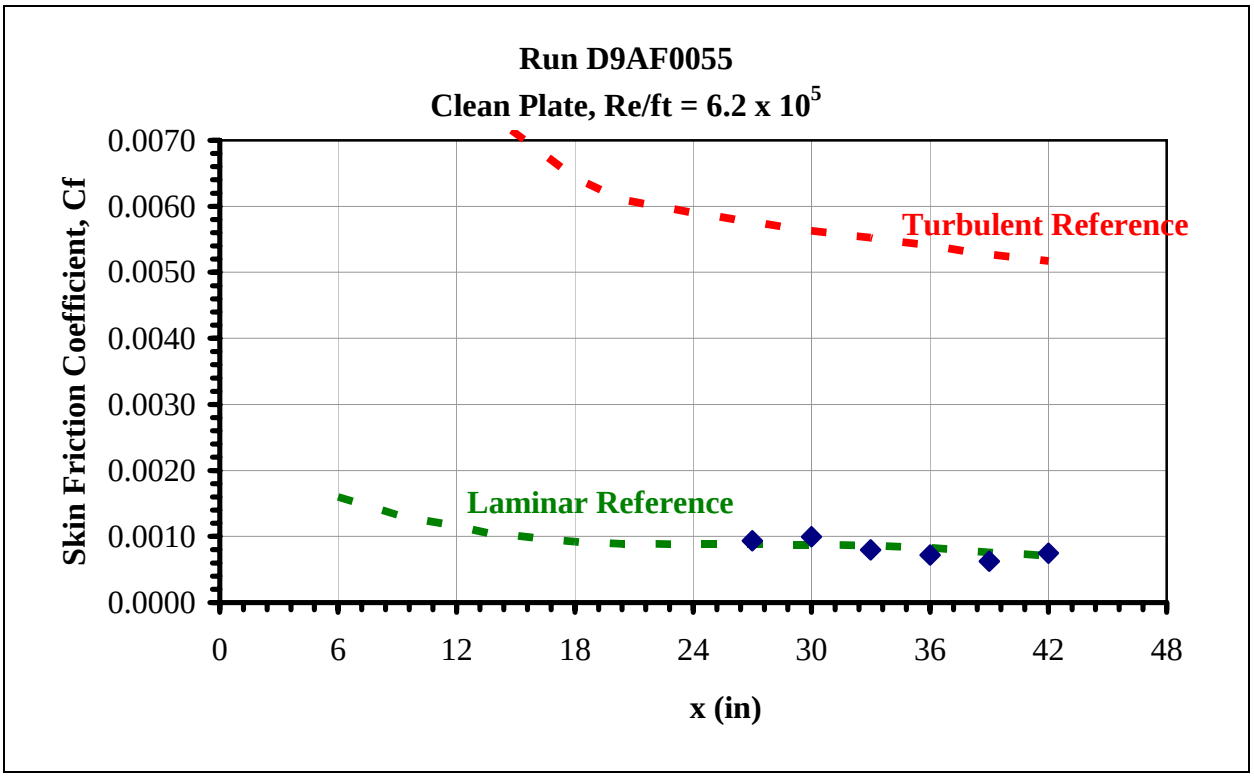

Figure 30. Clean plate skin friction distribution, run D9AF0055

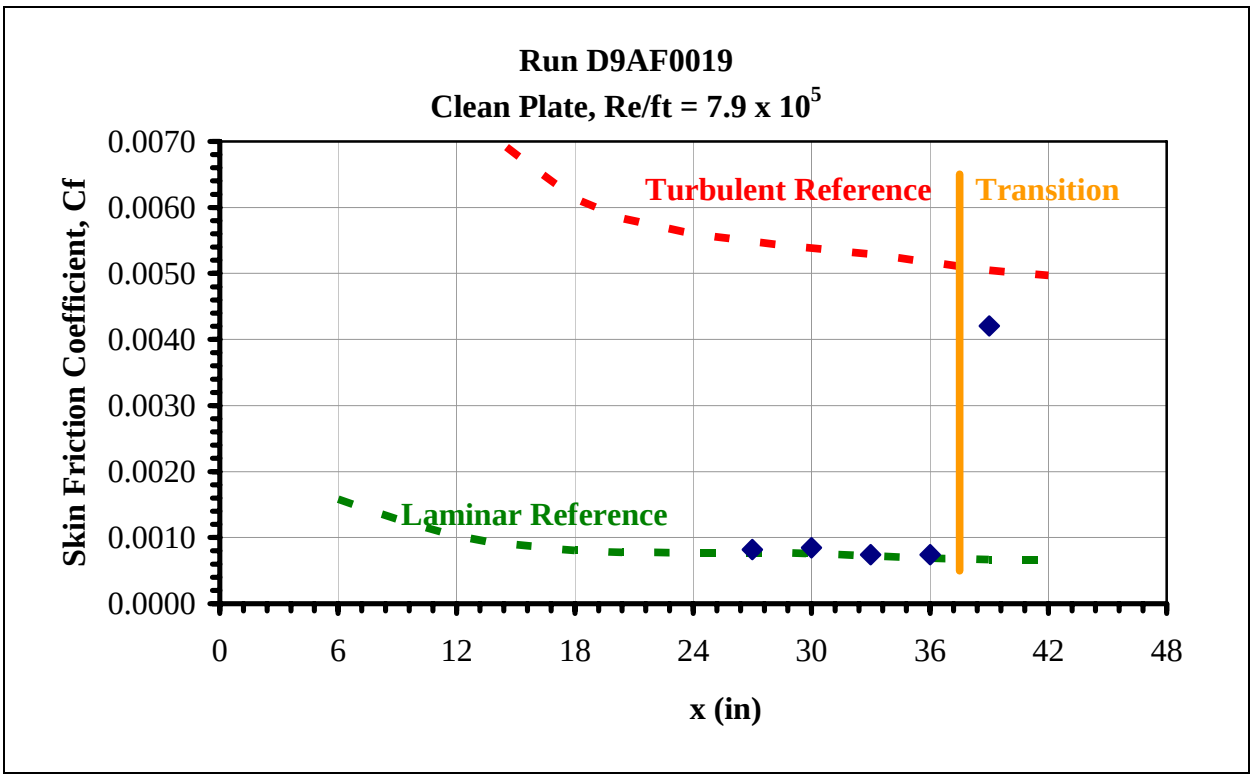

Figure 31. Clean plate skin friction distribution, run D9AF0019

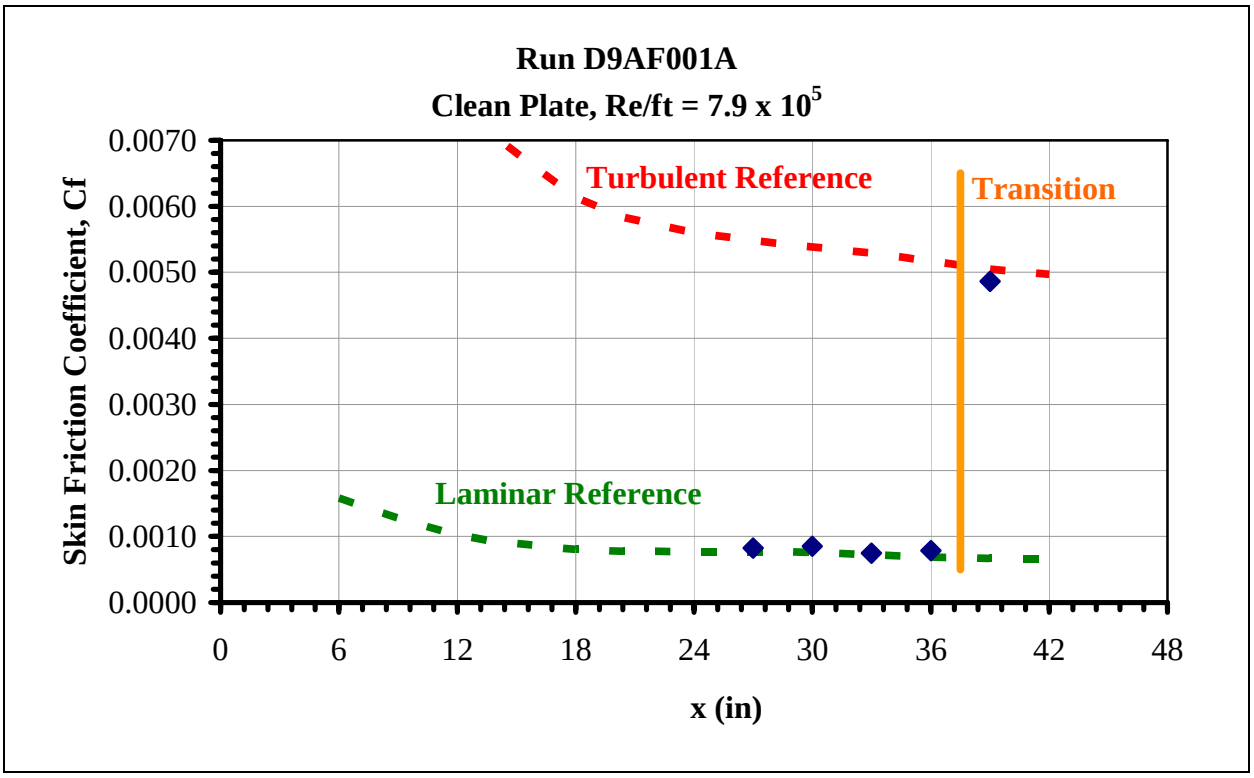

Figure 32. Clean plate skin friction distribution, run D9AF001A

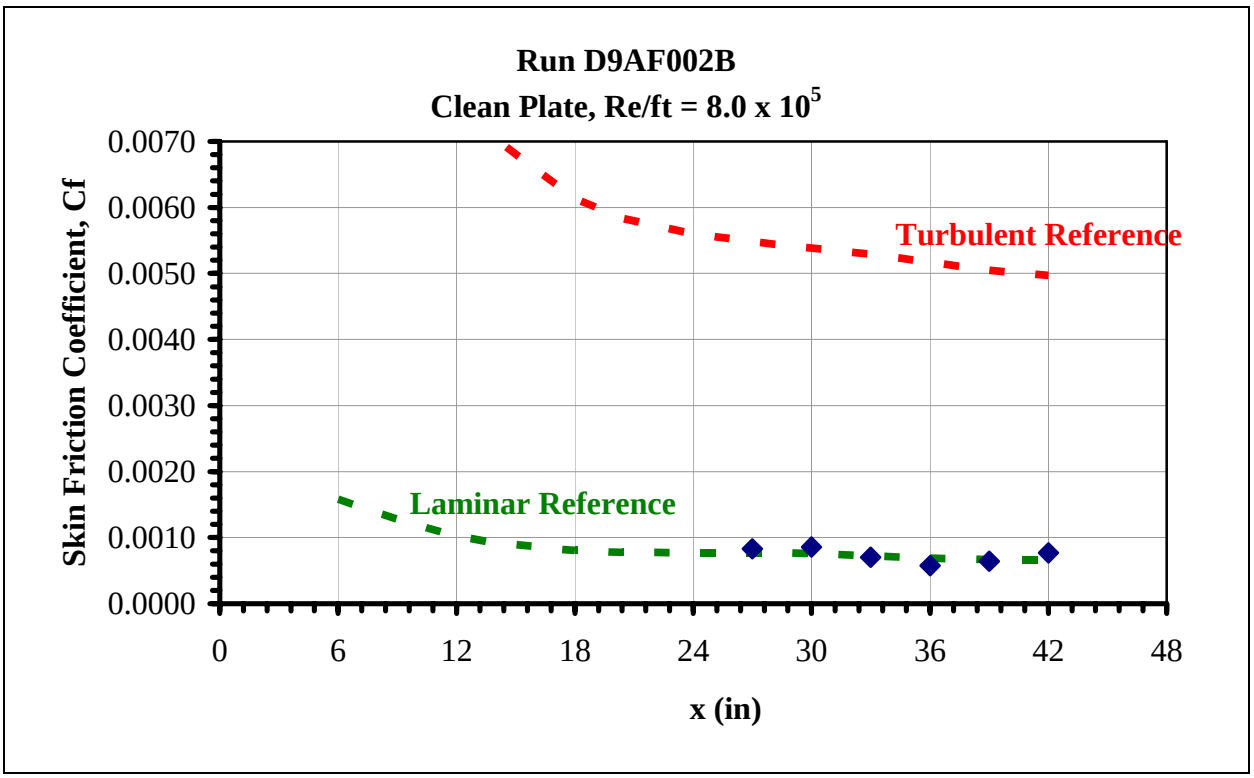

Figure 33. Clean plate skin friction distribution, run D9AF002B

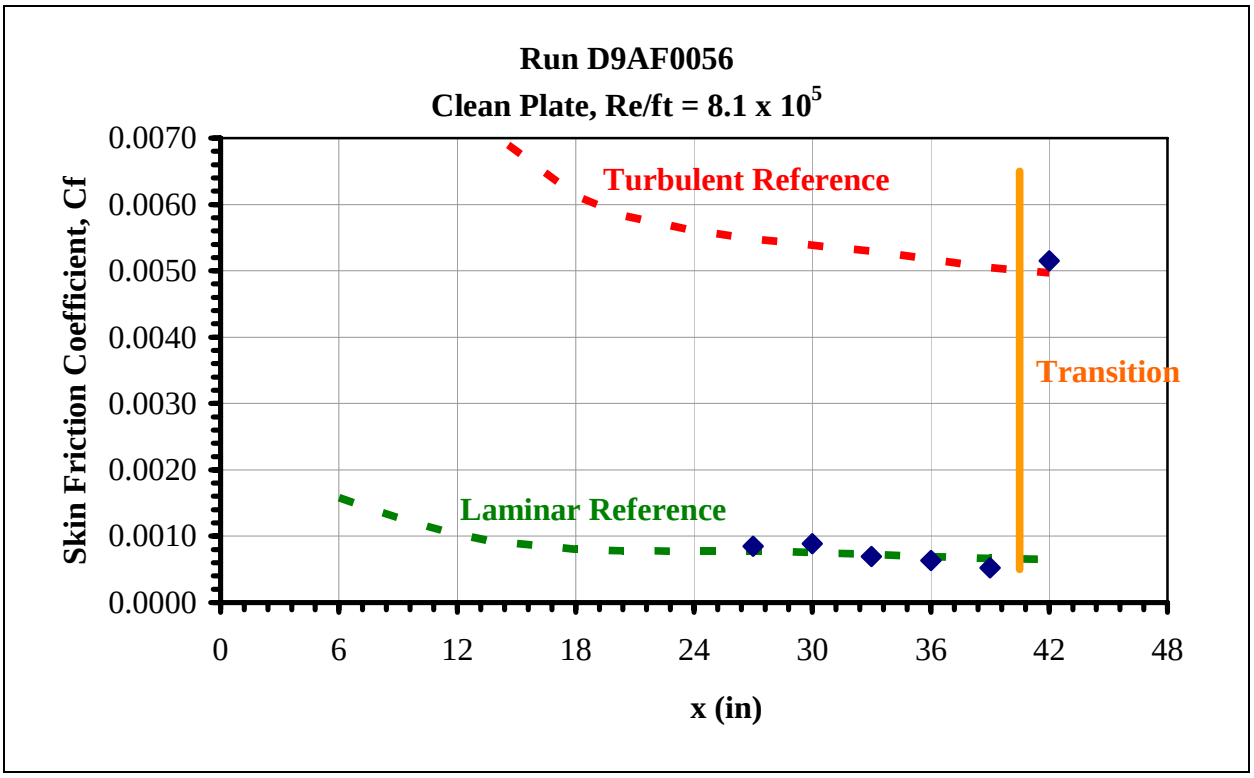

Figure 34. Clean plate skin friction distribution, run D9AF0056

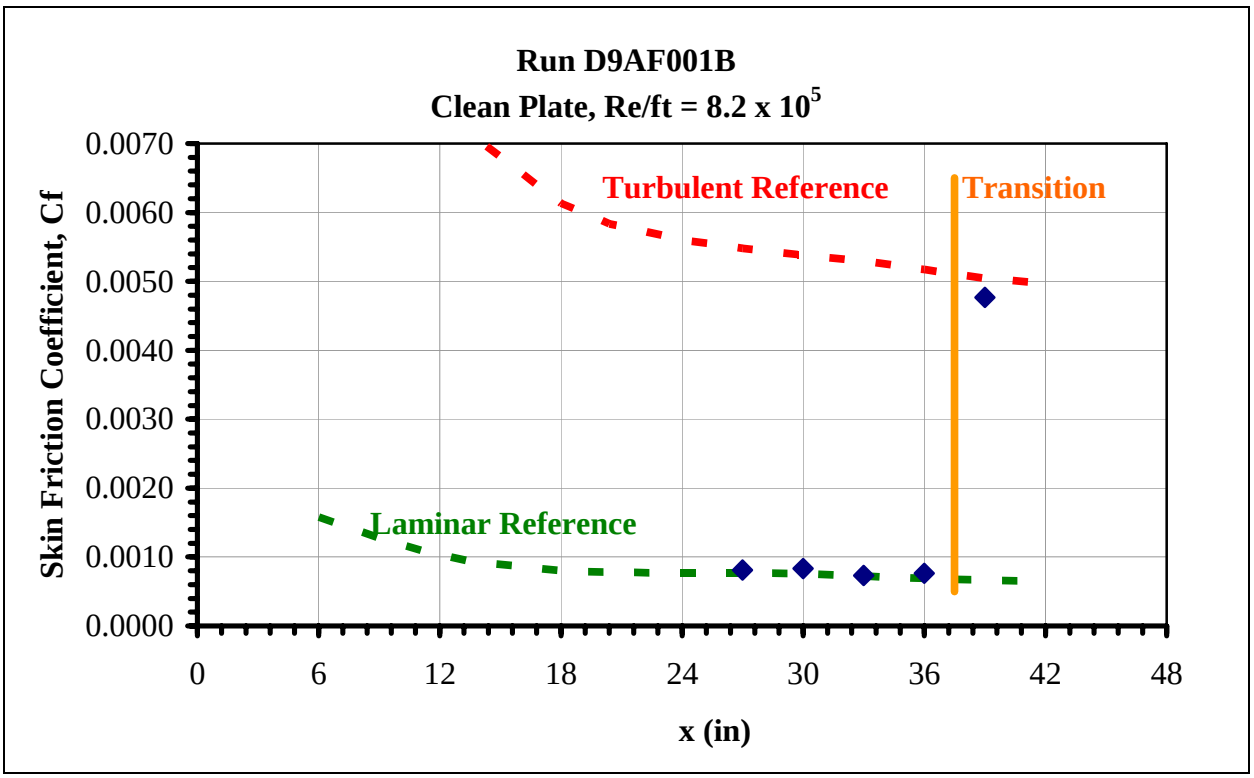

Figure 35. Clean plate skin friction distribution, run D9AF001B

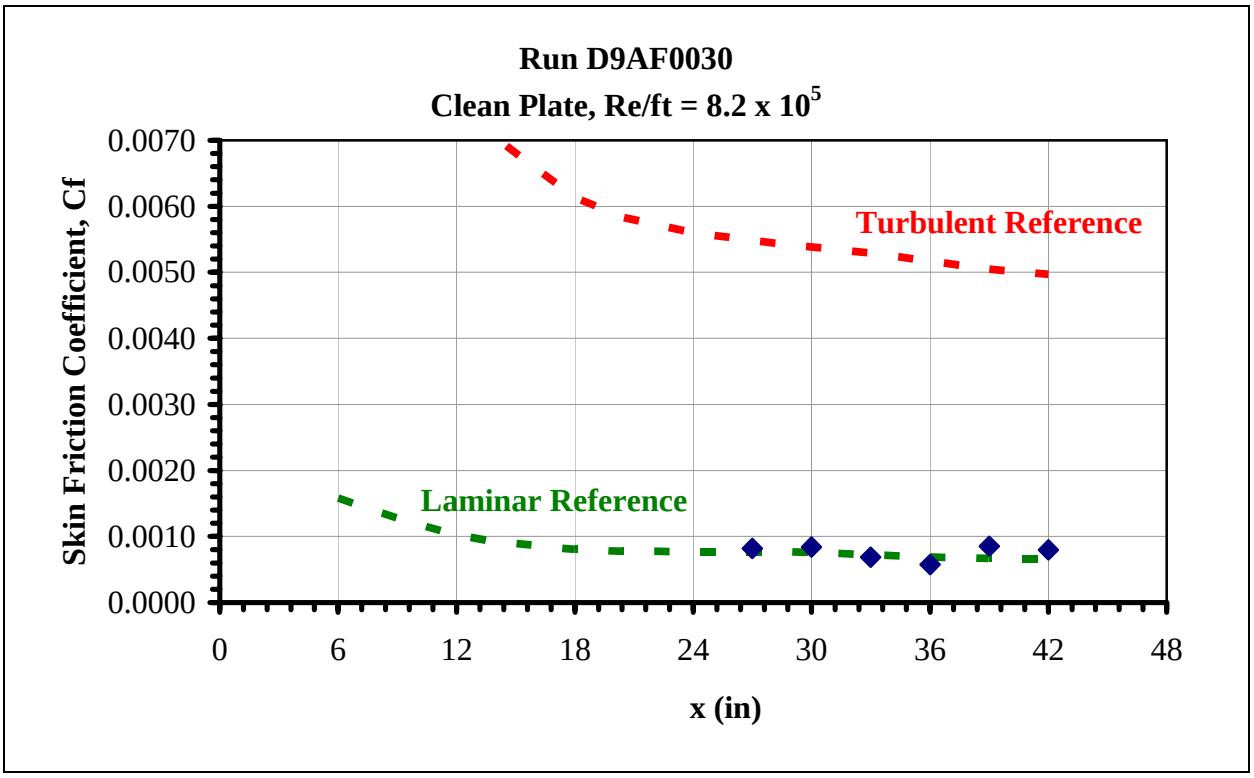

Figure 36. Clean plate skin friction distribution, run D9AF0030

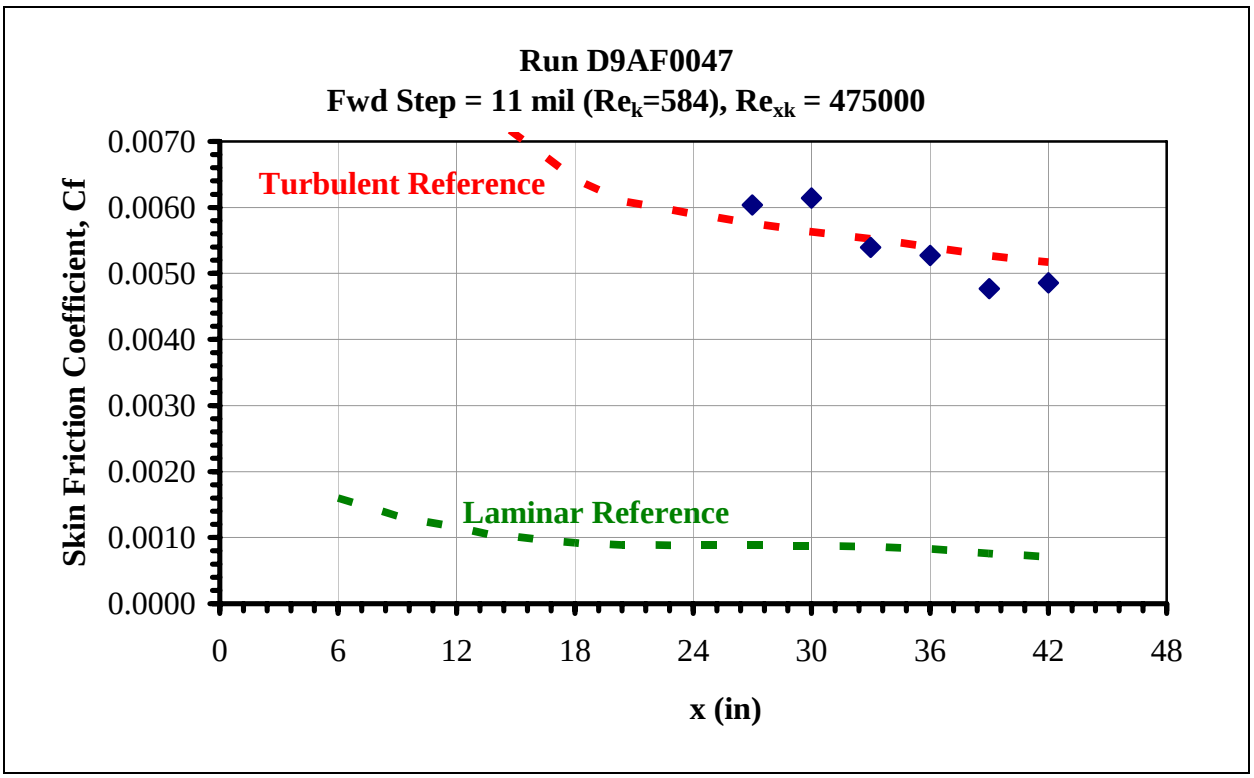

Figure 37. Forward step skin friction distribution, run D9AF0047

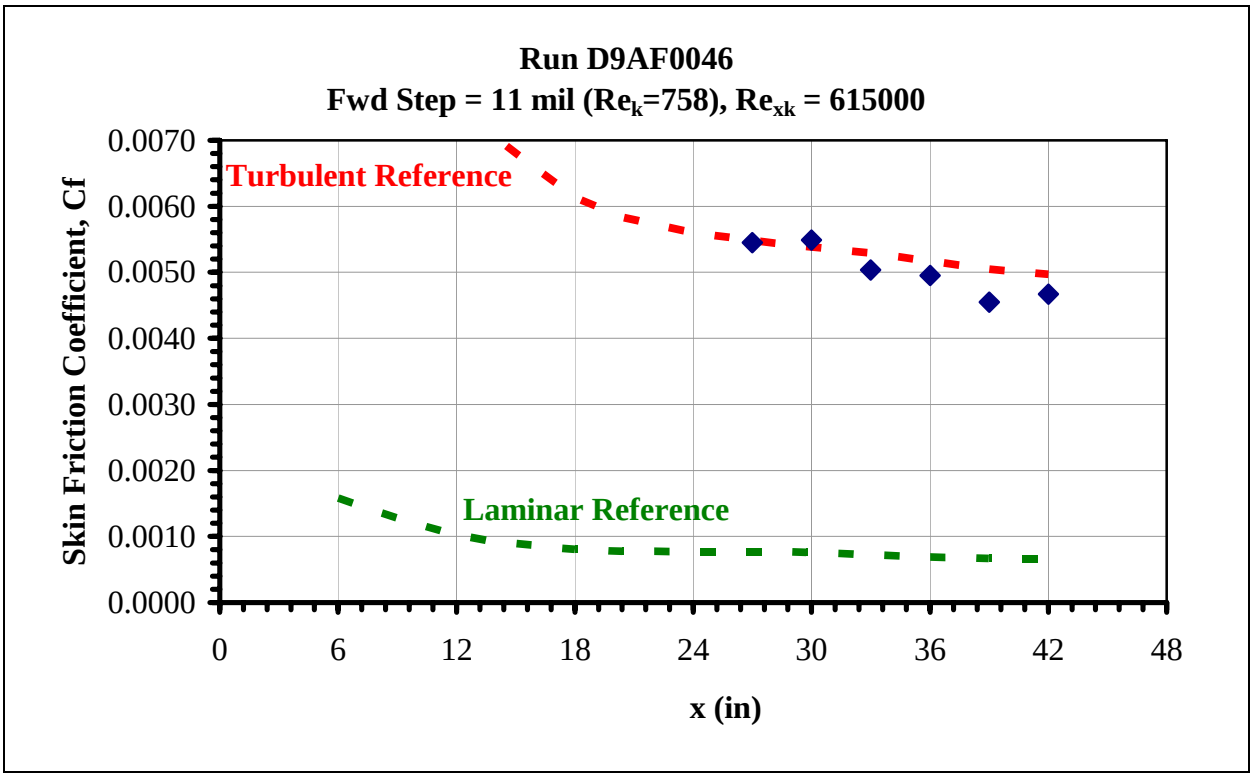

Figure 38. Forward step skin friction distribution, run D9AF0046

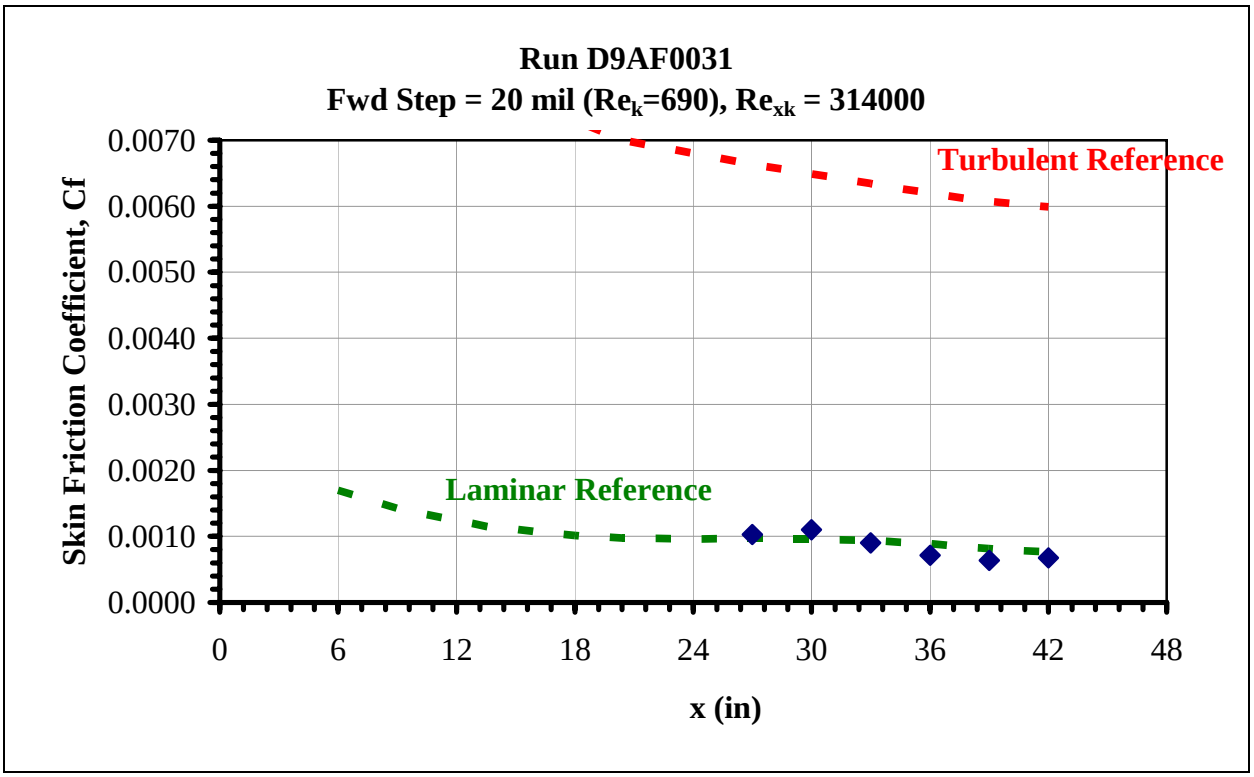

Figure 39. Forward step skin friction distribution, run D9AF0031

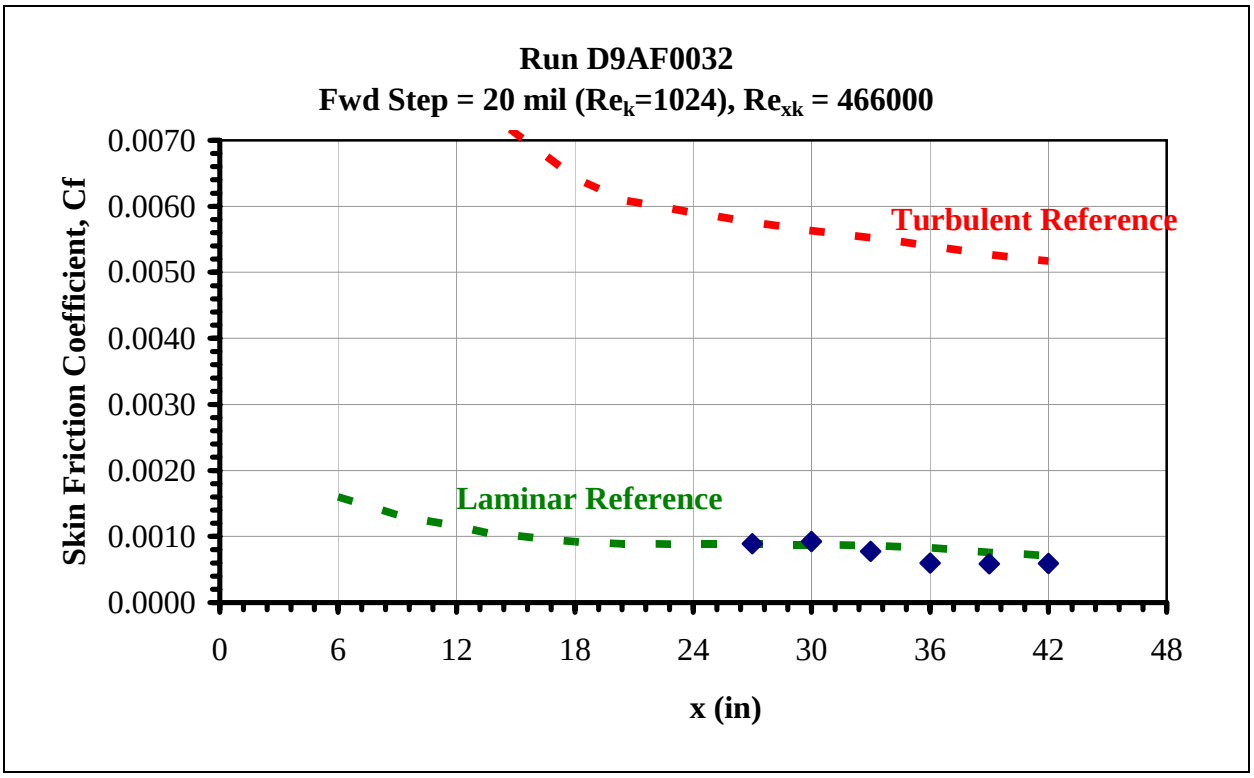

Figure 40. Forward step skin friction distribution, run D9AF0032

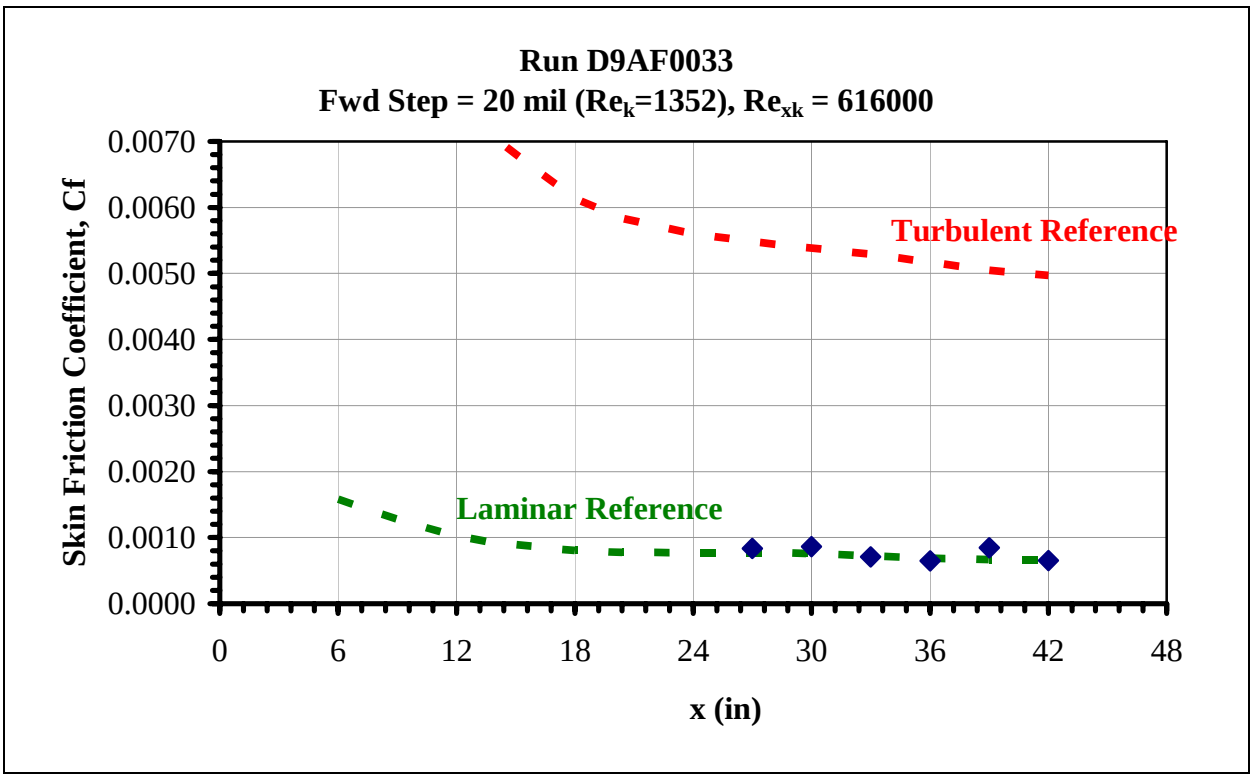

Figure 41. Forward step skin friction distribution, run D9AF0033

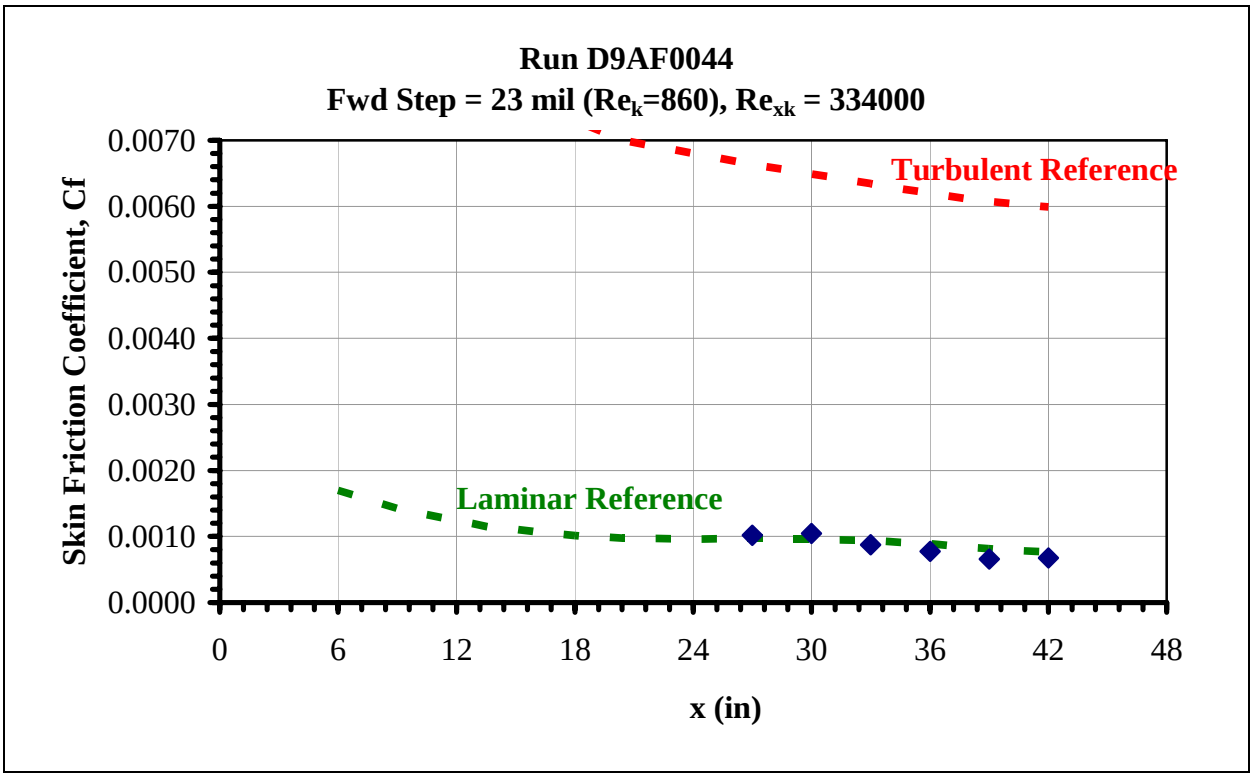

Figure 42. Forward step skin friction distribution, run D9AF0044

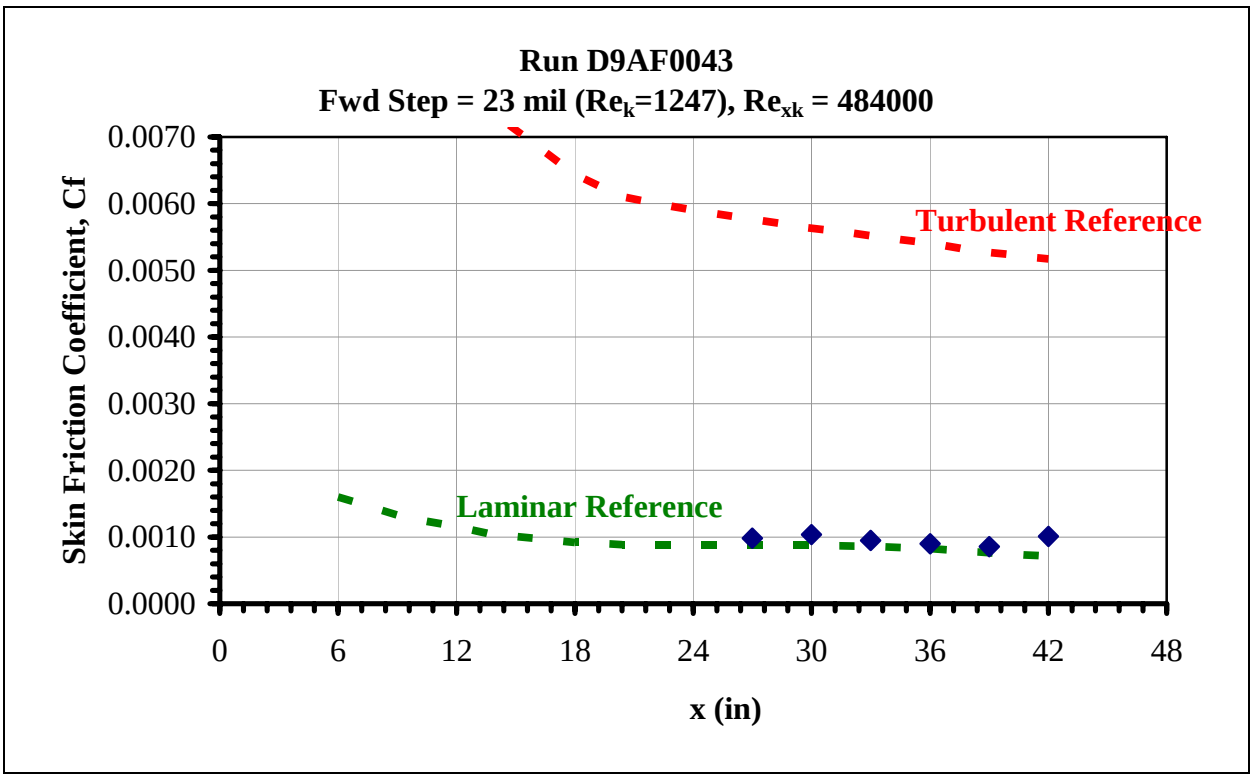

Figure 43. Forward step skin friction distribution, run D9AF0043

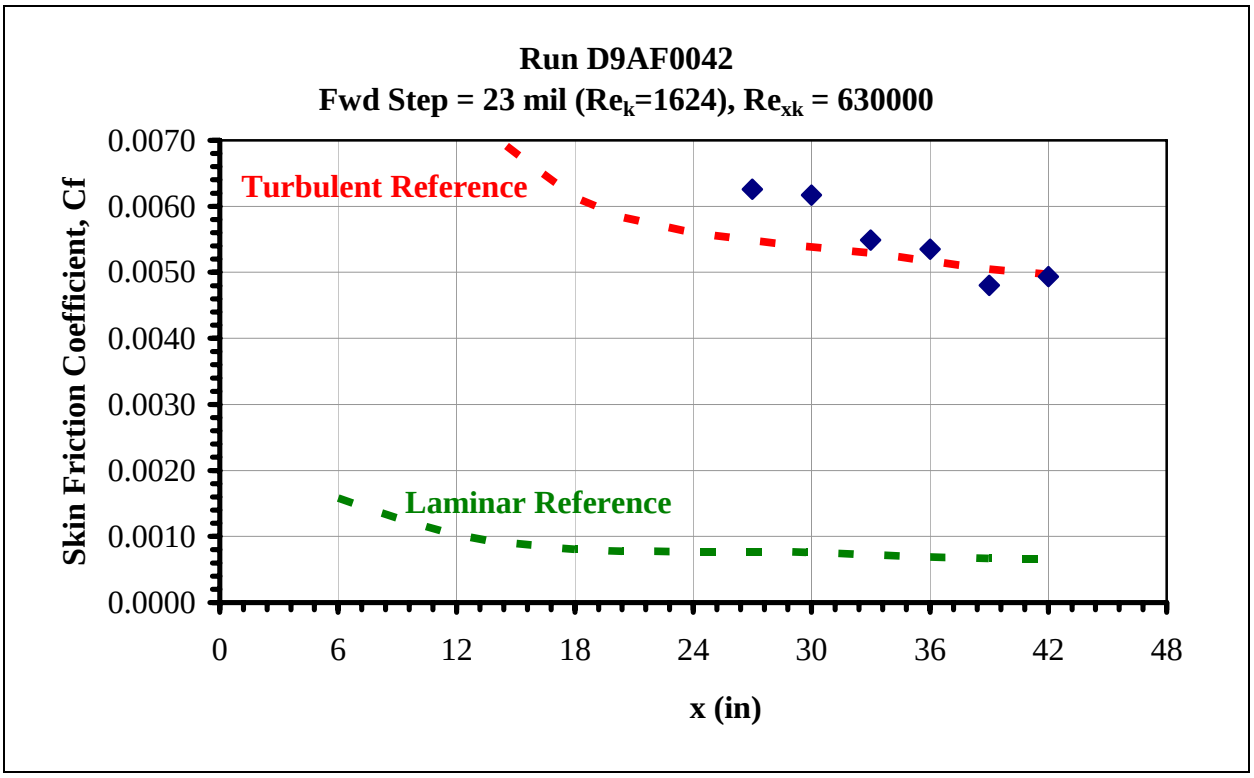

Figure 44. Forward step skin friction distribution, run D9AF0042

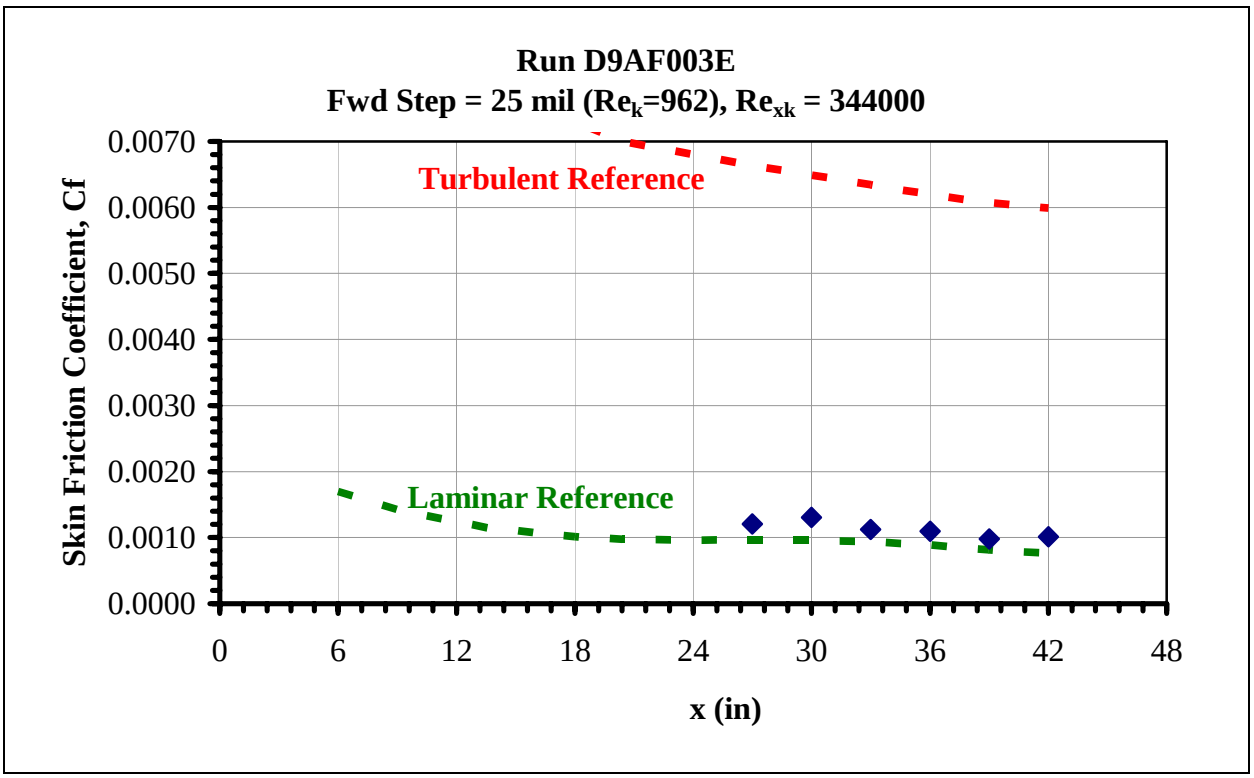

Figure 45. Forward step skin friction distribution, run D9AF003E

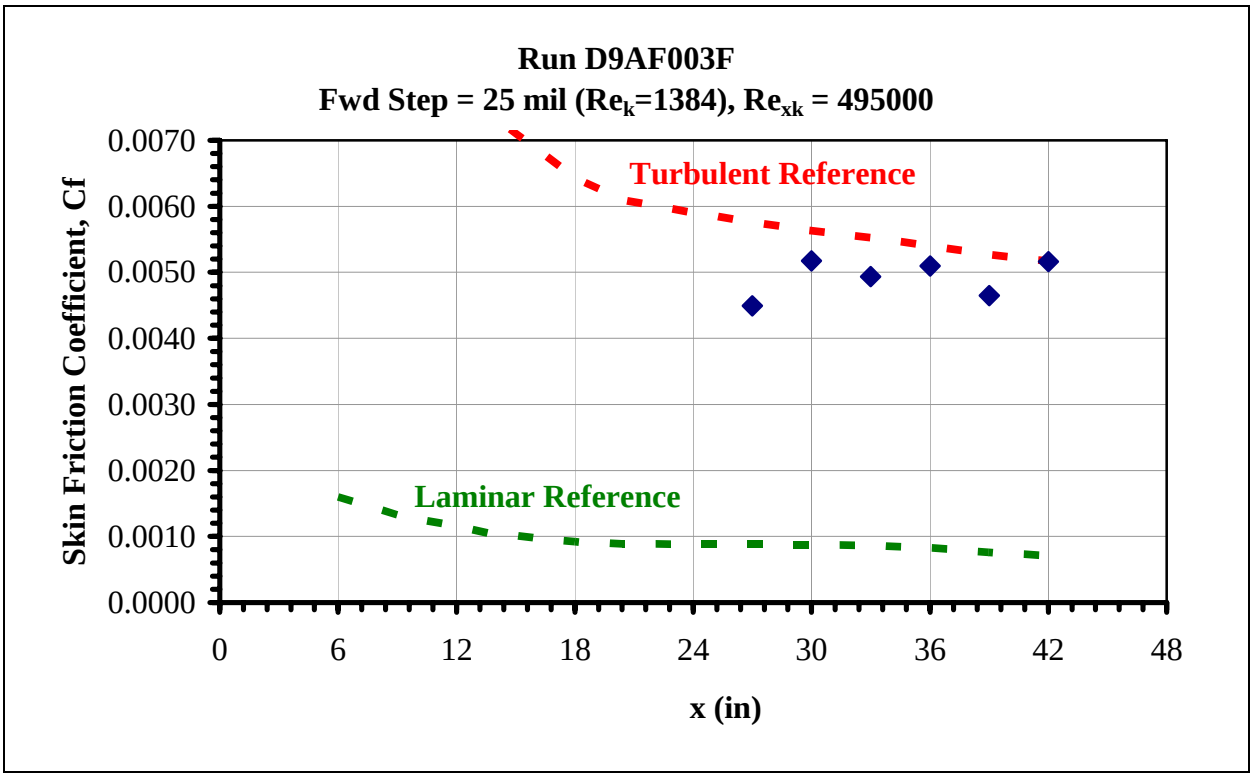

Figure 46. Forward step skin friction distribution, run D9AF003F

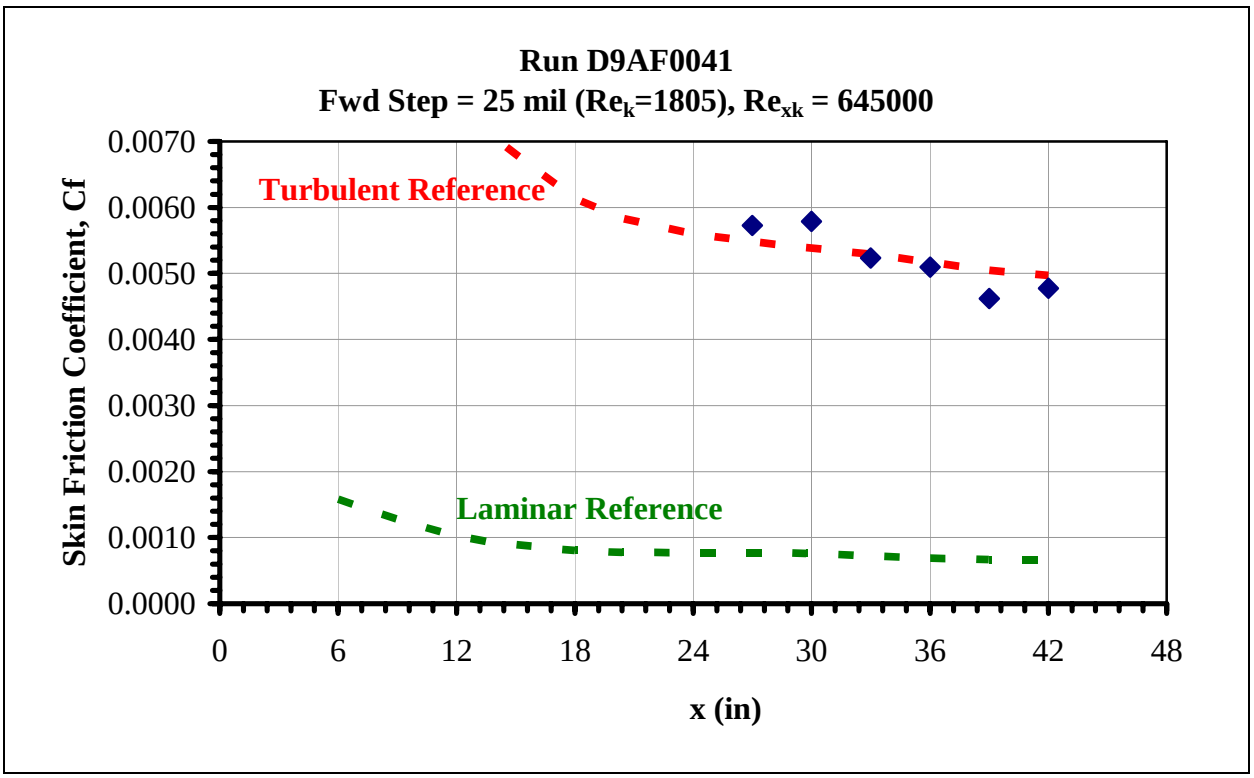

Figure 47. Forward step skin friction distribution, run D9AF0041

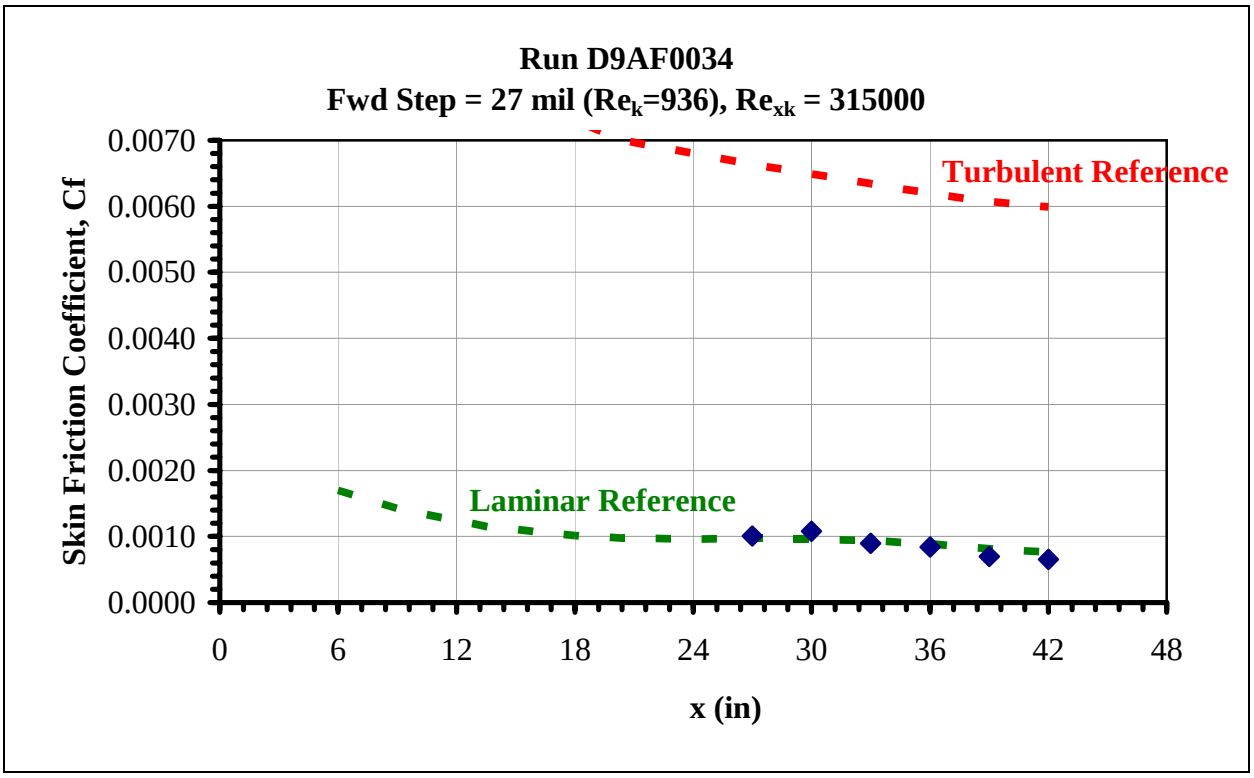

Figure 48. Forward step skin friction distribution, run D9AF0034

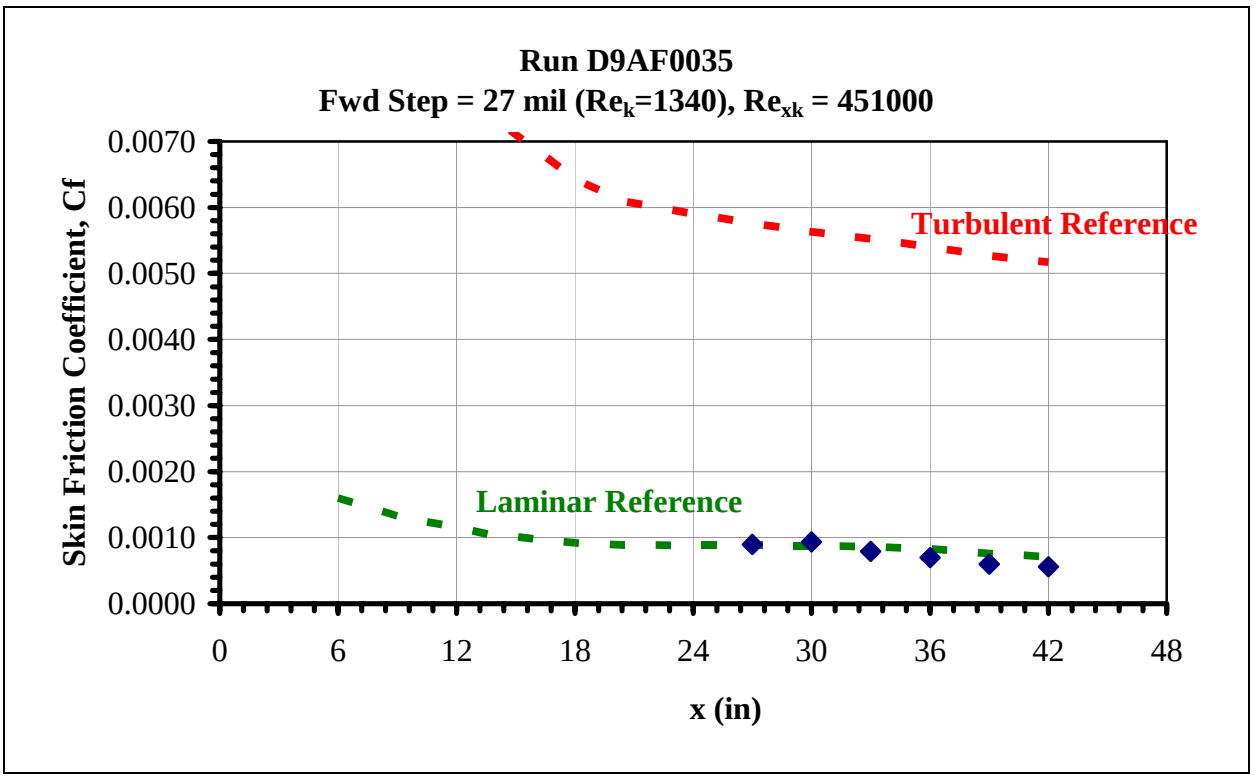

Figure 49. Forward step skin friction distribution, run D9AF0035

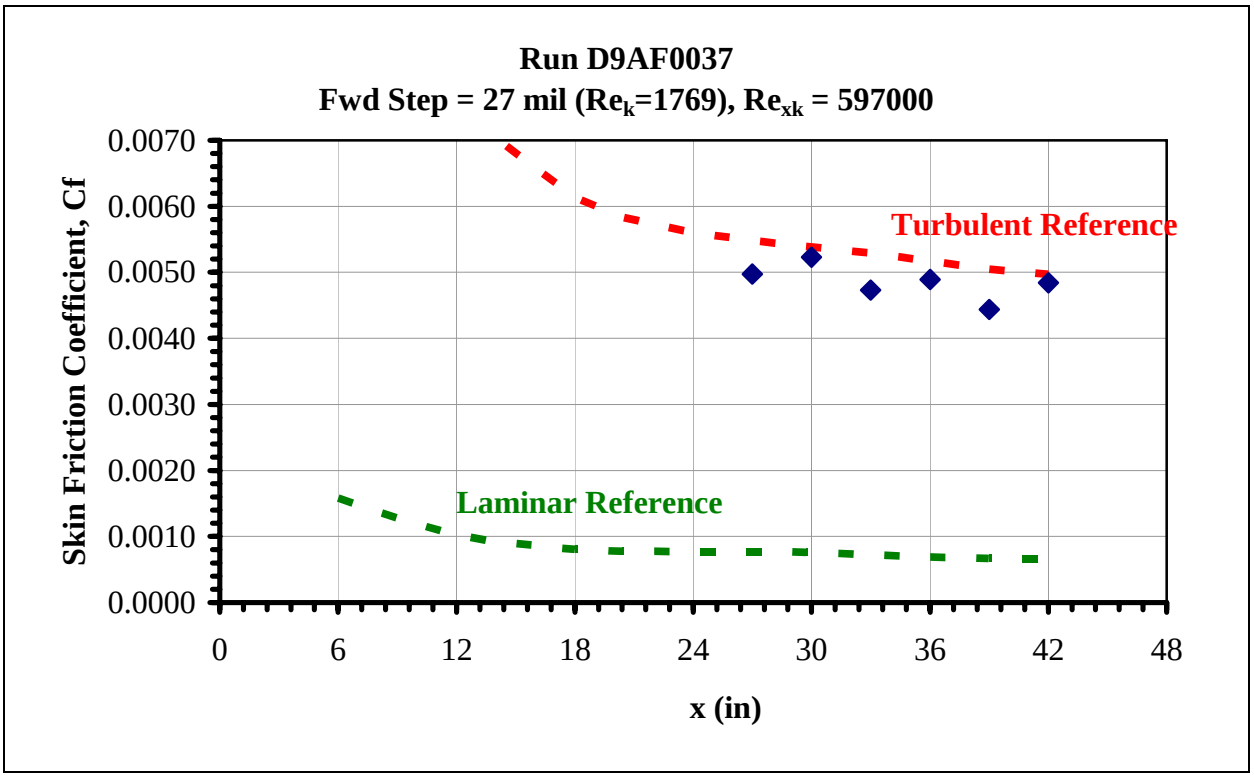

Figure 50. Forward step skin friction distribution, run D9AF0037

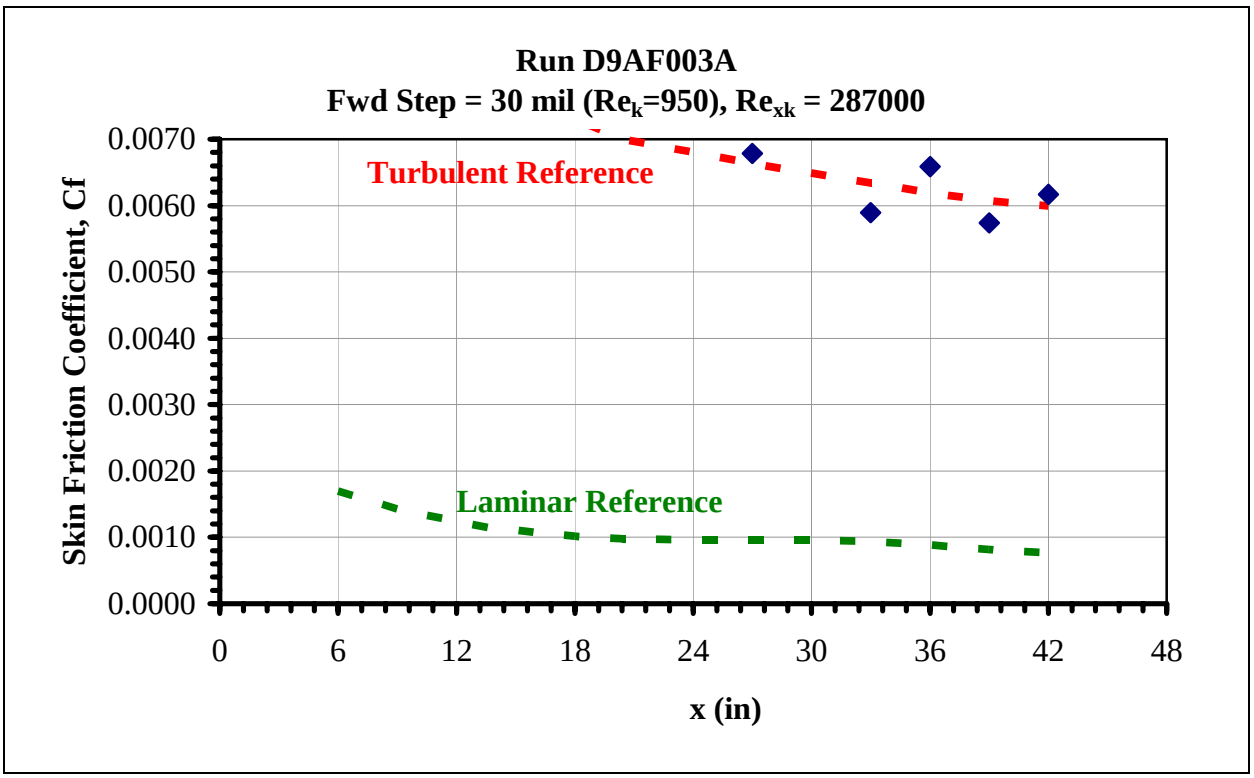

Figure 51. Forward step skin friction distribution, run D9AF003A

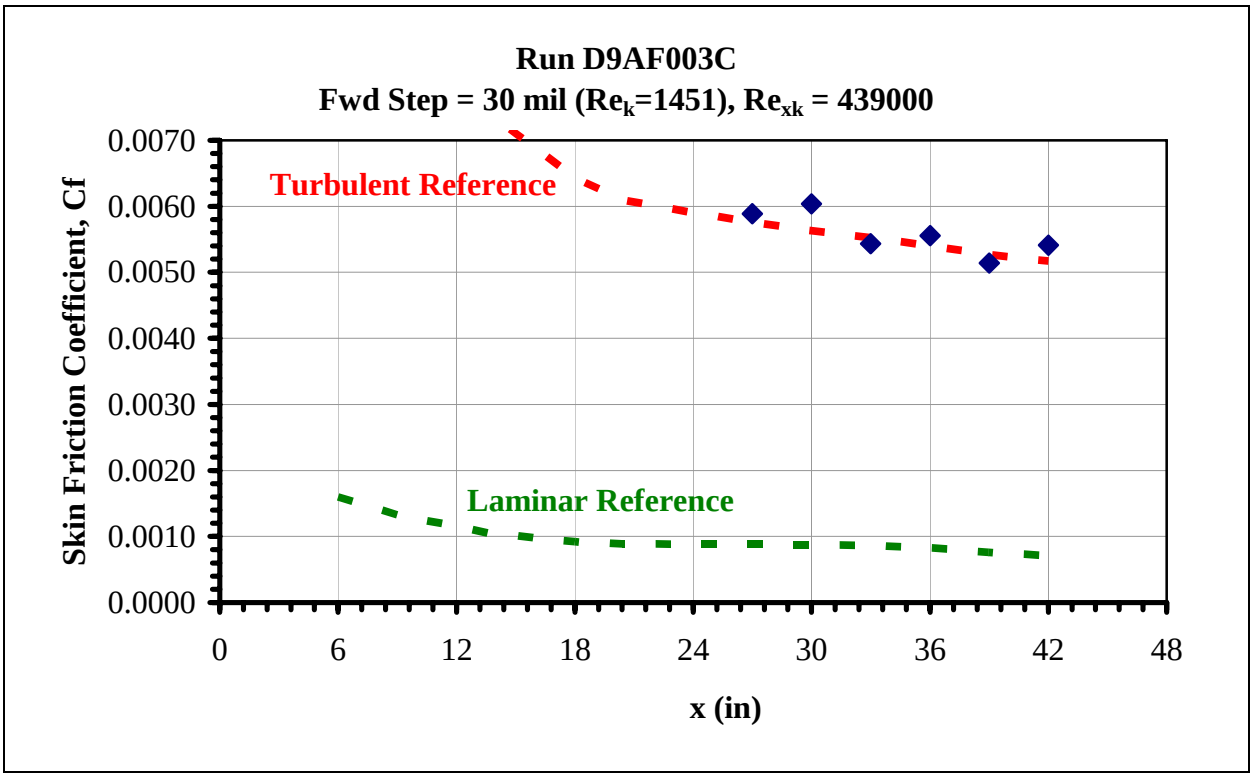

Figure 52. Forward step skin friction distribution, run D9AF003C

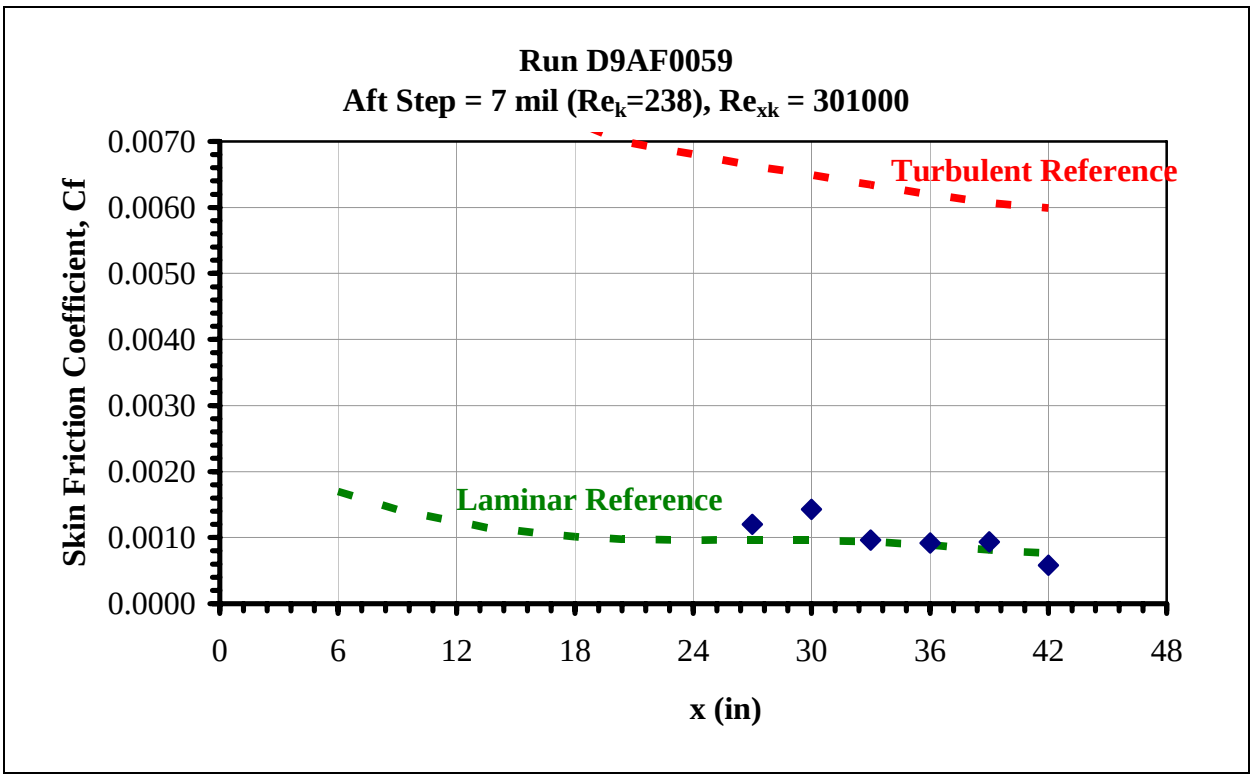

Figure 53. Aft step skin friction distribution, run D9AF0059

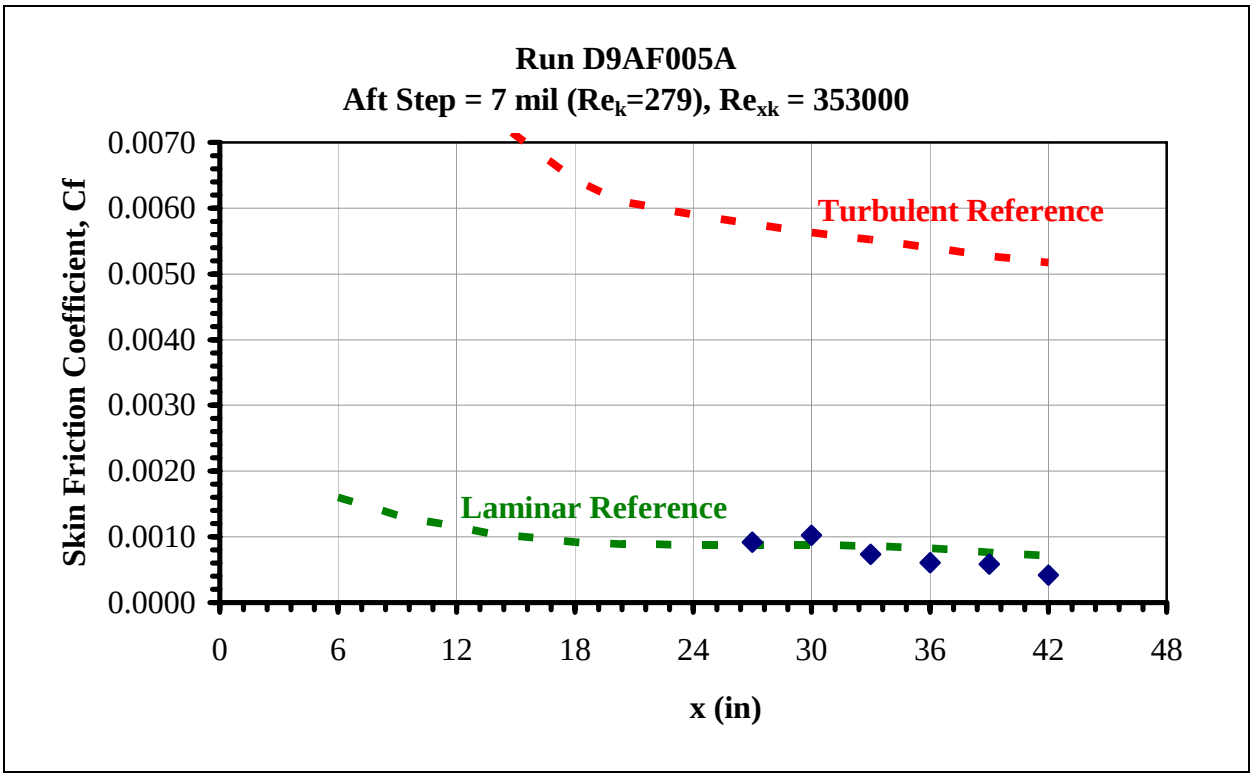

Figure 54. Aft step skin friction distribution, run D9AF005A

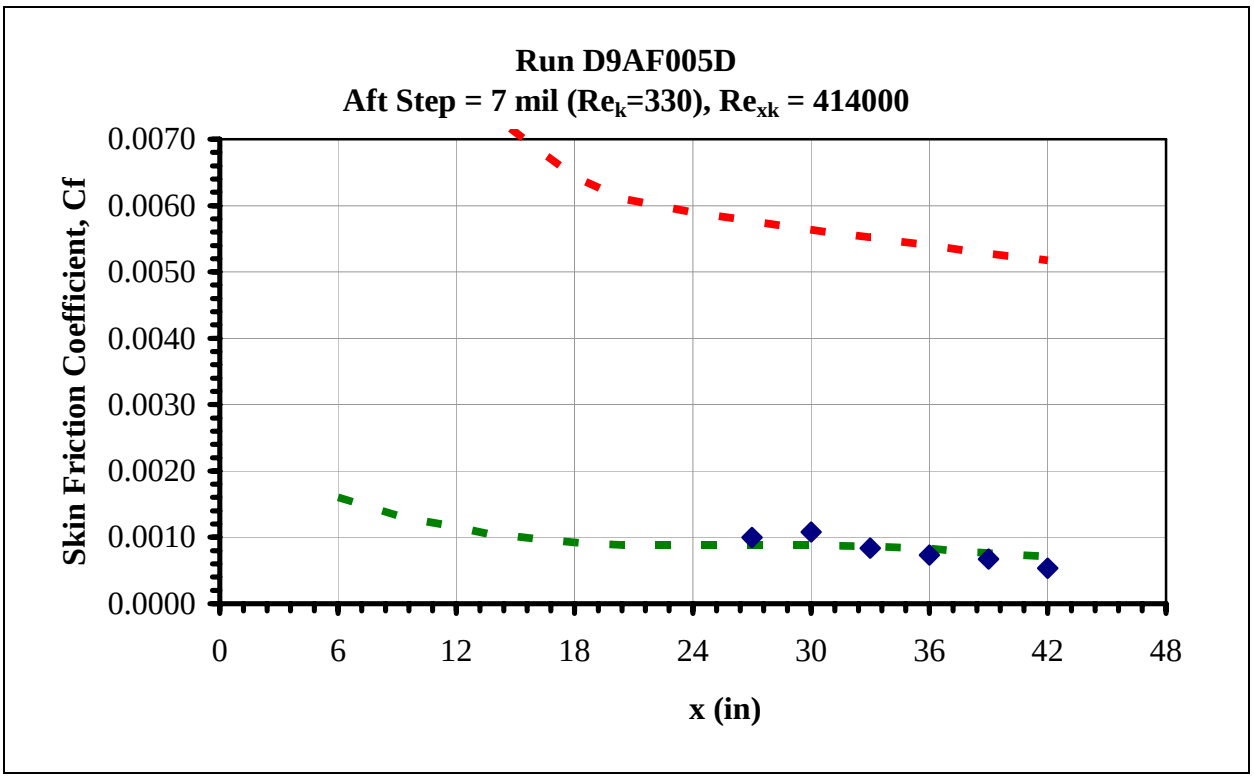

Figure 55. Aft step skin friction distribution, run D9AF005D

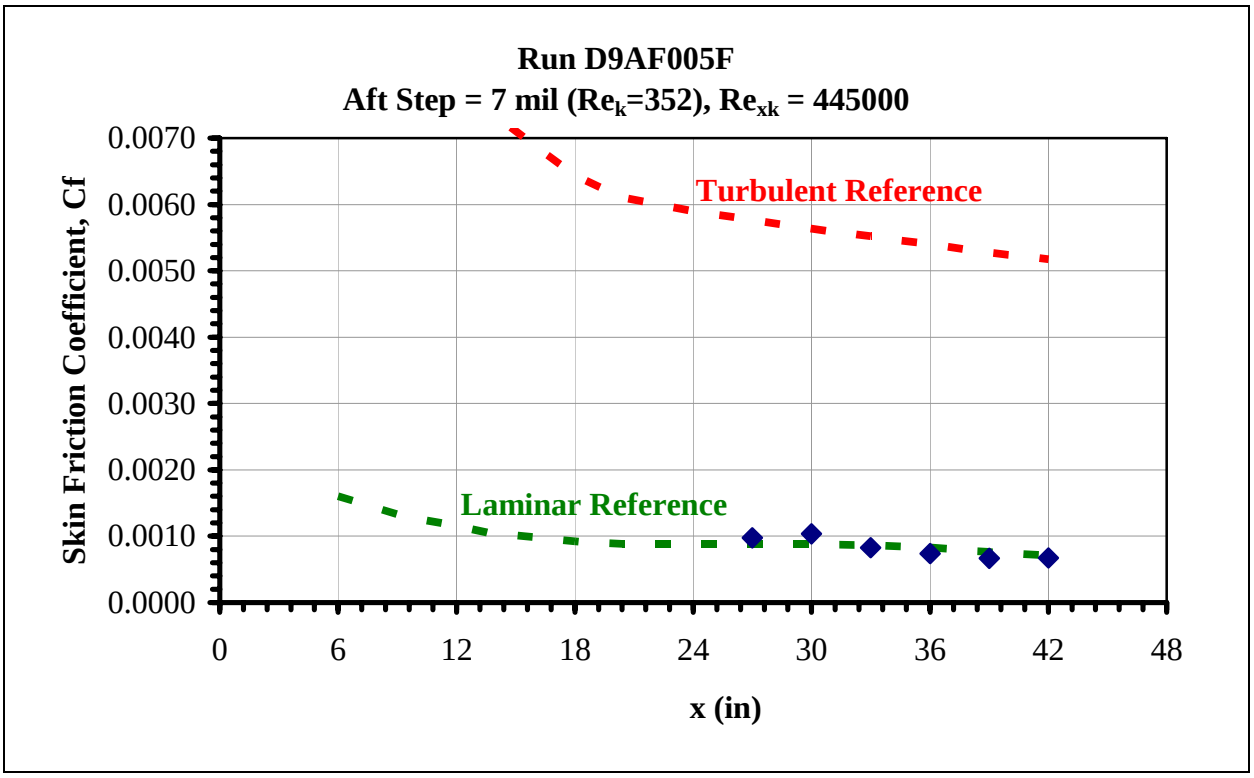

Figure 56. Aft step skin friction distribution, run D9AF005F

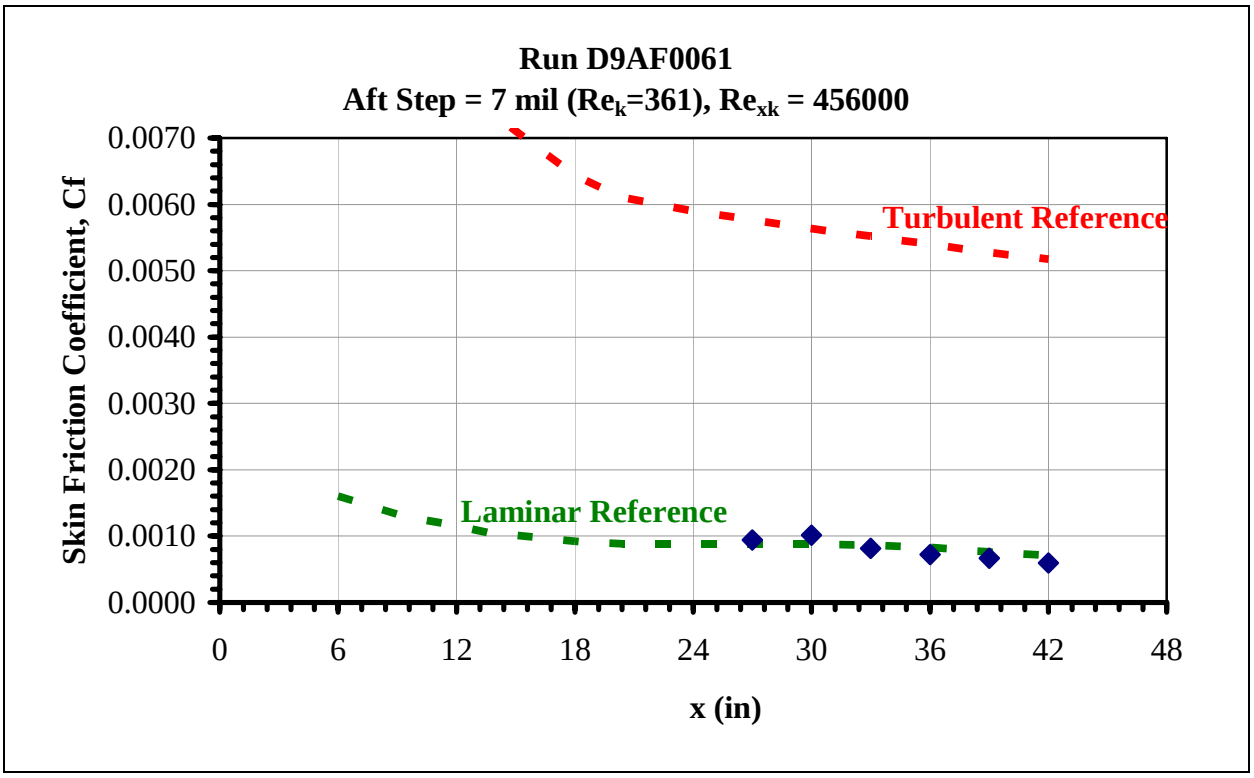

Figure 57. Aft step skin friction distribution, run D9AF0061

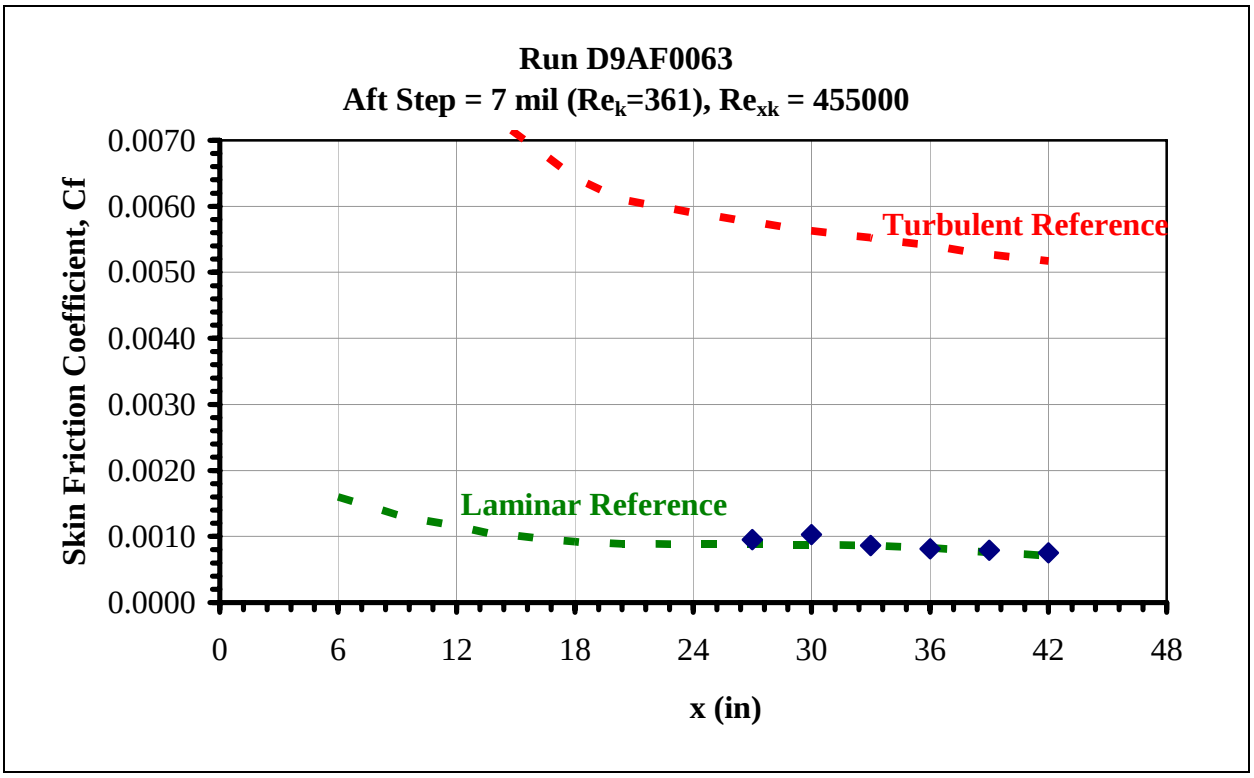

Figure 58. Aft step skin friction distribution, run D9AF0063

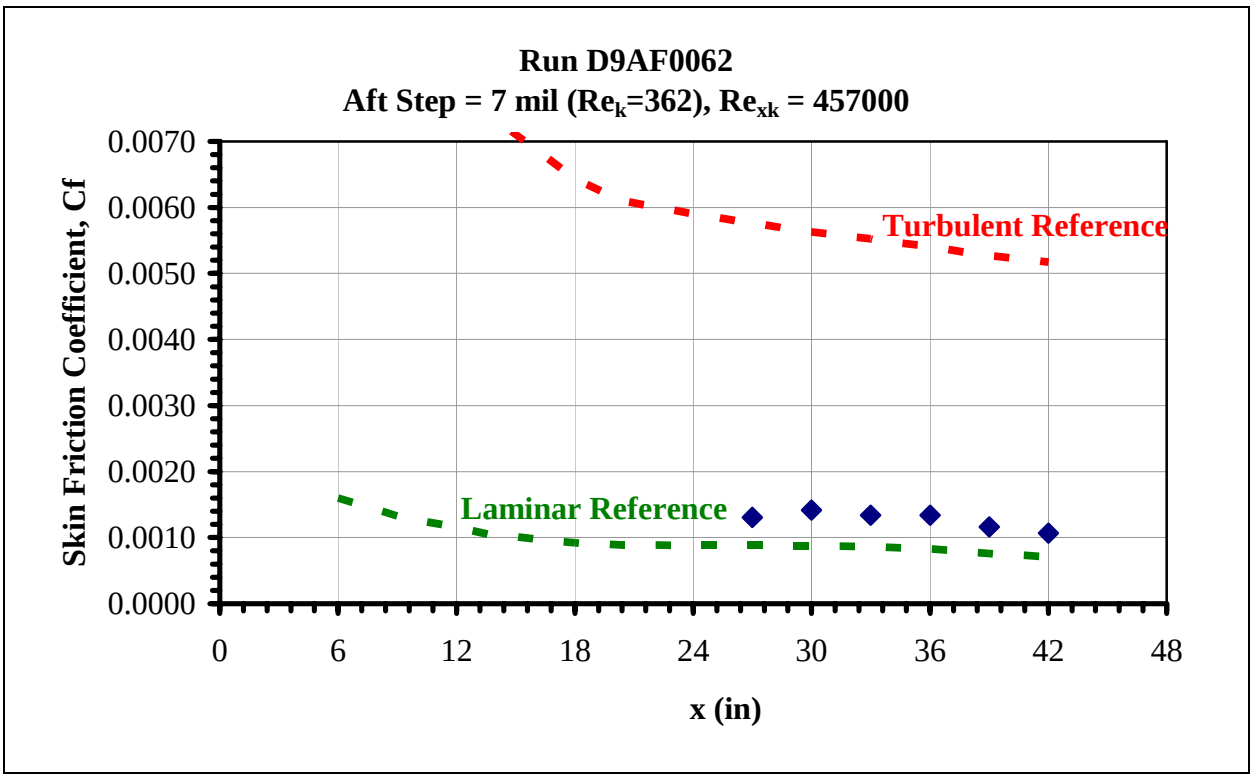

Figure 59. Aft step skin friction distribution, run D9AF0062

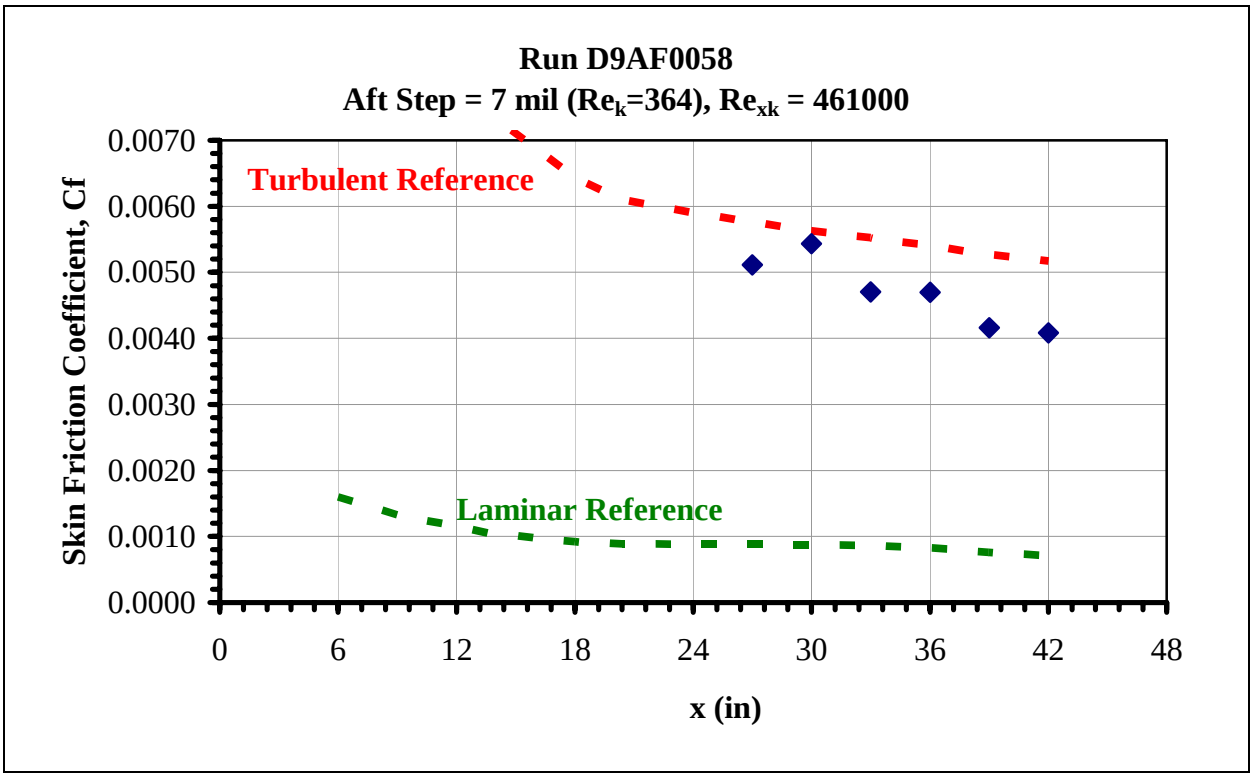

Figure 60. Aft step skin friction distribution, run D9AF0058

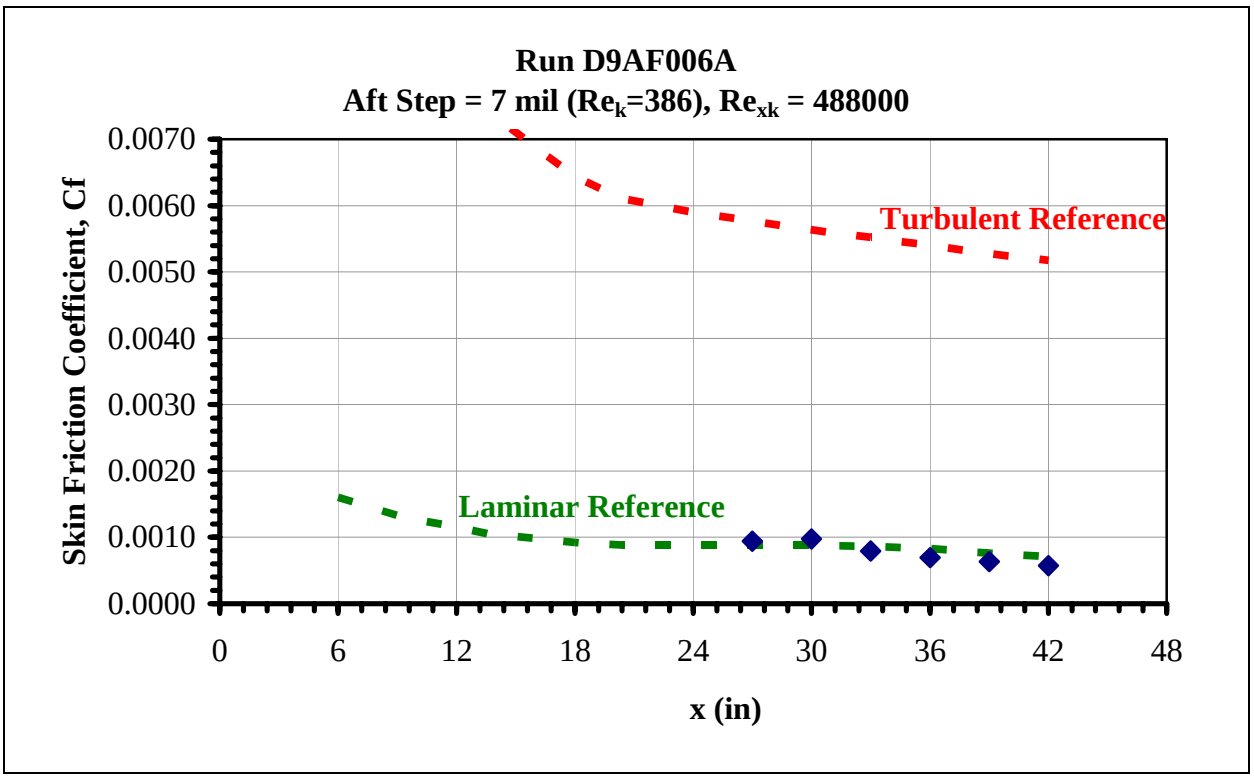

Figure 61. Aft step skin friction distribution, run D9AF006A

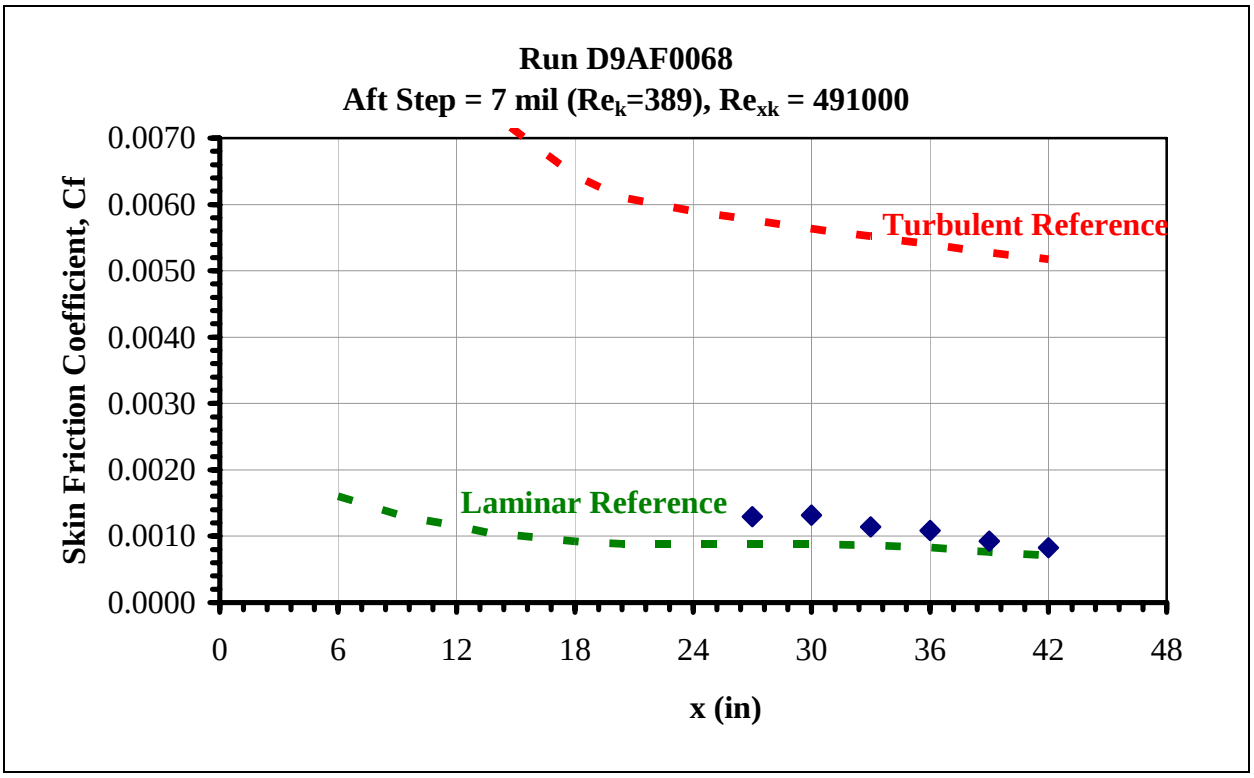

Figure 62. Aft step skin friction distribution, run D9AF0068

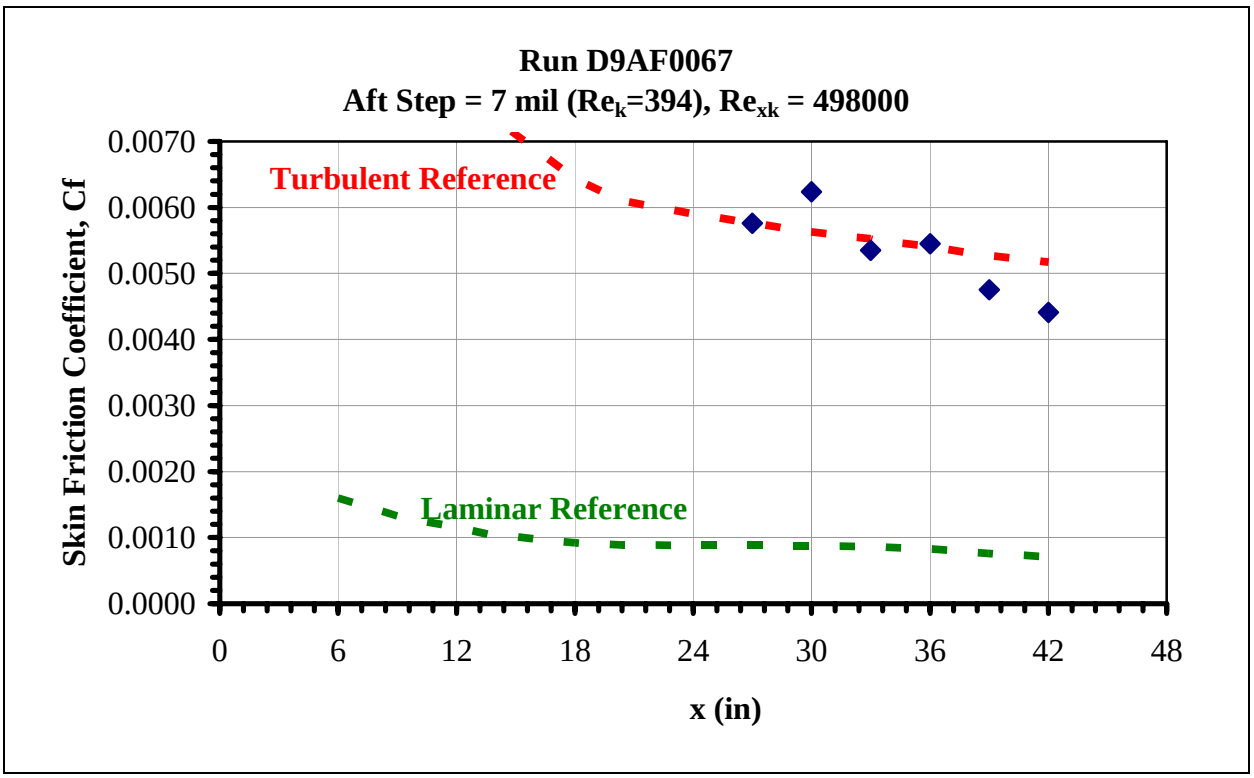

Figure 63. Aft step skin friction distribution, run D9AF0067

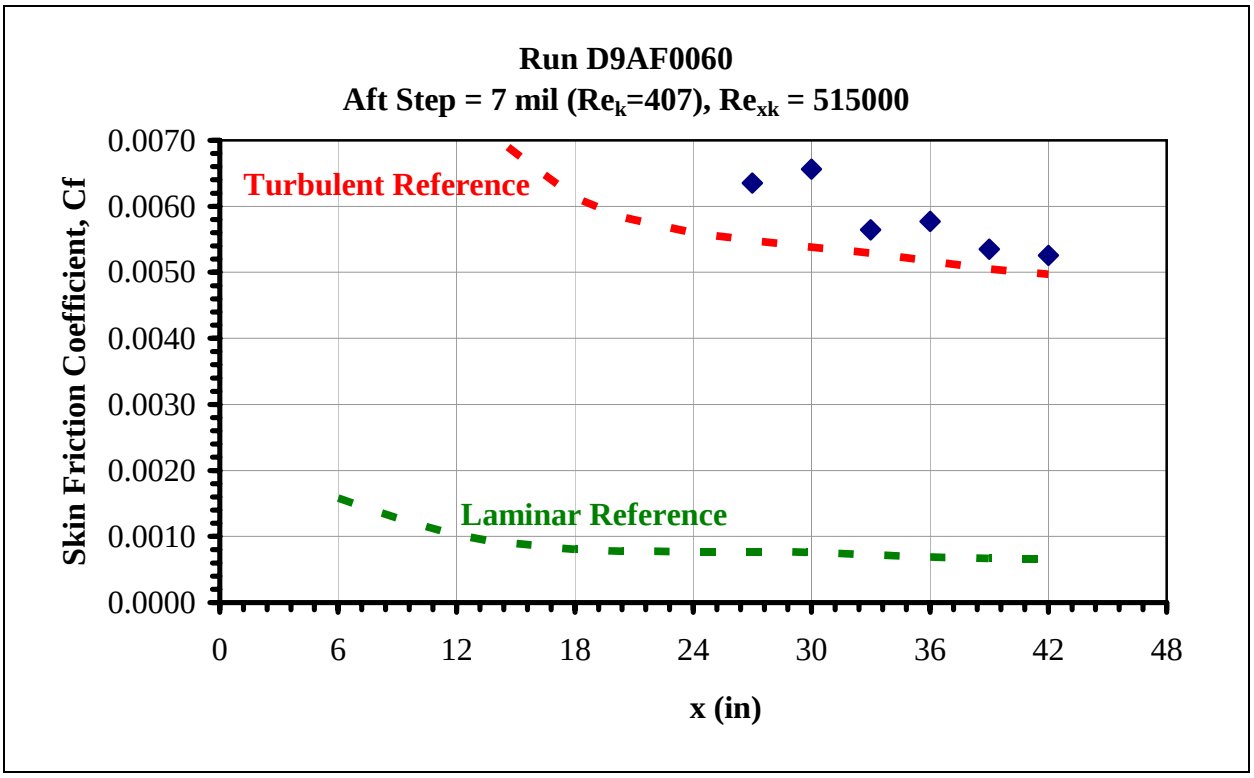

Figure 64. Aft step skin friction distribution, run D9AF0060

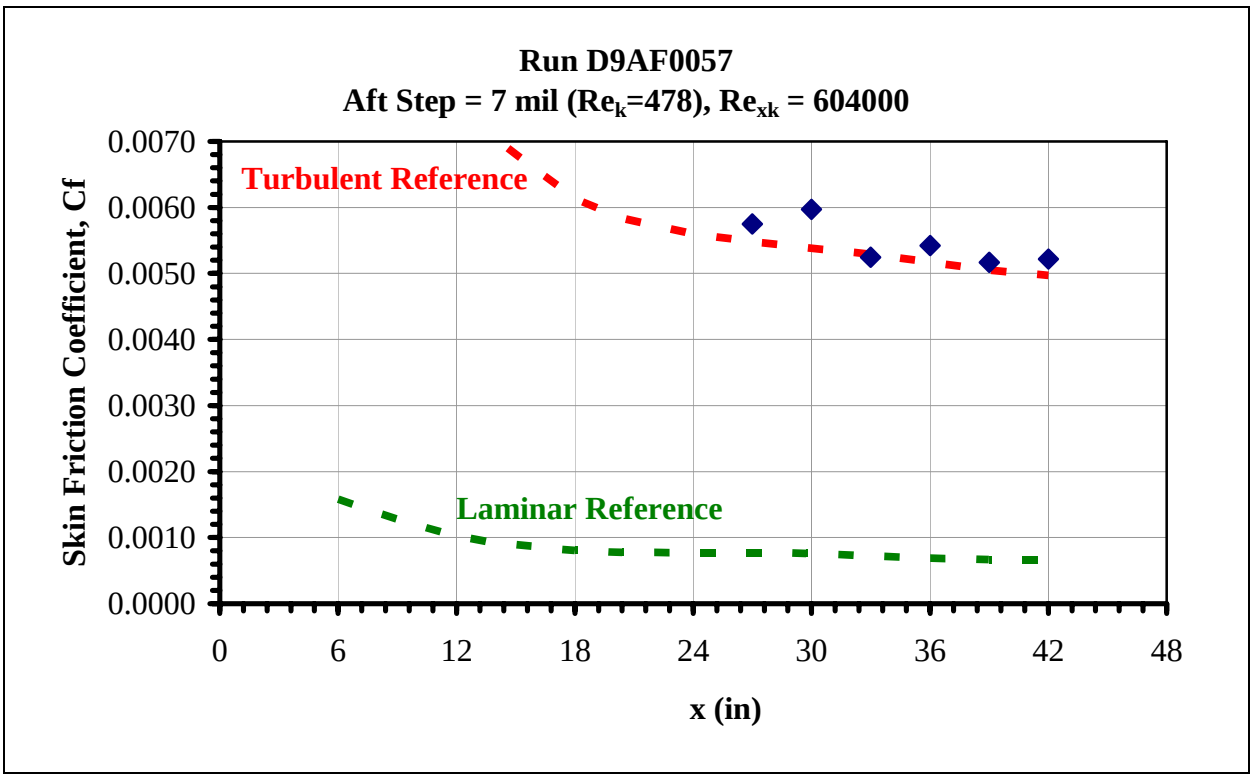

Figure 65. Aft step skin friction distribution, run D9AF0057

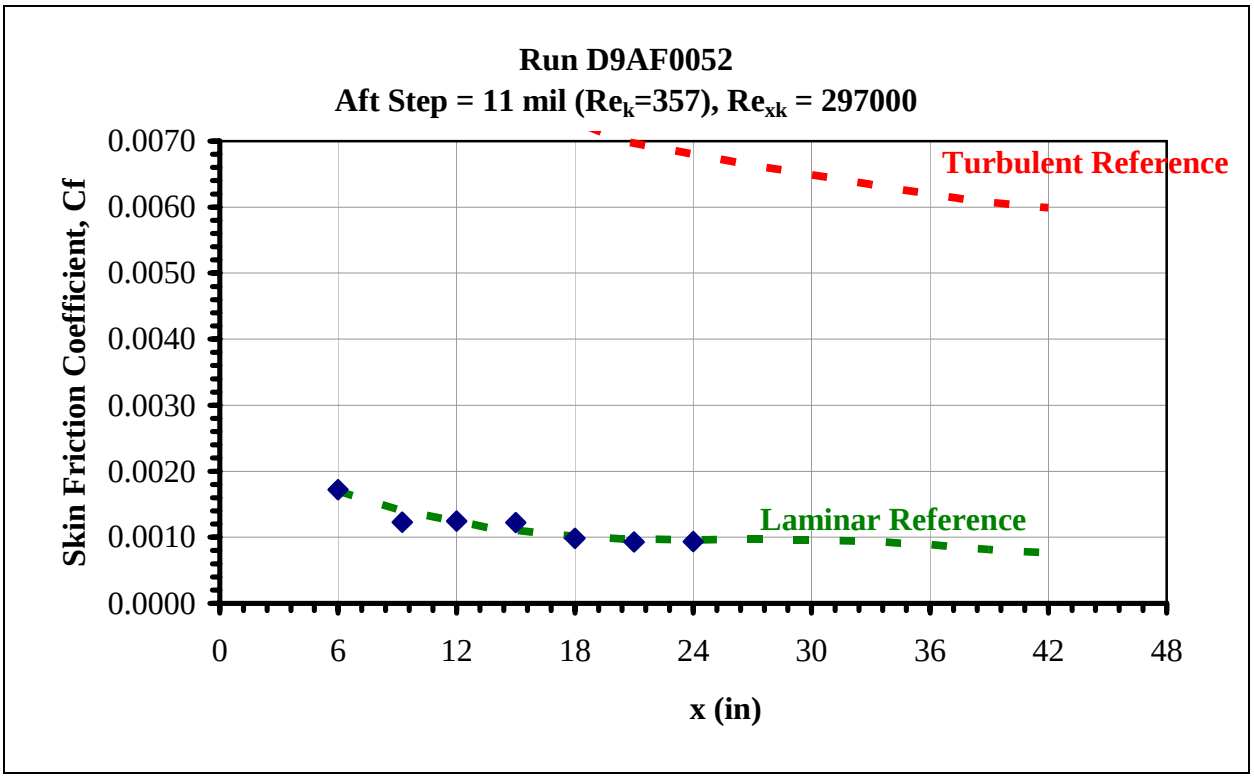

Figure 66. Aft step skin friction distribution, run D9AF0052

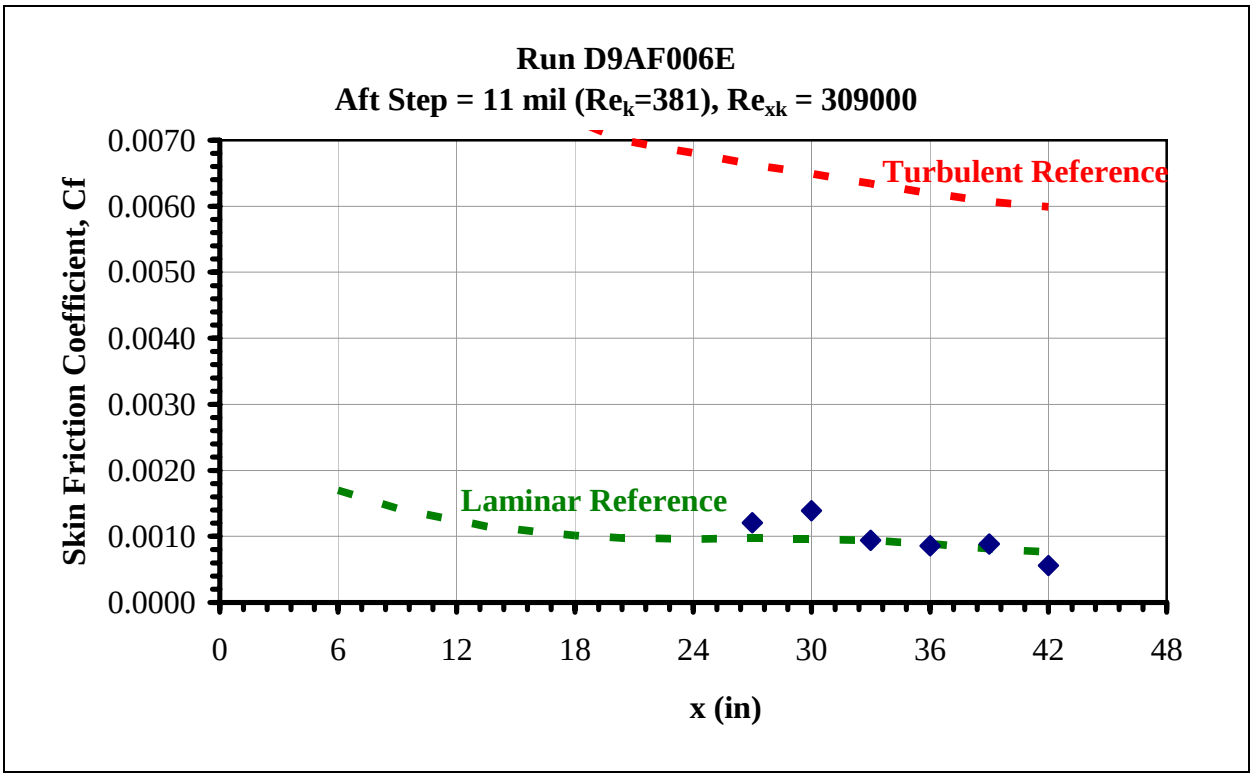

Figure 67. Aft step skin friction distribution, run D9AF006E

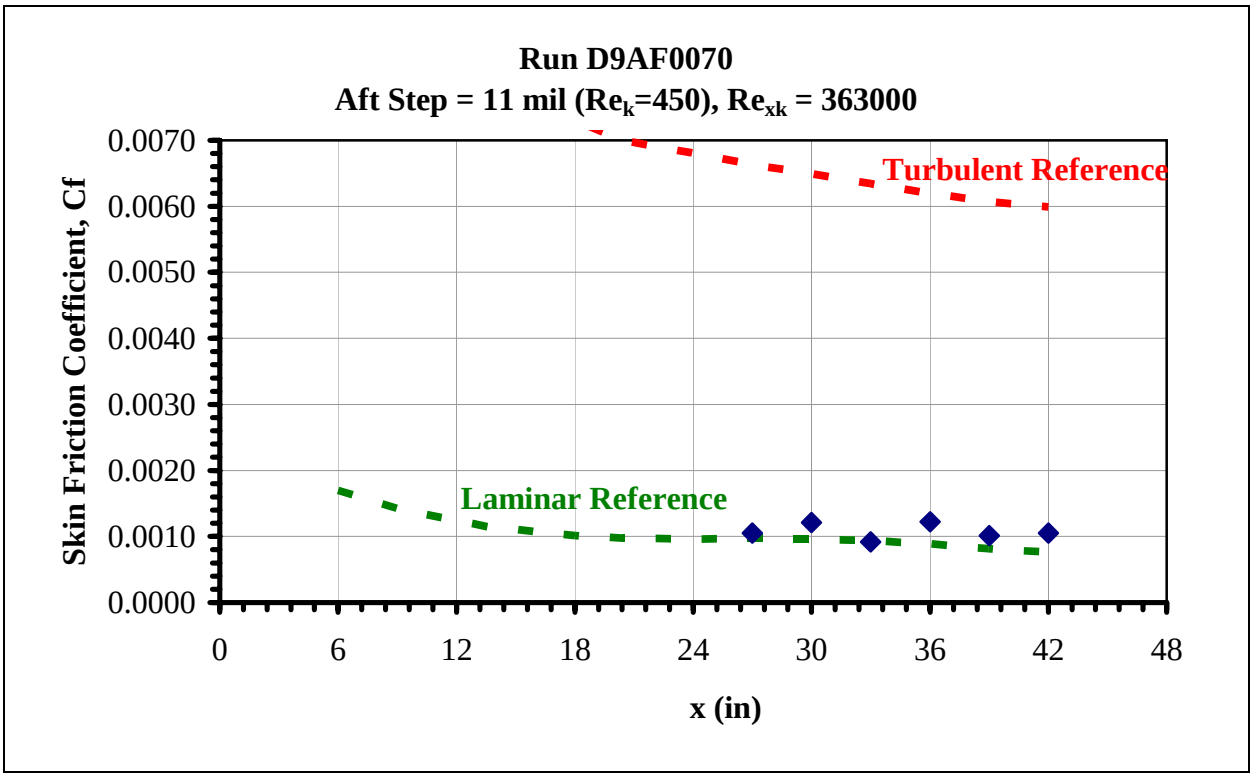

Figure 68. Aft step skin friction distribution, run D9AF0070

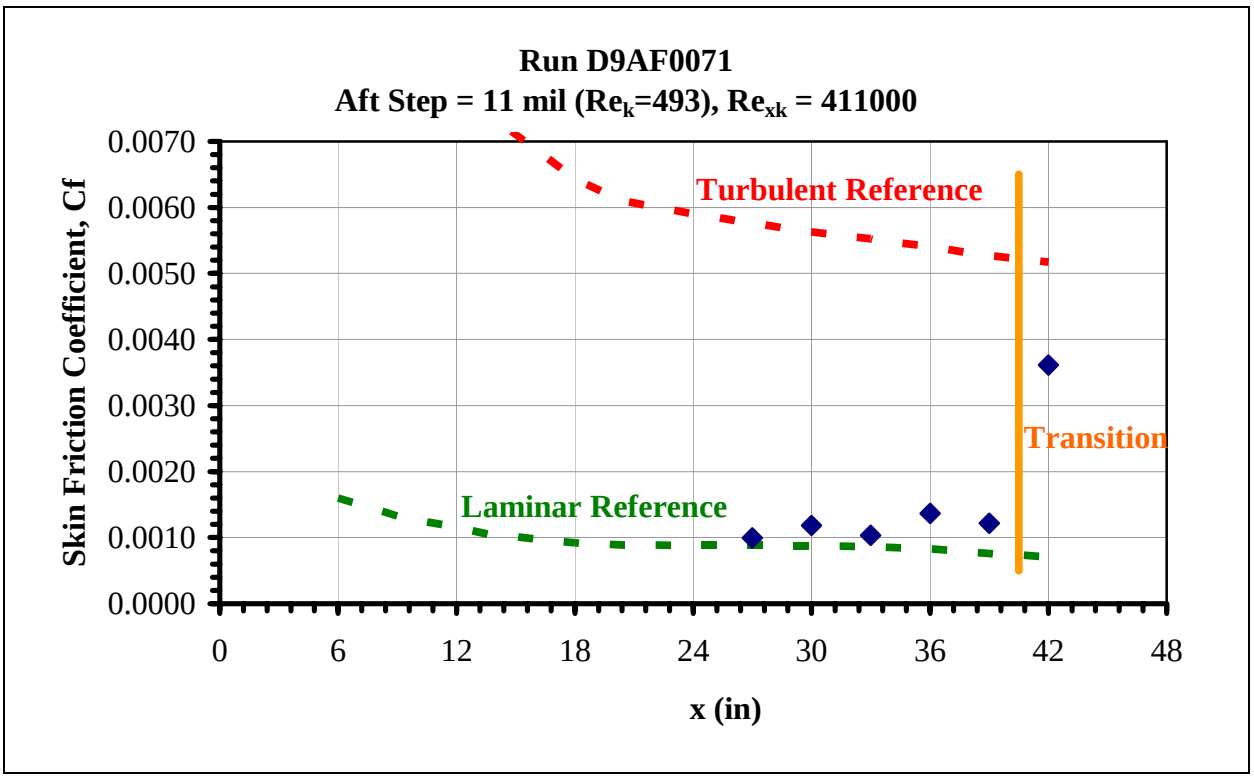

Figure 69. Aft step skin friction distribution, run D9AF0071

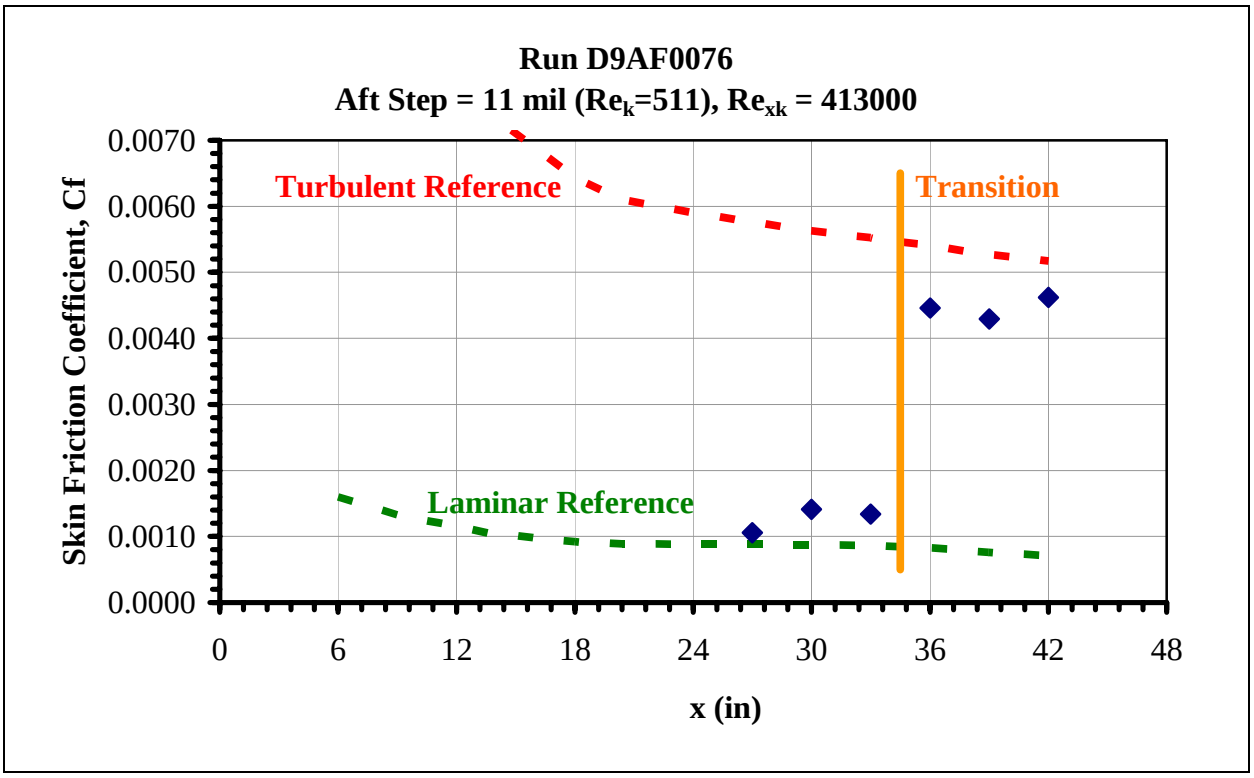

Figure 70. Aft step skin friction distribution, run D9AF0076

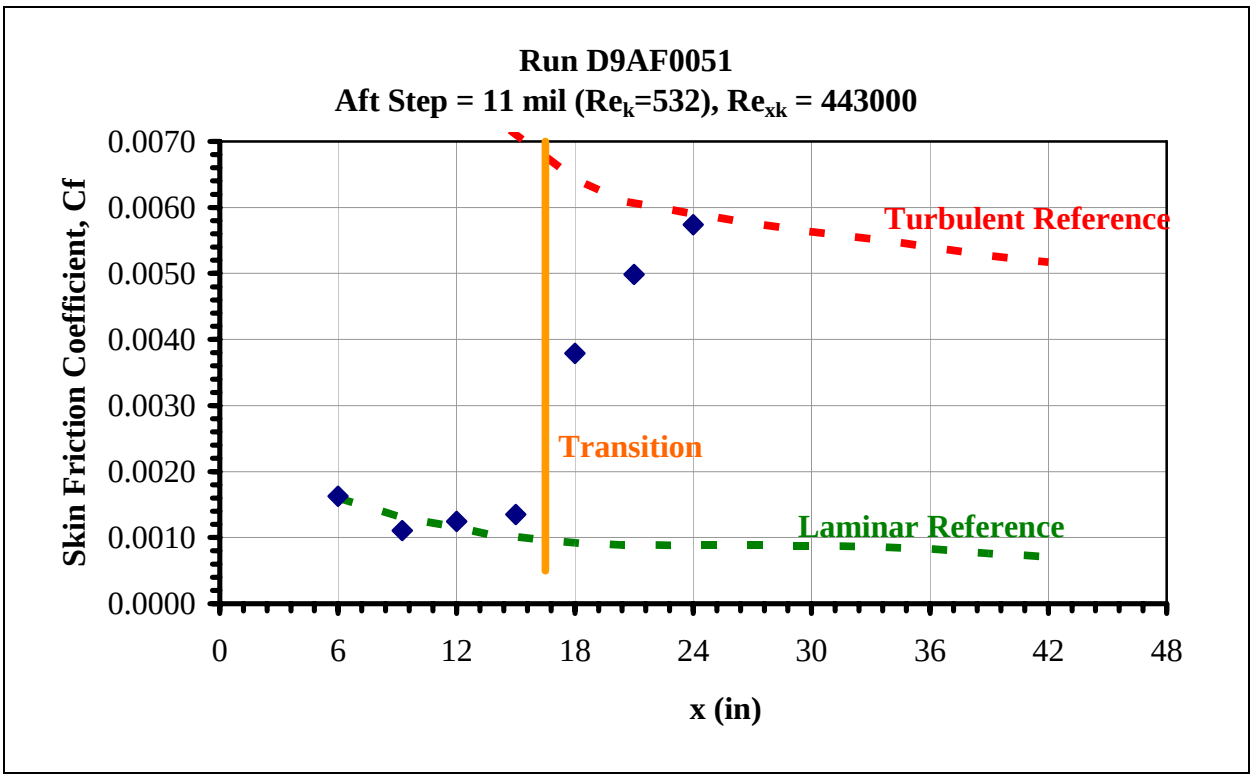

Figure 71. Aft step skin friction distribution, run D9AF0051

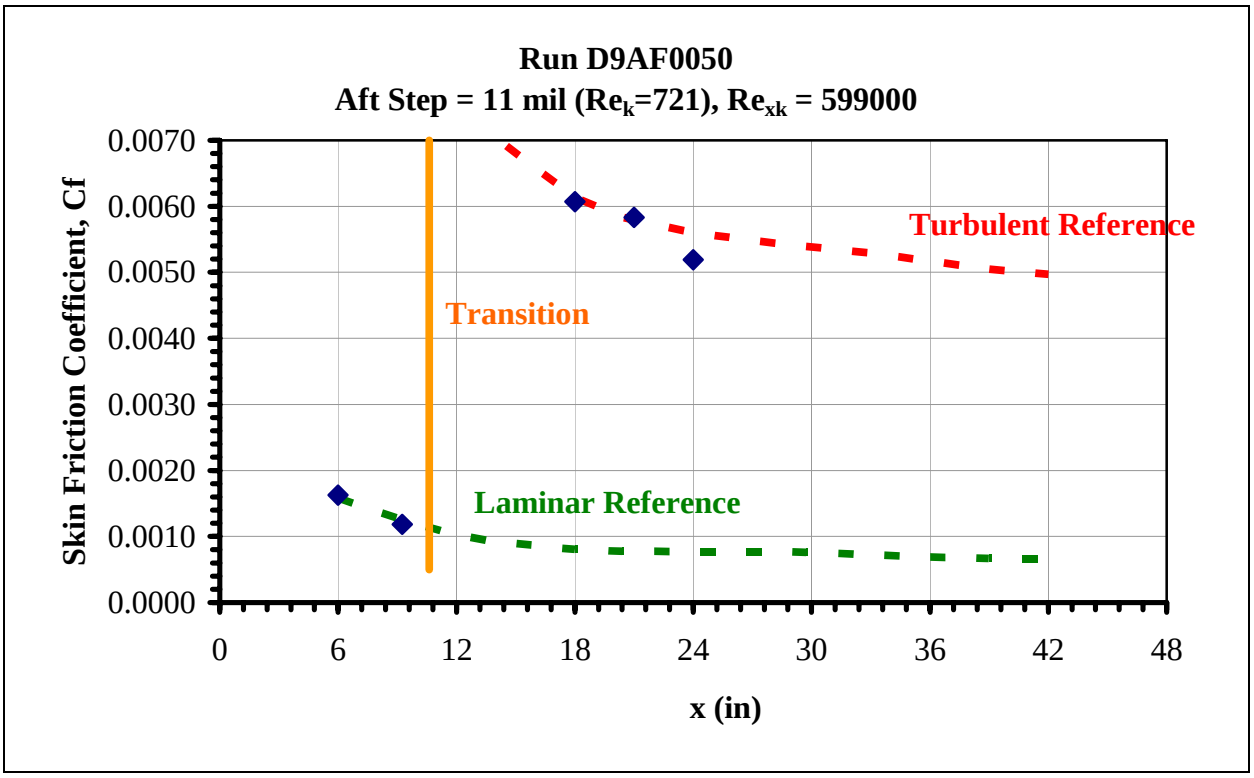

Figure 72. Aft step skin friction distribution, run D9AF0050

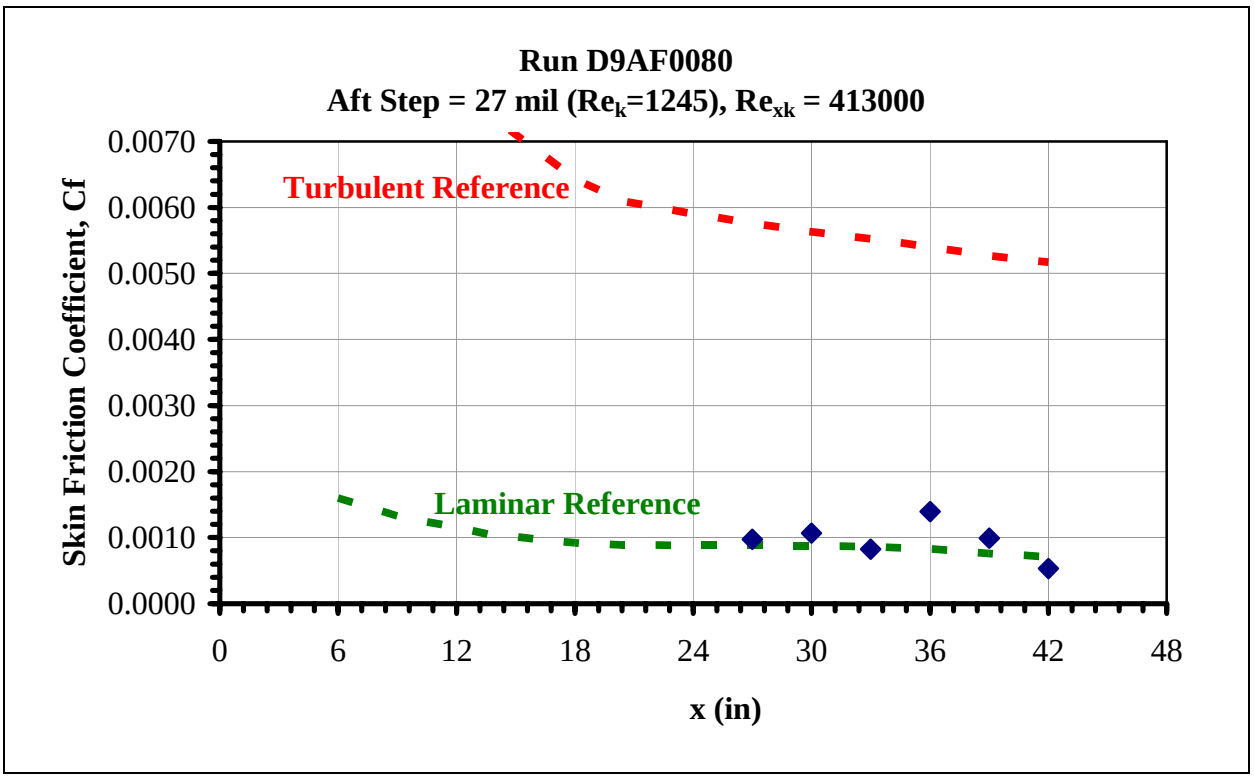

Figure 73. Aft step skin friction distribution, run D9AF0080

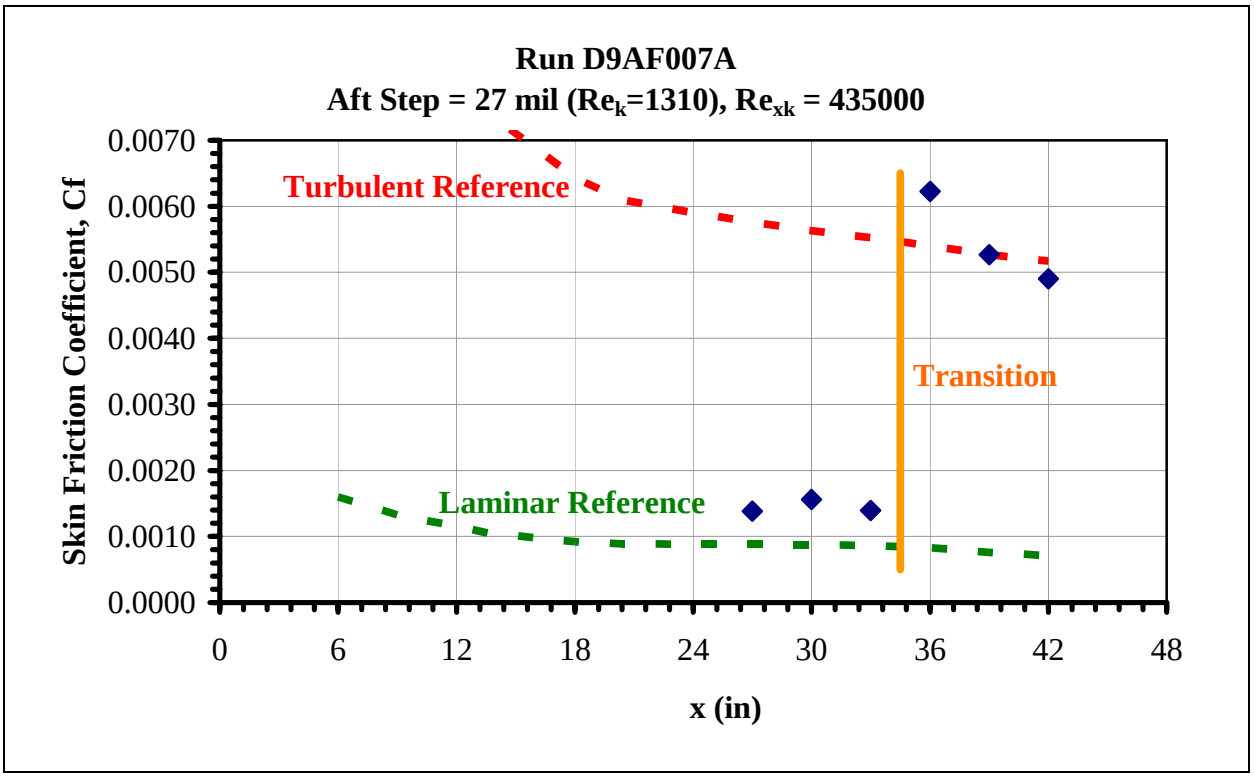

Figure 74. Aft step skin friction distribution, run D9AF007A

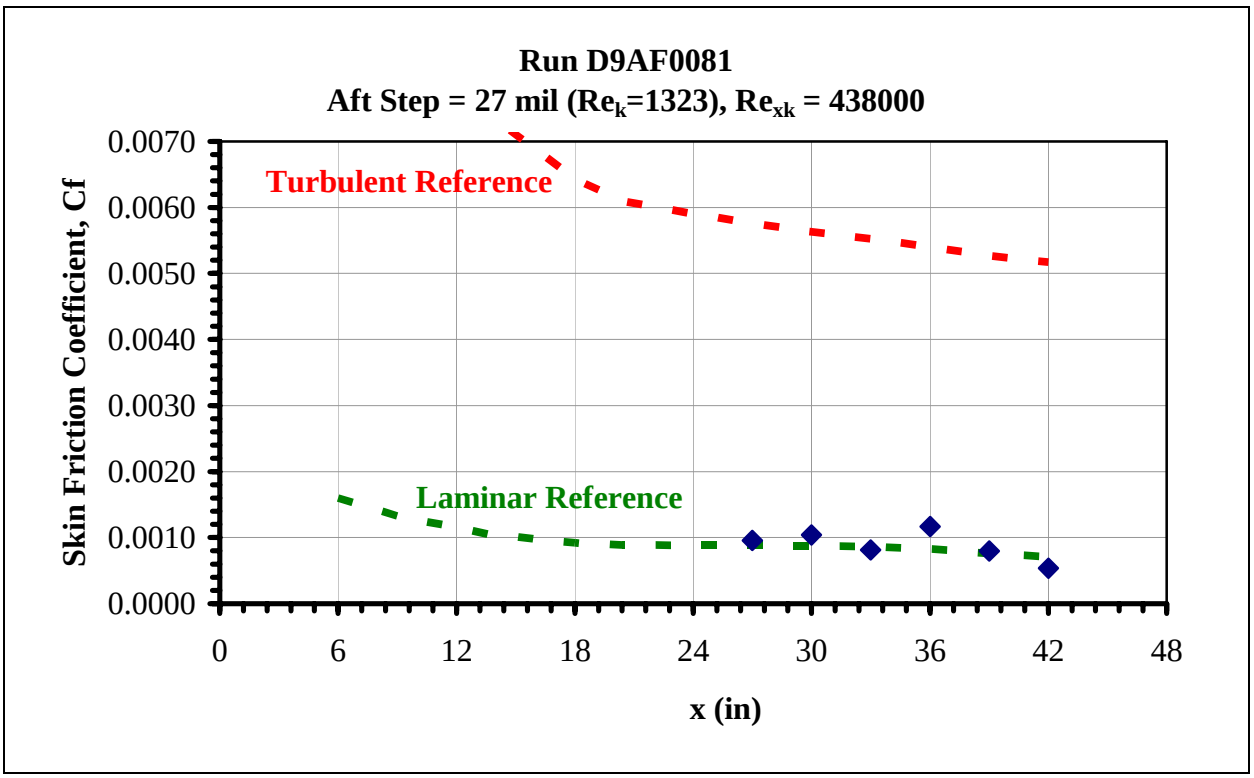

Figure 75. Aft step skin friction distribution, run D9AF0081

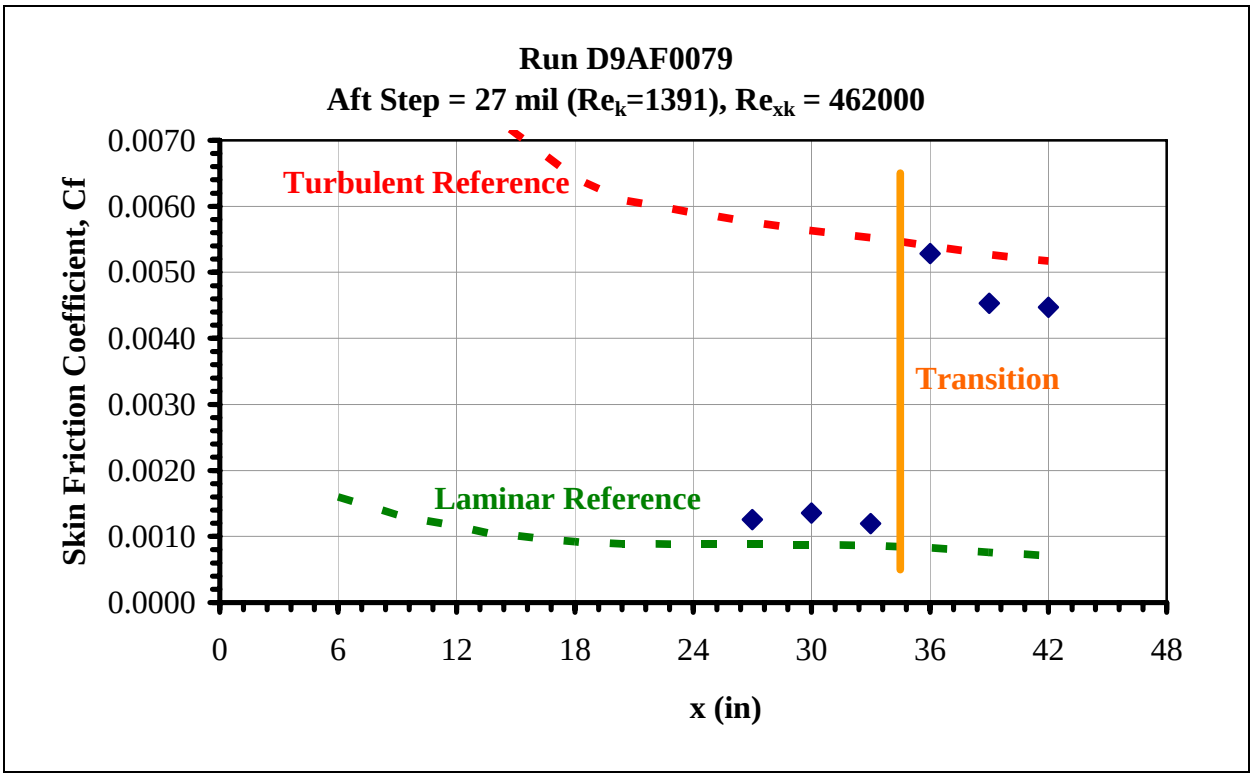

Figure 76. Aft step skin friction distribution, run D9AF0079

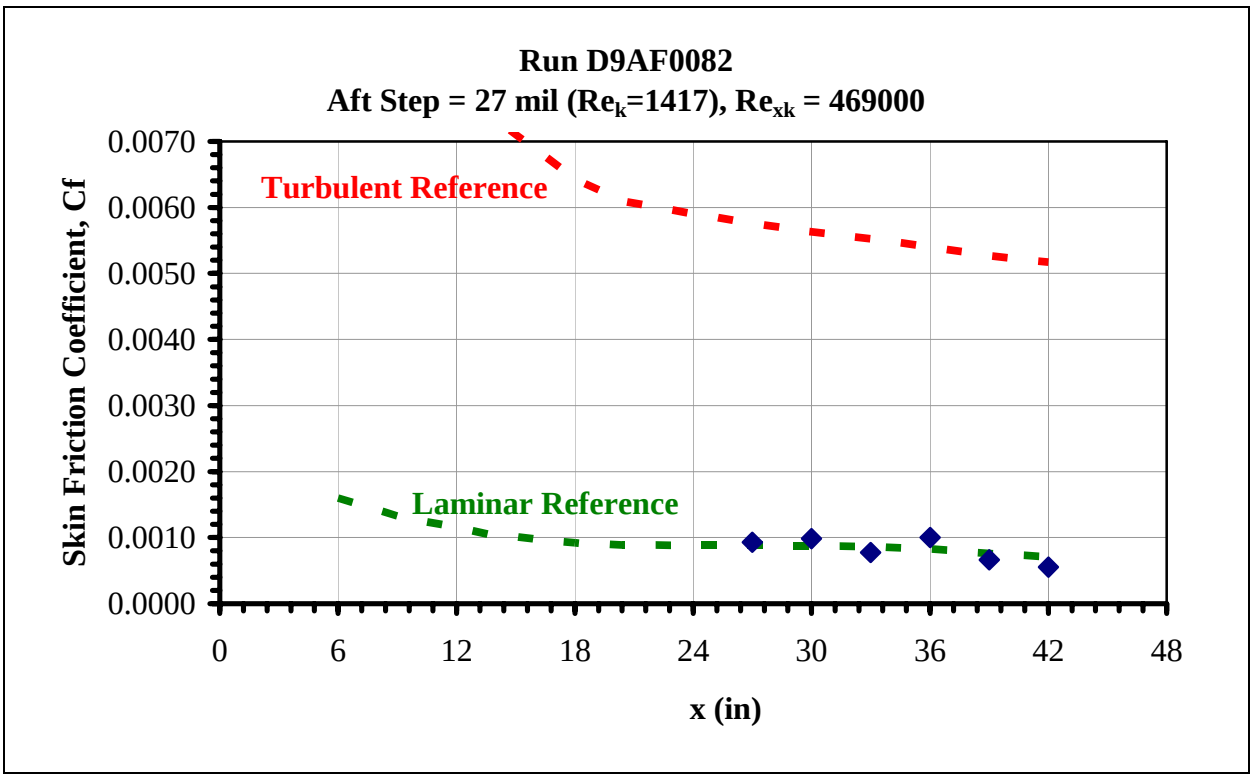

Figure 77. Aft step skin friction distribution, run D9AF0082

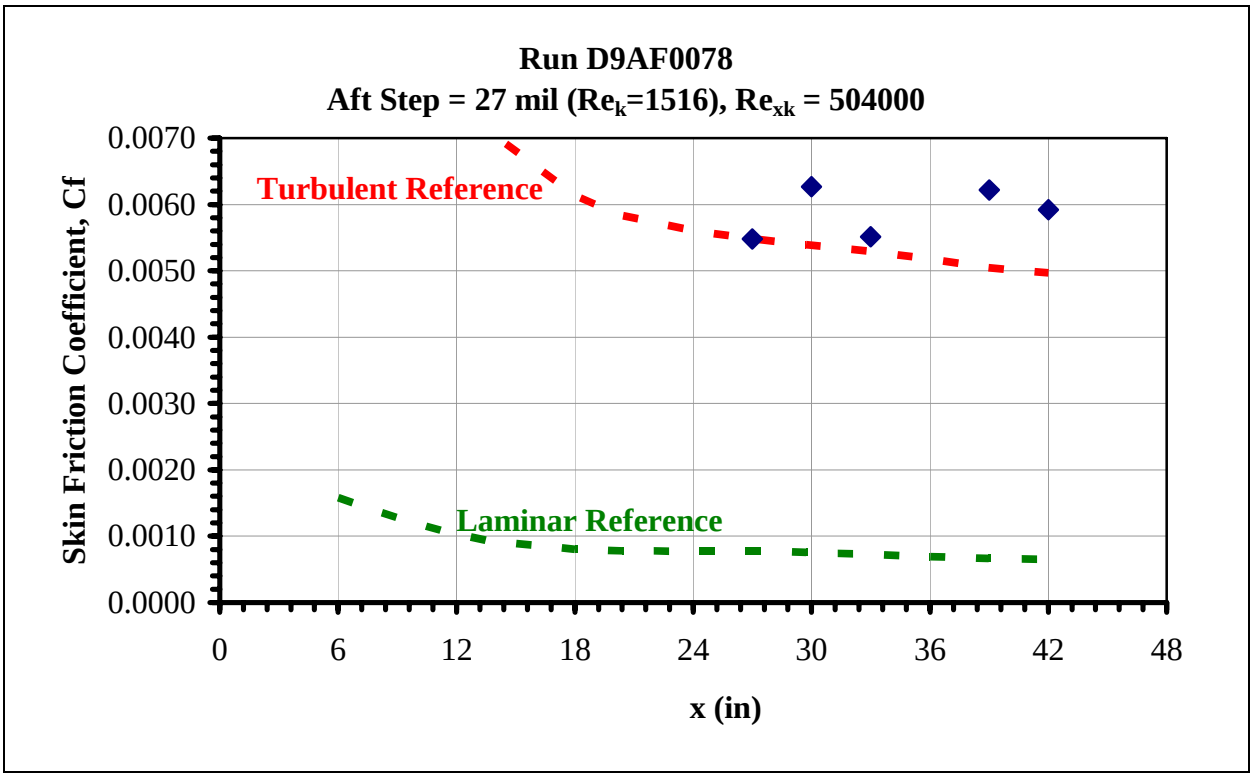

Figure 78. Aft step skin friction distribution, run D9AF0078

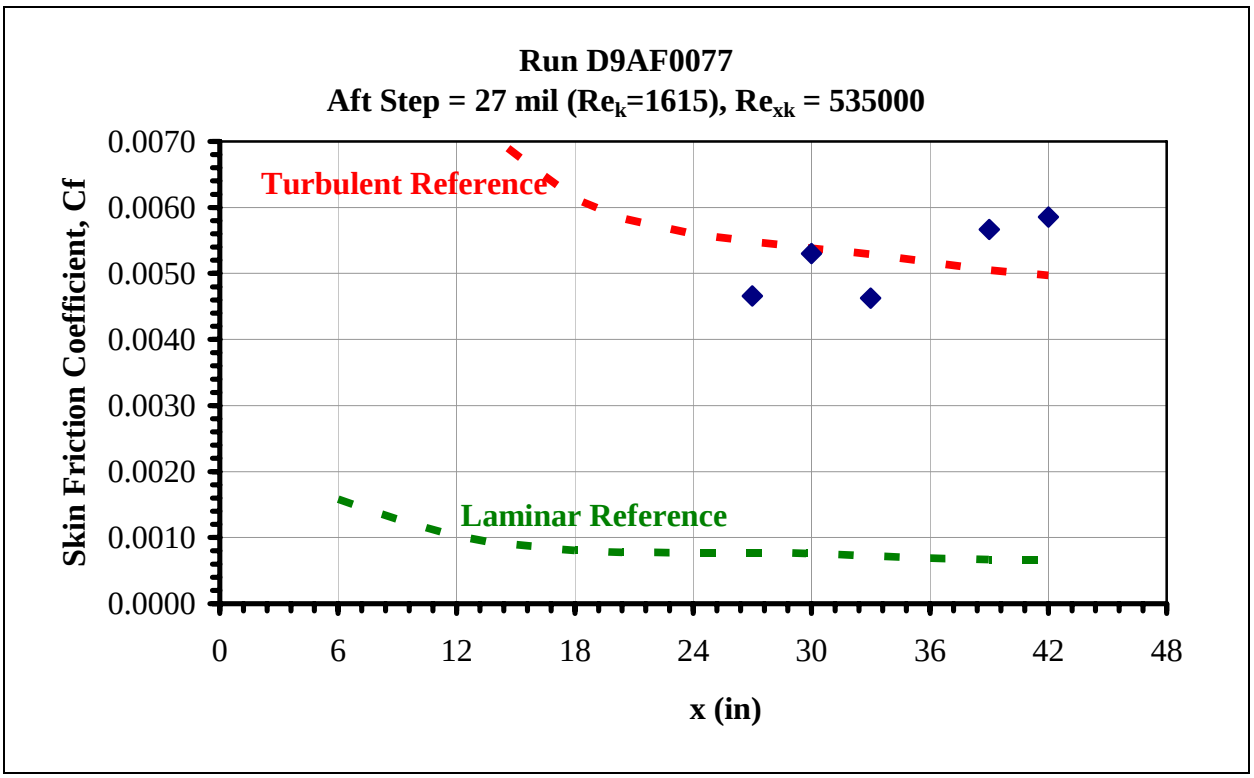

Figure 79. Aft step skin friction distribution, run D9AF0077

2.4.4 Boundary Layer Transition Trends

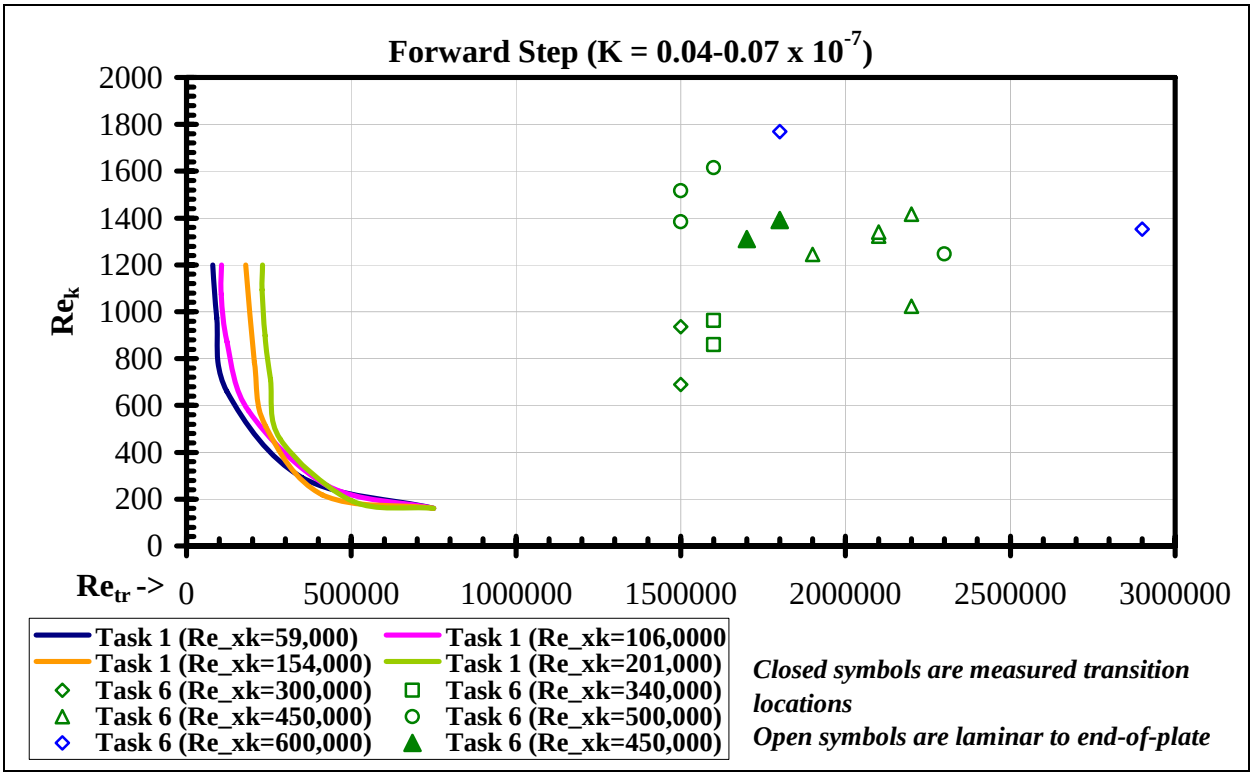

Figure 80. Re_k vs. Re_{tr} transition trend, forward steps

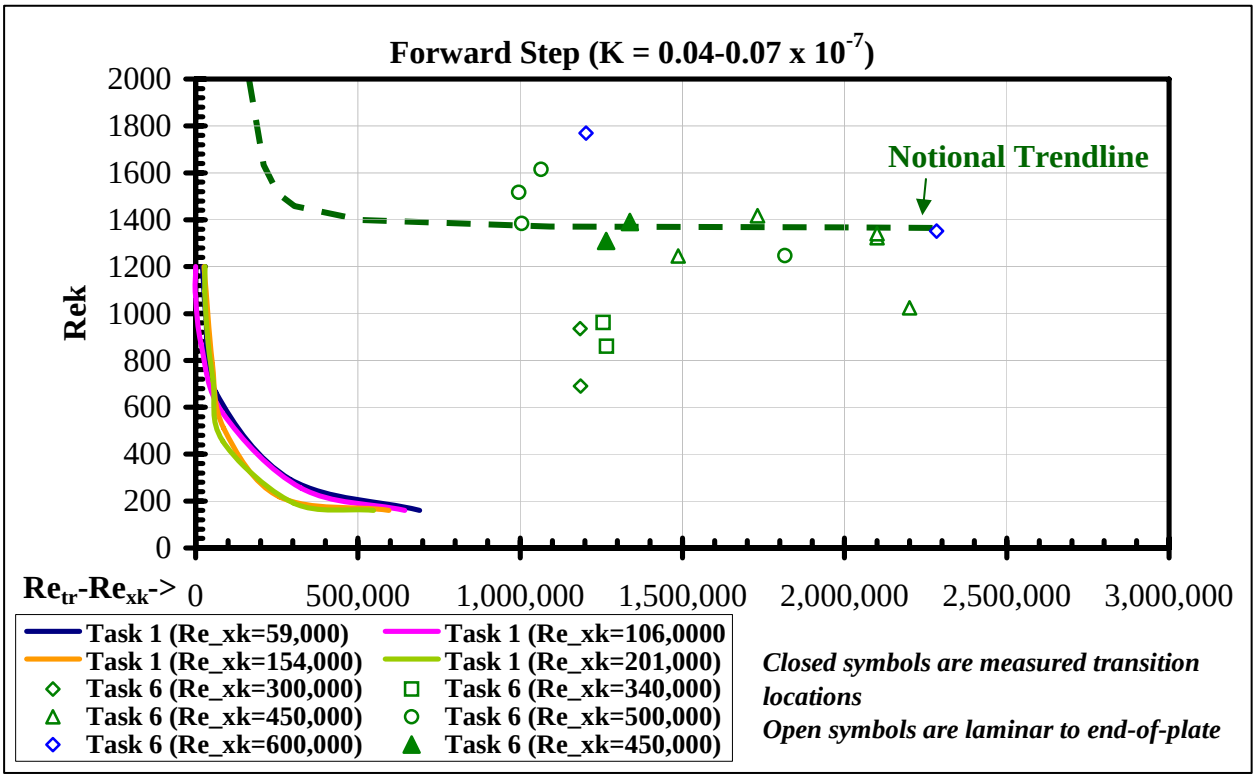

Figure 81. Re_k vs. (Re_{tr} - Re_{xk}) transition trend, forward steps

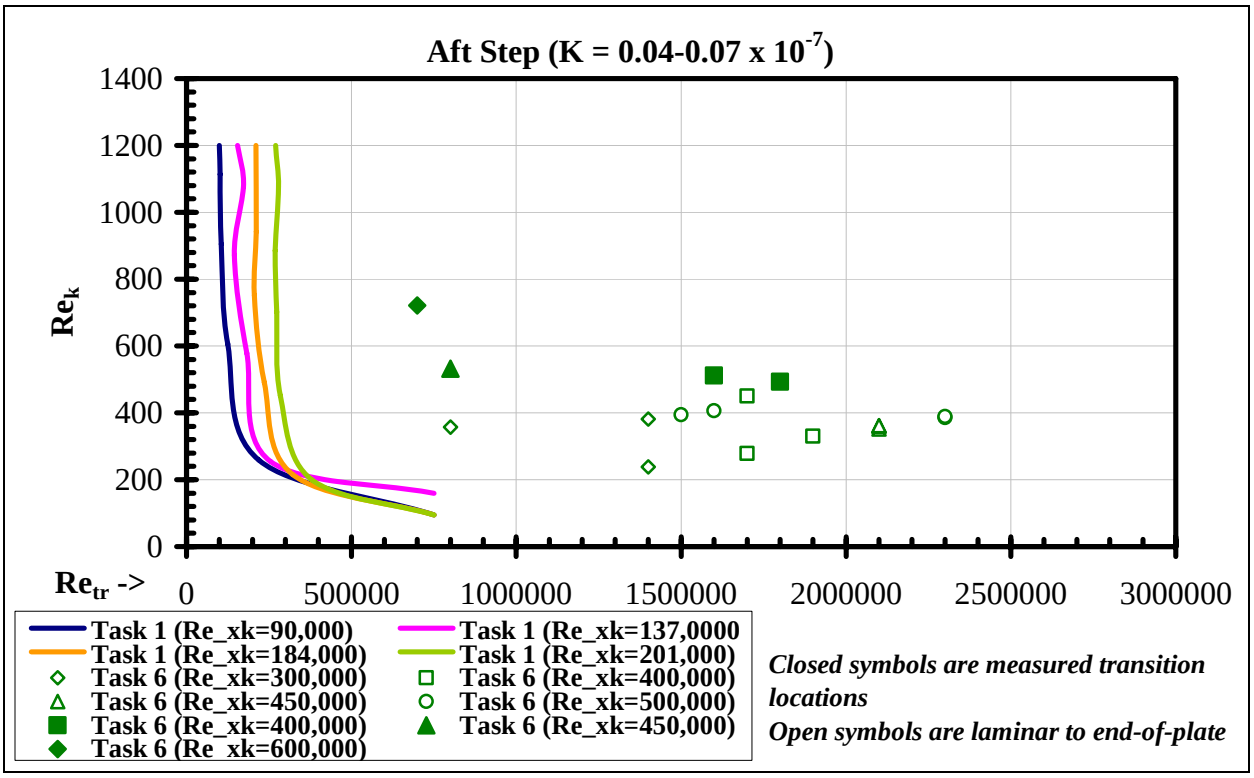

Figure 82. Re_k vs. Re_{tr} transition trend, aft steps

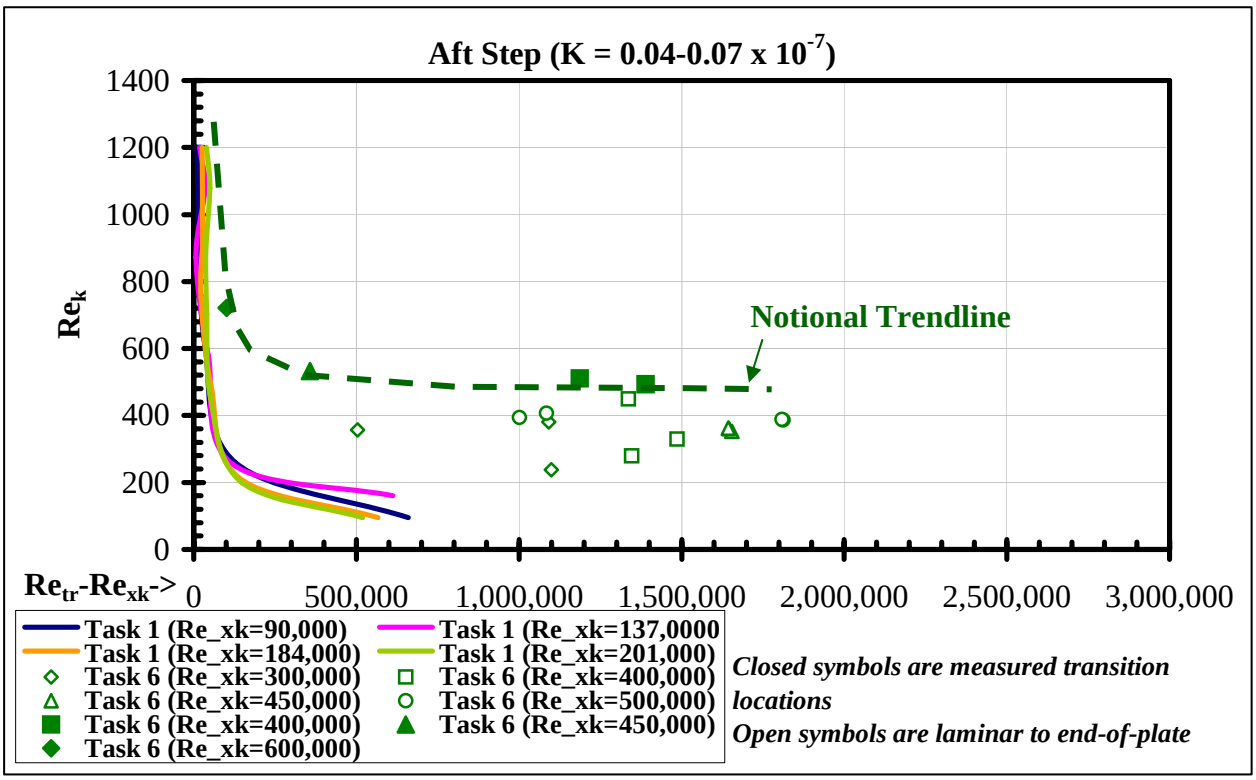

Figure 83. Re_k vs. (Re_{tr} - Re_{xk}) transition trend, aft steps

3.0 Conclusions

The dashed trendlines in Figures 81 and 83 are hypothetical, and are certainly not provable with the limited data we have to date. However, the Task 6 data does indeed suggest a dramatically different trendline compared to the Task 1 data, which represents a highly favorable shift in the transition trend. The Task 6 results indicate a potential for substantial reductions in the required manufacturing tolerances.

While the reason for the large discrepancy is unclear, the one major difference between the Task 1 and Task 6 testing is the flow quality of the facility. While the Task 1 wind tunnel has very good flow quality for boundary layer studies, the Towing Wind Tunnel has free-air conditions; one would expect this to be better, but the profound differences seen in the Task 6 data were not expected.

The implication is not that the Task 1 results are invalid; rather, it is that the disturbance environment has a more significant effect than anticipated. Considering that the Task 1 results at zero pressure gradient (both steps and wire trips) matched well with the data in the literature, the Task 1 setup seems validated. The results of Task 1 showed that even very small favorable pressure gradients lead to a marked increase in the allowable step heights. The expectation going into Task 6 was that the same trends would be seen, simply extended to higher Reynolds numbers. Instead, the data is significantly shifted. The Task 6 results show greatly increased allowable step heights compared to the Task 1 data, presumably due to the superior disturbance environment. This suggested result is very promising for laminar flow flight vehicles in general.

The Task 6 test setup is more relevant to flight applications. Furthermore, testing at the Towing Wind Tunnel proved itself to be a feasible endeavor. Because of the possibility for dramatic reduction in manufacturing tolerances, further investigation of excrescence effects at higher Reynolds numbers at this facility is well worth pursuing.

4.0 Recommended Follow-On Activities

4.1 Extensive Experimental Investigation at Full-Scale Reynolds Numbers

Much more study would be required to validate the theory of substantially relaxed manufacturing tolerances due to the disturbance environment suggested by the Task 6 results. The disturbance environment at the Towing Wind Tunnel would need to be quantified experimentally first. An extensive experiment, on the scale of the Task 1 work, would be appropriate. For a potential Task 7, a larger chord and span model would be desirable. The Task 0 model, used in the Task 6 testing, was designed for a very different test setup and facility. A larger chord model would also allow the maximum Reynolds number to approximately double. A limited number of different models, in order to vary pressure gradient would also be desirable. Increased-capability instrumentation, capable of measuring more data at once, would also be recommended.

LIST OF ACRONYMS, ABBREVIATIONS, AND SYMBOLS

ACRONYM	**DESCRIPTION**
2-D	Two-dimensional
km	Kilometer
m	Meter
mAhr	Milli-Ampere hour
psi	Pounds per square inch
Re	Reynolds number
t	Ton
U	Velocity
Ue	Boundary layer edge velocity
V	Volt
y	Height above surface
C_f	Skin friction coefficient
C_p	Coefficient of pressure
K	Pressure gradient parameter
Re_k	Excrescence height Reynolds number